TITANIUM DIOXIDE NANOPARTICLES: PROTEIN ADSORPTION AND CELLULAR INTERACTIONS

A Dissertation
Presented to
The Academic Faculty

by

Sabiha Runa

In Partial Fulfillment
of the Requirements for the Degree
Doctor of Philosophy in the
School of Chemistry and Biochemistry

Georgia Institute of Technology
August 2017

TITANIUM DIOXIDE NANOPARTICLES: PROTEIN ADSORPTION AND CELLULAR INTERACTIONS

Approved by:

Dr. Christine Payne, Advisor
School of Chemistry and Biochemistry
Georgia Institute of Technology

Dr. Christoph Fahrni
School of Chemistry and Biochemistry
Georgia Institute of Technology

Dr. Wendy Kelly
School of Chemistry and Biochemistry
Georgia Institute of Technology

Dr. Dong Qin
School of Materials Science and Engineering
Georgia Institute of Technology

Dr. Bridgette Barry
School of Chemistry and Biochemistry
Georgia Institute of Technology

Date Approved: [July 19, 2017]

ACKNOWLEDGEMENTS

My gratitude towards those who made my research endeavors possible is endless. First of all, I thank Christine Payne, for being my research advisor and mentor, providing me guidance and multiple opportunities to expand my experiences, both personally and professionally. I also thank my collaborators, Melissa Kemp and Melike Lakadamyali, for their assistance and for inadvertently becoming my role models.

Along with my supervisors, I thank my research lab and peers, especially Alexandra Hill, Emilie Warren, and Linda Kippner, who have taken time to serve as my mentors by training my hands in lab and my mind at the blackboard. Dhanya Jayaram, Dipesh Khanal, and Michael Hussey provided valuable conversations and guidance on my projects, and I am honored to call them coauthors in my publications.

Along this journey, I extrapolated mentors in Lizanne DeStefano, Steven Taylor and Maureen Rouhi. Your patience and willingness to work with an inexperienced writer and molding her into a reporter and investigator has enriched my life at Georgia Tech, allowing me to create my own legacy. I thank you immensely for the opportunity to work with you.

Every journey comes with realizing those who have provided substantial love, friendship, and guidance. However, I realize my limitations in acknowledging all those who have crossed my path, even if for the duration of an elevator ride, and changed my life in ways that cannot be defined as small, as all changes are impactful. For those hearts, please know that you made me who I am today.

At last, I thank my family for their unconditional support through this entire journey. There are infinite blessings in having my parents be my best friends through this process. I thank my Mom, Dad, and my siblings for every opportunity they gave me to realize my potential and push me to be the best version of myself inside and out. My dream of earning a PhD has been for you, with you, and most of all, because of you.

TABLE OF CONTENTS

LIST OF TABLES

LIST OF FIGURES

LIST OF SYMBOLS AND ABBREVIATIONS

µg	microgram
µL	microliter
A549	adenocarcinoma human alveolar basal epithelial
AF647	AlexaFluor 647
BET	Brunauer, Emmett and Teller
BSA	bovine serum albumin
BS-C-1	African green monkey kidney epithelial
C_T	threshold cycle
DLS	dynamic light scattering
DMPO	5,5-dimethyl-1-pyrroline N-oxide
DNPH	dinitrophenylhydrazine
DTT	dithiothreitol
E171	food grade titanium dioxide
EMCCD	electron multiplying charge-coupled device
EPR	electron paramagnetic resonance
FBS	fetal bovine serum
H_2DCF	2',7'-dichlorofluorescein
H_2DCFDA	2',7'-dichlorodihydrofluorescein diacetate
H_2O_2	hydrogen peroxide
HeLa	adenocarcinoma human cervical
IPA	isopropanol
kDa	kilodalton

LDH	lactate dehydrogenase
MB	methylene blue
MDA	malondialdehyde
MEM	minimal essential medium
mg	milligram
mL	milliliter
MTT	3-(4, 5-dimethylthiazolyl-2)-2, 5-diphenyltetrazolium bromide
MW	molecular weight
NBT	nitroblue tetrazolium
NP	nanoparticle
P25	industrial titanium dioxide
PBS	phosphate buffered saline
PDI	polydispersity index
PEG	polyethylene glycol
PEL	permissible exposure limit
PI	propidium iodide
PRDX/Prx	peroxiredoxin
PS	polystyrene
rcf	relative centrifugal force
ROS	reactive oxygen species
RT-PCR	reverse transcriptase polymerase chain reaction
SDS-PAGE	sodium dodecyl sulfate-polyacrylamide gel electrophoresis
SEM	scanning electron microscopy
SOD	superoxide dismutase
STORM	stochastic optical reconstruction microscopy

TA	terephthalic acid
TEM	transmission electron microscopy
TiO_2	titanium dioxide
UV	ultraviolet
UV-Vis	ultraviolet-visible
XPS	x-ray photon spectroscopy
ZP	zeta potential

SUMMARY

Titanium dioxide nanoparticles (TiO_2 NPs) are used in many applications from photocatalysis to pigmentation. Their presence in commercial products such as paints, sunscreens, cosmetics, and food motivates interest in understanding how these nanoparticles interact within a cellular environment. Previous studies have linked TiO_2 NPs to oxidative stress. The following dissertation characterizes this response and its oxidation-based mechanism in an *in vitro* setting.

We note that oxidative stress occurs after a 24 hour incubation with low, nontoxic concentrations of TiO_2 NPs. This intracellular change, characterized by the alteration in gene expression of the peroxiredoxin family of anti-oxidant enzymes, is further examined in relation to the reactivity of the nanoparticle surface and to the adsorbed serum proteins, or the protein corona. Both industrial and food grade TiO_2 NPs generated hydroxyl radicals and superoxides. These reactive oxygen species further oxidize serum proteins and the plasma membrane.

The experiments and studies detailed in this dissertation have utilized spectroscopic and microscopy techniques to observe NP-induced oxidation responses. Through fluorescence microscopy, we show a visual map of protein adsorption onto the NP surface and note that a NP-cellular system is one that is dynamic, with several oxidative responses. The chapters that follow introduce several novel findings regarding how titanium dioxide nanoparticles induce various molecular changes on multiple levels in a cellular environment.

CHAPTER 1. INTRODUCTION

1.1 Titanium Dioxide Nanoparticles

The investigation of metal oxide nanoparticles (NPs) spans decades, focusing on the tunability of their semiconducting properties and understanding the mechanism of chemical reactions in which they participate.[1-6] Through a culmination of optimized synthesis techniques and applied research, titanium dioxide (TiO_2) NPs have evolved to be a common NP used in many applications. Several synthetic production processes for TiO_2 nanostructures exist and are detailed in literature. Variation in size, shape, surface stability, and crystal structures can be attained with each method, giving new physical and chemical properties that are still being studied to this day.[1-3, 5, 7]

NP properties are a direct result of identity and crystal phase. The anatase and rutile phases of TiO_2 NPs are used in industry and studied for their participation in photocatalysis.[8] Industrial grade TiO_2 NPs, often referred to as Degussa P25, are 80/20 mixture of anatase and rutile phases.[9-10] Food grade TiO_2 NPs, denoted as E171 food additive are anatase phase.[2] In terms of biocompatibility, rutile TiO_2 NPs are less cytotoxic than anatase.[4, 7] However, the anatase phase has been reported to have higher photocatalytic activity than the rutile phase.[4]

1.1.1 Common Uses of TiO_2 NPs

The intrinsic properties of TiO_2 NPs make for a multitude of applications ranging from catalysis to aesthetics. Primary uses are shown in Figure 1. TiO_2 NPs can be found in various sunscreens and cosmetics to absorb ultraviolet light, protecting the dermal layer

from sunlight and consequential damage including inflammation, dermal matrix breakdown, and photoaging leading to various skin conditions.[11-12] The peak absorbance of the P25 Degussa industrial grade particles was found to be 330 nm (Chapter 4).

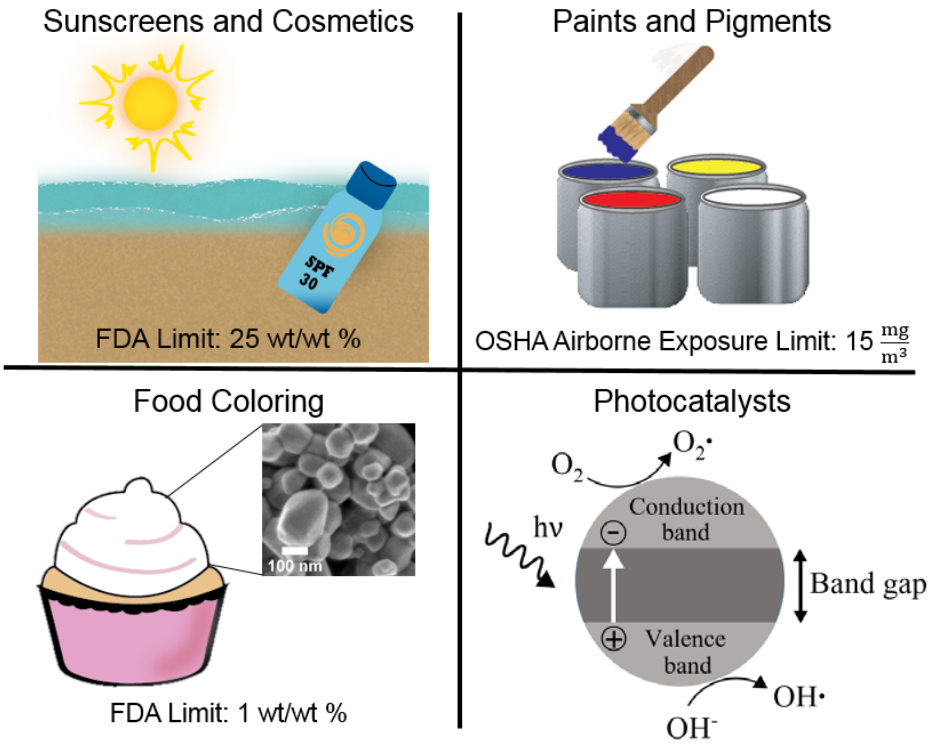

Figure 1 Common uses of TiO_2 NPs.

TiO_2 NPs scatter light and are highly opaque, with a refractive index of 2.54 for anatase and 2.79 for rutile.[2] Due to these properties, they are added to paints, plastics, and paper to provide a white coloring and opacity. Additionally, the NPs are added to foods such as gums, confectionary, and drink powders as a colorant.[4, 13-14]

The photocatalytic properties of TiO_2 NPs were discovered in 1972, where reactive oxygen species (ROS) were produced from splitting water in the presence of ultraviolet light (Figure 1).[1-2, 5] The band gap of TiO_2 is 3.2 eV.[4] Using the equation for photon energy,

this band gap energy approximates that photocatalysis of TiO_2 is activated by ultraviolet light below 385 nm. The research sector has been driven to fully understand and utilize the ultraviolet irradiation of TiO_2 to generate favourable reactions in solar cells or to photocatalyze the degradation of organic pollutants.[1, 5, 8]

TiO_2 photocatalysis is tunable by the addition of noble metals, other semiconductors, or oxides. Studies investigating these heterogeneous systems have found expanded applicability of TiO_2. Sato *et al.* discovered that a Pt/TiO_2 composite could photocatalyze the decomposition of water into H_2 and O_2, a reaction that TiO_2 alone cannot initiate.[15] Chen *et al.* noted that Pt/TiO_2 and Pd/TiO_2 both increased the rate of alcohol oxidation relative to TiO_2 alone.[8] The addition of graphene oxide, an insulator, has also shown to enhance charge transport.[1] Taken together, the full potential for TiO_2 composites remains undiscovered and is still being explored.

1.1.2 Public Health Perspectives: The Biological Relevance of TiO_2 NPs

As the production of TiO_2 NPs increases, so does the risk for exposure. Assessments on NP exposures investigate inhalation, ingestion and dermal absorption.[16-18] Smijs *et al.* confirm that the NPs applied to the skin do not penetrate the skin, making the main exposure pathways for TiO_2 NPs are inhalation (respiratory), with high probability occurring during the synthesis phase, and ingestion through presence in foods and through environmental exposure.[12]

In regards to respiratory toxicology, several studies have linked adverse effects to TiO_2 exposure. Lee *et al.* observed increases in the incidence of pneumonia, tracheitis, and rhinitis upon TiO_2 inhalation exposure for two years in rats.[17] Chronic exposure at 250

mg/m^3 resulted in bronchioloalveolar adenomas. Heinrich *et al*. found similar lung tumor formation in rats after 18 months of exposure.[16] Additionally, a lung tumor rate of 32% is reported after 24 months TiO_2 exposure followed by 6 months of clean air. Broadening studies to humans, Pelclova *et al.* examined the concentration of several oxidative stress markers in workers exposed to TiO_2. The exhaled breath condensate for each worker was examined, and increases were observed for 8-hydroxy-2-deoxyguanosine (8-OHdG), 8-hydroxyguanosine (8-OHG), 5-hydroxymethyl uracil (5-OHMeU)) and oxidized proteins o-tyrosine (o-Tyr), 3-chlorotyrosine (3-ClTyr) and 3-nitrotyrosine (3-NOTyr).[18]

In terms of occupational health, respiratory studies of these NPs vary in testing methods, NP-of-interest size and dosage. Frysek *et al.* assessed workers in TiO_2 production factory environments and found no correlation between NP exposure and cancer.[19] Similar results were found by Boffeta *et al.*, in a study assessing lung cancer and NP exposure. No association was found, determined by an odds ratio of 0.9 with a 95% confidence interval.[20] It is important to note that reporting of individual responses, existence of previous health conditions, as well as the details on the TiO_2 particle size introduce biases within each study.[21] In terms of public health, exposure assessments require the collaboration between the science, medical, and public health community. The molecular mechanistic approaches, such as those detailed in this text, provide one way to connect *in vitro* findings to informing public health research, expanding the methodologies performed in exposure assessment.

Studies regarding NP ingestion have suggested a correlation between TiO_2 NPs and inflammation. Bettini *et al.* observed the development of inflammation in the colon of rats

orally administered with E171 NPs.[22] Scaling down, *in vitro* assessments have also linked TiO_2 NPs to inflammation and oxidative stress.[23]

Regulations for TiO_2 within the United States is overseen by multiple departments. Usage of TiO_2 for dermal protection is regulated by the Food and Drug Administration (FDA) operated under the United States Department of Health and Human Services, where the upper limit of NPs is 25% of the weight of the sunscreen or protectant.[24] The FDA limits the amount of titanium dioxide in foods to 1% of the weight of the product.[13, 25] To address the safety of workers exposed to titanium dioxide during its production in factories, the Occupational Safety and Health Administration under the United States Department of Labor has set the permissible exposure limit (PEL) for titanium dioxide is 15 mg/m^3 averaged over an 8-hour timeframe.[26] It is important to note that the PEL is designated for TiO_2 and not specific to nanoscale material. The National Institute for Occupational Safety and Health (NIOSH) has classified ultrafine TiO_2 as a potential carcinogen and recommends an exposure limit of 0.3 mg/m^3 over a 10-hour timeframe.[26]

1.2 Oxidative Stress

1.2.1 The Implications of Oxidative Stress

While reactive oxygen species (ROS) are a natural occurrence in the body, an imbalance in their concentrations leads to oxidative stress.[27-29] Under physiological conditions, ROS produced in the body include hydrogen peroxide, hydroxyl radicals, superoxides, nitric oxides, and peroxynitrites, with each implicated in specific biological pathways.[30-33] ROS participate in the natural homeostatic processes of such as cell metabolism, cell migration, cell-cell signalling, and apoptosis.[34-35] Given the short life

cycle of ROS and their ability to diffuse short distances, their role in many localized reactions seems apparent. ROS are also known to activate the mitogen-activated protein kinase (MAPK) cascades which are responsible for cell growth and differentiation.[28]

Separate from the phenomenon of ROS occurrence, oxidative stress has been implicated in various diseases including cancers, diabetes, cardiovascular disease, and rheumatoid arthritis.[36-37] Oxidative stress has also been linked to the aging process.[28, 38]

Through sophisticated regulatory pathways, the body modulates ROS levels on the cellular and subcellular levels. Antioxidants are present in the mitochondria, endoplasmic reticulum, nucleus, and cytoplasm and reduce local ROS into more stable molecules.[33, 39] When ROS levels are uncontrolled, they oxidize biomacromolecules.[40-42] The resulting oxidative damage alters the biomacromolecule structure and function. DNA injury, lipid peroxidation, and protein oxidation are all examples of oxidative stress hallmarks. Oxidative stress can also initiate secondary responses such as inflammation. Shimizu *et al*. noted that oxidative stress in injured liver cells caused an overproduction of the hepatic stellate cells (HSCs) that produce collagen during hepatic fibrosis.[43]

The study of oxidative stress is traditionally carried about by studying oxidative stress biomarkers. Because direct studies of ROS is generally limited by their confinement within their environment and by their short half-life, biomarkers serve as indicators of biological pathways we wish to study. Oxidative stress biomarkers are molecules that interact with ROS and includes the gene expression of enzymes responsible for regulating ROS, such as superoxide dismutase and ferritin, or quantification of biologics, such as proteins, DNA, and lipids, oxidized by ROS.[44]

1.2.2 Nanoparticle-induced Oxidative Stress Response

Many studies, including our own, have linked TiO_2 NPs to oxidative stress.[9-10, 45-52] Toxicity resulting from oxidative stress is suggested to occur due to the combination of both the chemical reactivity of the NP surface as well as the physical and mechanical disruption of cellular processes by the NP. As suggested in Section 1.2.1, the ability for TiO_2 to generate direct and indirect cellular defense responses can contribute to overall acute toxicity when ROS is left unchecked by antioxidant activity.

1.3 Protein Corona

Upon injection into the blood stream or ingestion into the gastrointestinal tract, NPs encounter serum, the component of whole blood after the removal of red blood cells, white blood cells, and clotting factors. Through a thermodynamically driven process, serum proteins adsorb onto the surface on NPs, forming a corona.[53-57] A similar phenomenon occurs with NP inhalation with lung surfactant proteins. While not defined as serum, lung proteins can bind to the NP surface in a similar fashion as serum or plasma proteins.[58]

The protein corona serves as a mediating layer, interfacing between the cell and the NP. The corona can dictate cellular responses to the NP, triggering internalization, opsonization, and immune responses.[59-64] The adsorption process is defined by the Vroman effect, where proteins dynamically compete at the NP surface.[65] While proteins with higher mobility encounter the NP surface initially, forming a “soft” corona, a “hard” corona of higher affinity ultimately displaces these proteins.[55, 66]

A protein corona has been observed for many different NPs, including those comprised of metal, polymer, lipids, or protein,[50, 55, 57, 67-68] making it a parameter that must always be addressed when investigating NP-cell interactions.

1.3.1 Composition

The chemical forces attributed to protein adsorption are hydrophobic interactions, hydrogen bonding, electrostatic interactions, van der Waals interactions, and π-π stacking.[56] While each individual interaction is weak compared to covalent bonds, collectively these forces create a protein layer whose composition is dependent on NP identity, concentration, size, curvature, shape, surface modifications, and surface charge.[56] Specific to metal oxides, Deng *et al.* noted a NP-concentration dependent corona composition for TiO_2 and zinc oxide (ZnO) NPs, but not for silicon dioxide (SiO_2) NPs. While all three NPs possessed similar zeta potentials, corona composition varied.[68] The use of plasma as opposed to serum alone resulted also in the adsorption of clotting factor fibrinogen onto all three NP surfaces.

Serum properties also drive protein corona composition. Lesniak *et al.* found that silica NPs with a preformed corona incubated with A249 cells in the presence of serum proteins generated a different corona that that of the same NPs with a preformed corona in the presence of cells but the absence of serum proteins.[69] The biological consequences included stronger adhesion to the cell membrane and cell damage in the absence of serum proteins.

Figure 2 depicts the protein layer composition P25 TiO_2 NPs, where the hard corona comprises of higher affinity proteins while the soft corona (gray) is the remainder of serum.

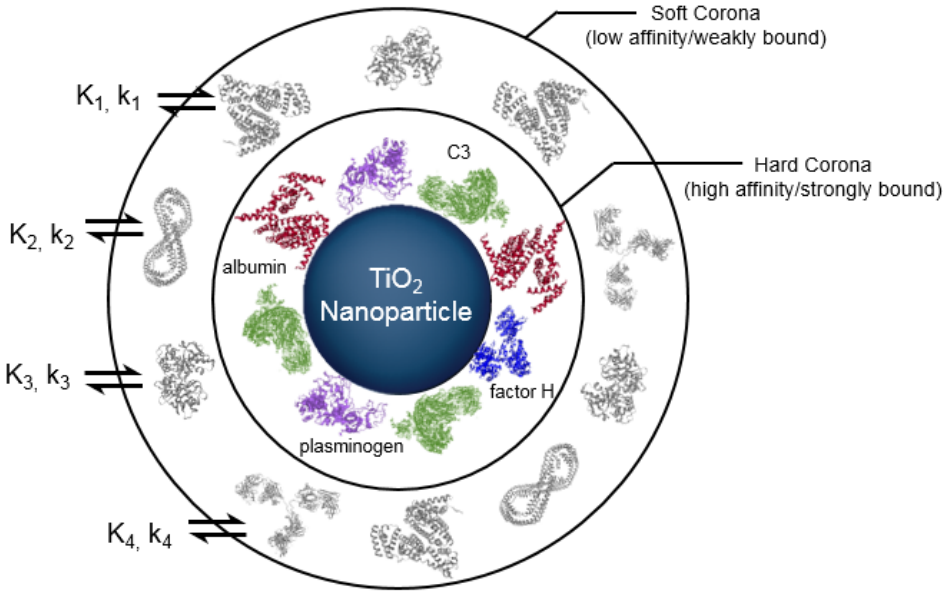

Figure 2 Schematic of the protein corona. Protein structures were obtained from the Protein Data Bank.

1.3.2 Spatial Distribution

While the composition of the protein corona has been widely investigated, the spatial distribution has not been fully elucidated. While thermodynamics drive protein adsorption, protein-protein interactions are inherent in the process. Through this, the distribution of the corona can be characterized.

Spatial mapping of the corona is still a recent endeavour, with few studies directly visualizing the protein distribution. Clemments *et al.* utilized super-resolution fluorescence microscopy and a sphere fitting model to map protein adsorption onto mesoporous silica

NPs.[70] Complete coverage was not observed, which is in agreement with protein coverage for hydrophilic surfaces. Thus, while it is inferred that the corona dictates NP-cellular interactions, a bare NP surface is also present, creating a more complex and diverse set of possible biological implications.

1.3.3 Structural and Molecular Modifications of Corona Proteins

The protein corona provides a stabilizing effect by reducing steric forces and minimizing surface energy of the NPs. Through this process, proteins can release free energy and partially denature, losing native structural properties. The partial loss of secondary structure of bovine serum albumin is documented upon adsorption on polystyrene, silver, gold, and zinc oxide NPs.[71-74] These are classic examples of NP driven molecular modifications of the protein corona. The consequences of modifications vary based on the modification and extent. Within our lab, Fleischer *et al.* observed that cationic PS NPs with a partially denatured BSA corona bound to scavenger receptors while anionic PS NPs with a native BSA corona bound to BSA receptors in BS-C-1 and CHO cells.[61]

Other modifications investigated in literature include charge-based and covalent alterations. Treuel *et al.* noted that charge modification of the albumin-based corona of quantum dots resulted in NPs more tightly bound onto the plasma membrane of Hela cells.[75] Covalent modified serum proteins also are reported to affect cell-NP interactions. A study by Morgan *et al.* conducted in the absence of NPs correlated oxidized serum proteins with an increase in disease activity in patients with systemic lupus erythematosus.[72]

These finding collectively suggest the molecular modifications of the protein corona contribute to cellular response. We discuss in Chapter 4 that in investigating covalent oxidation modifications of serum proteins, we find that oxidized protein corona leads to cellular oxidative stress.

CHAPTER 2. MATERIALS AND METHODS

2.1 Nanoparticles

2.1.1 Titanium Dioxide Nanoparticles

Titanium dioxide nanopowder (21 nm, #718467, Sigma-Aldrich, St. Louis, MO) were used for all experiments. For experiments in 25 cm^2 cell culture flasks (PCR, western blots, and PI staining), TiO_2 NPs were used at a concentration of 400 μg/mL. For experiments in 12 well plates or 24 well plates the concentration of NPs (270 and 160 μg/mL TiO_2 NPs, respectively) was scaled down based on the number of cells forming a monolayer on the surface of the culture dish to keep the ratio of NPs to cells constant. A TiO_2 NP diameter of 370 nm, based on dynamic light scattering (DLS) was used to calculate surface area. All experiments were carried out under in the absence of light.

2.1.2 Polystyrene Nanoparticles

Orange fluorescent carboxylate-modified NPs (200 nm, #F8809, Invitrogen/Thermo Fisher, Carlsbad, CA) were used for all polystyrene NP experiments. The NPs are fluorescent with an excitation wavelength of 540 and emission wavelength of 560 nm. The concentration of NPs for cellular experiments carried out in T25 flask of 20 pM was chosen to match the surface area of the TiO_2 NPs used in corresponding experiments. A polystyrene NP diameter of 200 nm, based on TEM data provided by Thermo Fisher, was used to calculate surface area. All experiments were carried out under dark light conditions.

2.2 Cell Culture

Human cervical carcinoma cells (HeLa, CCL-2 ATCC) were used for most experiments. Protein expression (western blotting) experiments were reproduced in African green monkey kidney epithelial cells (B-SC-1, ATCC) and lung epithelial carcinoma cells (A549, CCL-185, ATCC). All cell lines were maintained in a 5% carbon dioxide environment at 37^{o}C in Minimum Essential Medium, (MEM, Invitrogen, 61100) supplemented with 10% fetal bovine serum (FBS, Invitrogen, 10437028). For all NP-cell experiments, the NP concentration was adjusted for number of cells grown per given surface area. A hemocytometer was used to count cells after staining with trypan blue.

For gene and protein expression studies, cells were grown in 25 cm^2 culture flasks. For cell health assays, cell were grown in either 12 or 24 well plates. For fluorescence and brightfield microscope imaging, cells were maintained in 3.5 cm optical dishes (#P35G-1.5-14-C, MatTek, Ashland, MA).

2.3 Nanoparticle Characterization

2.3.1 Dynamic Light Scattering and Zeta Potential

The hydrodynamic diameter and zeta potential of TiO_2 and PS NPs were measured with a Malvern Zetasizer (Nano-ZS, Malvern Instruments, Worcestershire, England). Hydrodynamic diameter measurements were acquired from 13 runs per measurement. Zeta potential measurements was measured from 30 runs and calculated using the Smoluchowski approximation. Each sample was measured in triplicate.

For experiments conducted for NPs with FBS, TiO_2 NPs were incubated in MEM + 10% FBS for 30 at room temperature to allow a protein corona to form on the surface of the TiO_2 NPs. Excess FBS was removed by repeated centrifugation and resuspension in water (8,000 rcf, 15 min, x3). The remaining TiO_2-protein pellet was resuspended in nanopure water (18 MΩ) and sonicated for 10 minutes prior to measurements.

2.3.2 Transmission Electron Microscopy (TEM)

The size distribution of P25 TiO_2 NPs was determined through TEM. Imaging (JEOL 100 CX II) was carried out at the Center for Nanostructure Characterization at Georgia Tech. Images were obtained at 100 kV with 200k× magnification. A mean diameter of TiO_2 NPs and their aggregates was determined by measuring the greatest distance between two boundaries of 100 NPs or 10 distinct aggregates using ImageJ software.

2.3.3 Scanning Electron Microscopy (SEM)

Food grade TiO_2 NPs imaging was performed at the Center for Nanostructure Characterization at Georgia Tech using a SU8200 Ultra-high resolution scanning eletron microscopy (Hitachi, Krefeld, Germany) at 1 kV with 3500x magnification. A mean diameter of TiO_2 NPs and their aggregates was determined by measuring the greatest distance between two boundaries of 35 distinct NPs or aggregates using ImageJ software.

2.3.4 BET Analysis

BET analysis was carried out using the ASAP 2020 Plus Physisoption (Micromeritics, Norcross, GA). For sample preparation, P25 TiO_2 NPs (1.2 grams) were

dried under high vacuum at 110 ^{o}C overnight. Analysis was performed using the N_2 adsorption-desorption isotherms. Chamber equilibration and degassing was achieved after 35 s prior to N_2 addition. Relative and absolute pressure readings were taken at 77 K over 25 minutes and plotted against quantity adsorbed.

2.4 Cell Health Assays

For all cell health assays, experiments were carried out on three distinct samples and significance was determined by a two-tailed student's t-test.

2.4.1 MTT Assay

Mitochondrial activity was measured using the Vybrant MTT (3-(4,5-dimethylthiazol-2-yl)-2,5-diphenyltetrazolium bromide) Cell Proliferation Assay Kit (#V13154, Life Technologies). Cells maintained for MTT assay experiments were cultured in 12-well (#62406-165, VWR). Absorbance values were measured at 540 nm with a SpectraMax M2e plate reader (Molecular Devices, Sunnyvale, CA) and normalized to cells without NP treatment (control).

2.4.2 Lactate Dehydrogenase Assay

A Pierce LDH (lactate dehydrogenase) Cytotoxicity Assay Kit (#88953, Thermo Fisher) was used for cells cultured in 24-well plates (#62406-159, VWR). LDH activity was characterized by measuring absorbance at 490 nm and subtracting background absorbance at 680 nm. Values were quantified with a SpectraMax M2e plate reader (Molecular Devices, Sunnyvale, CA).

2.4.3 Propidium Iodide Staining

Propidium iodide (PI) staining (#P1304MP, Invitrogen) was carried out for cells cultured in 25 cm^2 flasks. Prior to PI addition, cells were removed from the flask surface by a 10 minute incubation with Accutase (#A6964, Sigma-Aldrich). The resulting cell suspension was distributed into 1 mL aliquots and pelleted (5000 rcf, 7 minutes, room temperature), followed by resuspension in PI solution (2 µg PI/mL PBS) for 15 minutes. Cells were filtered with a cell strainer (#352340, Falcon) into 5 mL round-bottom tubes (#352058, Falcon) for flow cytometry (Accuri C6, Becton Dickinson). PI fluorescence was detected using the FL-2 filter.

2.5 Reverse Transcriptase Polymerase Chain Reaction (RT-PCR)

HeLa cells at ~60% confluency were incubated with NP treatment noted in the text. Cells were lysed after 24 hours and mRNA was extracted using an RNeasy Mini Kit (#74104, Qiagen, Hilden, Germany) and QIAshredder (#79656, Qiagen). RNA was further purified using the RNase- Free DNase Set (#79254, Qiagen) to remove genomic DNA. The sample volume was adjusted in subsequent experiments to ensure equal amounts of RNA were used for cDNA conversion. Following RNA extraction, cDNA synthesis was performed using a RT^2 First Strand Kit (#330401, Qiagen). Real-time PCR was performed using a RT^2 Profiler PCR Array (Human Oxidative Stress Plus, PAHS-065YC, #330231, Qiagen) in combination with RT2 SYBR Green ROX qPCR Mastermix (#330522, Qiagen). A StepOnePlus Real-Time PCR System (Applied Biosystems) was used as the real time cycler. The first cycle was 10 min at 95 °C, and the 40 subsequent cycles were at 95 °C for 15 s and 60 °C for 1 min. Data analysis was performed using the GeneGlobe

Data Analysis Center (Qiagen) by selecting a baseline threshold cycle (C_T) of 35 and normalizing against housekeeping genes (beta actin (ACTB), beta-2-macroglobulin (B2M), glyceraldehyde-3-phosphate dehydrogenase (GAPDH), hypoxanthine phosphoribosyltransferase 1 (HPRT1), and large ribosomal protein P0 (RPLP0)). The average CT across housekeeping genes was subtracted from the C_T for the gene of interest for each sample to normalize for cDNA content (normalized ΔC_T). Normalized ΔC_T values were averaged across samples before calculating $2^{-\Delta C_T}$ to provide relative expression levels, as previously described. All arrays were performed with triplicate sets of RNA isolation for statistical analysis.

2.6 Western Blotting

After treatment noted in text for 24 hours, cells were lysed with a 1% Triton X-100 lysis buffer with protease inhibitor (#78441, Halt, Pierce, Rockford, IL) for 30 min at 4°C. Lysate was separated with centrifugation (14,000 rcf, 20 min, 4°C). Protein concentration was determined using a BCA assay (#23227, Thermo Fisher). Lysate (20 µg) was diluted 1:1 in Laemmli loading buffer (#BP-110R, Boston BioProducts) and run on a tris-glycine SDS gel (#456-1094, Bio-Rad, Hercules, CA) at 230 V for 35 min and transferred to a PVDF membrane (100 V, 45 min). The membrane was blocked (#MB-070 Rockland Immunochemicals) for 1 hr at 4°C. Primary antibodies were added and incubated overnight at 4 °C in blocking buffer and the membrane was washed with TBS-Tween (3 times, 10 min). Peroxiredoxin 1 (#ab41906, Abcam) and peroxiredoxin 4 (ab59542, Abcam) were diluted at 1:5,000 and actin (#ab3280, Abcam) at 1:10,000. Secondary antibodies were incubated for 1 hour at 4 °C in blocking buffer (1:10,000, #926-68021 and #926-32212,

LI-COR). The membrane was washed twice with TBS-Tween for 10 minutes and then once with TBS. Blots were imaged with an Odyssey Imager (LI-COR) and quantified by densitometry (ImageJ).

2.7 Proteomics

TiO_2 NPs (400 μg/mL) and polystyrene NPs (151 pM) were incubated in a 10% v/v solution of FBS for 30 min at room temperature. Unbound and weakly bound proteins were removed from the NPs by centrifugation and resuspension in water (8000 rcf, 15 min, 4 °C, 4×). These washed NPs, with only tightly bound proteins remaining on the surface, were loaded onto a gel, as previously described for the Western blots. Running the protein−NP complexes on a gel separated the protein from the NPs and the SDS loading buffer prior to mass spectrometry. The gel was run (130 V) for 8 min. The gel was stained with SimplyBlue SafeStain (#LC6060, Thermo Fisher) for 1 h, and the entire, unresolved band was submitted for proteomics (Bioproximity, Chantilly, VA). Protein abundance was determined by spectral count of each protein family.

2.8 Reactive Oxygen Species Confirmation

2.8.1 General ROS Probe: H_2DCFDA

2',7'-dichlorodihydrofluorescein diacetate, or H_2DCFDA (#C6827, Invitrogen/Thermo Fisher) can be oxidized to highly fluorescent 2',7'-dichlorofluorescein (H_2DCF) by ROS. H_2DCFDA was first deacetylated to produce non-fluorescent H_2DCF for use in cell-free assays. Specifically, 50 μg of H_2DCFDA was dissolved in 50 μL of DMSO. 50 μL of

methanol was added to the solution followed by 25 μL of 2 M KOH. This solution was vortexed and then incubated at 37 °C for one hour. It was neutralized to pH 7 with HCl prior to use. After a 1 h room temperature incubation with H_2DCF (5 μM in phosphate-buffered saline (PBS)) TiO_2 NPs (400 μg/mL) were removed (8000 rcf, 15 min, ×3) from the solution prior to measurement (Excite: 488 nm; Emit: 523 nm, RF-5301PZ fluorometer, Shimadzu).

2.8.2 Hydroxyl Radical Probe: Terephthalic Acid

Terephthalic acid (TA, 2 mM, #100210, Sigma-Aldrich) was added to an aqueous suspension of TiO_2 NPs (2 mg/mL, 1 hr, room temperature). As with the H_2DCFDA assay, TiO_2 NPs were removed (8000 rcf, 15 min, x3) from the solution prior to measurement. Fluorescence intensity of the hydroxyl radical-oxidized product was measured at 434 nm (Excite: 312 nm).

2.8.3 Superoxide Probe: Nitroblue Tetrazolium

Nitroblue Tetrazolium (NBT, 2 mM, #298839, Sigma-Aldrich) was incubated with TiO_2 NPs (2 mg/mL, 1 hr, room temperature), which were removed (8000 rcf, 15 min, x3) prior to measurement. Superoxide-mediated oxidation of NBT to form insoluble formazan was characterized by a decrease in the NBT absorption at 259 nm (DU 800 Spectrophotometer, Beckman Coulter).

2.8.4 Radical Trapping and Electron Paramagnetic Resonance

Aqueous suspensions of TiO_2 NPs (10 mg/mL) and 5,5-dimethyl-1-pyrroline-N-oxide (DMPO, 0.02 M, #D5766, Sigma-Aldrich) were drawn into quartz EPR capillaries

(#Q-.4X.55, Wilmad-LabGlass) and then inserted into quartz EPR tubes (Wilmad-LabGlass). Spectra were recorded on an EMX EPR 100 X-band spectrometer (Bruker).

2.8.5 Methylene Blue

P25 TiO_2 NPs at various concentrations (0.01-15 mg/mL) were incubated with 6 μM MB in Millipore water under constant stirring. For dark experiments, the mixture was covered in foil. For light conditions, the mixture was continually irradiated using a hand held UV lamp (Entela UL3101, longwave). After incubation, the NPs were removed through a series of centrifugation steps detailed in Section 2.9.1 and Section 4.2.1 (Figure 13), followed by UV-Vis measurement. MB concentration was measured from 0-135 minutes at 15 minute increments.

2.9 NP-Mediated Oxidation and Oxidation Assays

2.9.1 TiO_2 NP-Mediated Oxidation of Serum Proteins

TiO_2 NPs (P25, 400 μg/mL) were incubated with FBS (10%) in MEM, identical to cell culture conditions, for 30 min in the dark with constant rocking. This mixture was centrifuged (8000 rcf, 15 min, ×3) to remove the TiO_2 NPs (Figure 13a and 13b). We used DNPH to confirm that this 30 min exposure to TiO_2 NPs oxidized the serum proteins. Polystyrene NPs (20 pM) were added to the supernatant of the oxidized proteins allowing a corona to form on the surface of the polystyrene NPs. The protein–polystyrene NP mixture was then transferred to cell culture flasks prior to PCR and western blotting experiments.

2.9.2 Protein Oxidation

A dinitrophenylhydrazine assay was used to determine serum protein oxidation. TiO_2 NPs (400 μg/mL) or polystyrene NPs (20 pM) were incubated with 10% FBS (3 mg/mL) in the dark with constant vortexing. After 30 min, the NPs were removed from the mixture by centrifugation (8000 rcf, 15 min). The protein solution was then incubated with DNPH (10 mM, TCI America) in 6 M HCl for 15 min, allowing any oxidized proteins to react with the DNPH. To remove unbound DNPH prior to measurement, proteins were precipitated with 50 w/v trichloroacetic acid (Sigma-Aldrich) followed by centrifugation (14,000 rcf, 5 min) and washed in ethanol/ethyl acetate (x3). The pelleted proteins were resuspended in 6M guanidine hydrochloric acid. The concentration of bound DNPH (Abs: 370-385 nm) was measured with UV-Vis spectroscopy (DU 800, Beckman Coulter) and normalized against the concentration of protein (Abs: 280 nm).

2.9.3 Malondialdehyde Assay

A malondialdehyde (MDA) lipid peroxidation assay was carried out for cells grown in 25 cm^2 flasks. For the assay, the cells were not washed prior to conducting the assay to ensure both cells adhered onto the flask and detached were accounted for. A cell scraper was used to removed cells from the flask. The assay was carried out according to the manufacturer's protocol (#K739-100, BioVision). Cells were homogenized using a Dounce homogenizer. Following incubation with thiobarbituric acid (1 hr, 95 °C), the MDA-TBA adduct absorbance was measured at 532 nm with a spectrophotometer (DU 800, Beckman Coulter). Protein concentration was measured at 280 nm.

2.10 TiO_2 Surface Modifications

2.10.1 Surface Passivation

5 g P25 TiO_2 NPs were added to 40 mL deionized water. The mixture was sonicated for 3 minutes. The mixture (pH = 3.3) was heated to about 95° C followed by addition of 0.08 g citric acid 50% solution, lowering the pH to 2.7. The pH was adjusted with 1 M NaOH to a range of 9-9.5. The neutral pH was maintained by adding 1 M HCl while adding 1.07 g sodium silicate drop wise over 14 minutes. The mixture was heated at 95° C for one hour at pH 9.5 with stirring. The pH was lowered to 7 by adding 1 M HCl while 0.9 g sodium aluminate was added drop wise over 10 minutes. The heat was turned off and the mixture was stirred for 20 minutes at pH of 7. The temperature after 20 minutes was 75.5° C. The pH was adjusted to 6.0 ± 0.3 with HCl and stirred for 5 minutes. The final mixture was filtered, washed with deionized water. The mixture was dried for about 30 minutes to form a cake. Ethanol was added to cover the cake for about 15 minutes, then vacuum dried for 30 minutes. The cake was dried in a 125° C. oven on a tray overnight.

2.10.2 Plasma Treatment

P25 TiO_2 NPs were plasma cleaned for 10 min with a plasma cleaner (PDC-32G, Harrick Plasma, Ithaca, NY).

2.11 Microscopy

2.11.1 Conventional Microscopy

FBS used for imaging experiments was labelled with AlexaFluor647 (#A37566, ThermoFisher) and purified according to the manufacturer's instructions. Final labelled FBS (AF647-FBS) concentrations were determined by UV-Vis spectroscopy (abs=280 nm). TiO_2 NPs were incubated with AF647-FBS at ratio of 1 μg AF647-FBS: 1 μg TiO_2

NPs for 30 at room temperature to allow a protein corona to form on the surface. Excess FBS was removed by repeated centrifugation and resuspension in water (8,000 rcf, 15 min, x3). The final TiO_2 NP concentration after this washing process was determined by UV-visible spectroscopy (abs=330 nm). HeLa cells were then incubated with the AF647-FBS-TiO_2 NP complexes (124 μg/mL).

Epifluorescence microscopy was performed with an inverted microscope (Olympus IX71, Tokyo, Japan) using a 60x, 1.20 N.A. objective (Olympus). A xenon lamp was used as a light source and images were acquired (5 ms) with a Cy5 filter cube and EMCCD camera (#DU-897, Andor, South Windsor, CT). Brightfield microscopy using the same microscope system was used to image the TiO_2 NPs. Image analysis was carried out in ImageJ. Brightness and contrast settings for all epifluorescence images were set equal. Mean intensities were measured for 30 NPs, or NP aggregates, from 3 separate images from 2 distinct experiments for each experimental condition.

2.11.2 Single Molecule Localization Microscopy

Bovine serum albumin (BSA, #12657, Merck, Darmstadt, Germany) was labelled with AlexaFluor 647 (#A37566, ThermoFisher) and purified according to the manufacturer's instructions. TiO_2 NPs were incubated with labelled BSA (AF647-BSA) at mass ratios of 0.01-10 mg of BSA/mg TiO_2, as noted in the text, for 30 minutes with constant vortexing in the dark. Following five wash steps (14,000 rcf, 10 minutes, 5 times) to remove residual AF647-BSA, the AF647-BSA-TiO_2 NPs were transferred to a glass coverslip for imaging. An imaging buffer of 5% glucose, 1% glucose oxidase/catalase, and 10% ethanolamine was added to samples prior to experiments.

The experimental setup used for the super-resolution stochastic optical reconstruction microscopy (STORM, 100x objective, 1.49 NA, Nikon Instruments) experiments has been described previously. In brief, stochastic imaging used activation at 405 nm followed by three collection frames at 647 nm excitation. Emission from the AF647-BSA was collected by an EMCCD camera with an exposure time of 20 ms per frame. The resulting direct STORM (dSTORM) images were reconstructed using custom software (Insight3) provided by Bo Huang, University of California, San Francisco.

CHAPTER 3. TITANIUM DIOXIDE NANOPARTICLES INDUCE CELLULAR OXIDATIVE STRESS

3.1 Introduction

The high level of use of titanium dioxide nanoparticles (TiO_2 NPs) as pigments and photocatalysts has been accompanied by extensive TiO_2 NP toxicity studies exploring a range of exposure routes (dermal, inhalation, intravenous, oral).[46, 48-49, 51, 54, 76-77] Of specific interest is the relationship between TiO_2 NP exposure and oxidative stress. On the cellular level, cytotoxicity and oxidative stress results range considerably depending on cell type, NP concentration, diameter, crystal phase (anatase, rutile, or mixed), and method of measurement.[9-10, 23, 45, 47, 78-82] Ultimately lab-to-lab variations in experimental parameters makes it difficult to compare results and draw firm conclusions. For example, studies of TiO_2 NPs with colon cancer cells (Caco-2) showed an increase in intracellular reactive oxygen species (ROS) based on a ROS-sensitive fluorescent dye, but no cytotoxicity.[23] Studies in the same cell line using protein markers of oxidative stress (glutathione, heme oxygenase-1, gamma-glutanyl cysteine synthetase), instead of bulk ROS measurements, did observe cytotoxicity, but without any detected oxidative stress.[78] Studies in human bronchial cells showed that 200 nm rutile TiO_2 NPs led to oxidative stress measured by DNA damage, micronuclei formation, and lipid peroxidation, but that 200 nm anatase TiO_2 NPs did not. Mixed anatase and rutile TiO_2 NPs were the most damaging.[45] In comparison, experiments with 100 nm anatase TiO_2 NPs in mouse fibroblast cells showed oxidative stress-mediated cytotoxicity and suggested rutile NPs were less toxic.[47] Other studies observed no oxidative stress in cells (mouse macrophages and human bronchial cells) following exposure to TiO_2 NPs (11 nm primary particles, ~600 nm diameter in water, 80% anatase/20% rutile).[9-10]

Our goal was to carry out a quantitative, mechanistic study of TiO_2 NPs and oxidative stress using the most common commercially-available TiO_2 NPs (P25, Aeroixde, Degussa) with a focus on the relationship between the NP-cell interface and cellular outcomes. NP concentrations were selected to maintain cell health to mimic long-term exposure under non-cytotoxic conditions. We then used PCR arrays to screen 84 oxidative stress-related genes following the incubation of human cells (HeLa) with TiO_2 NPs for 24 hrs. The array showed that expression of four members of the peroxiredoxin family of anti-oxidant enzymes were altered. These enzymes, responsible for the degradation of peroxides, are essential to the oxidative stress response of cells.[35, 83-86] Changes in peroxiredoxin gene expression of ~50%, increase and decrease, were observed in comparison to control cells not exposed to TiO_2 NPs. The changes observed for the peroxiredoxins were unique to TiO_2 NPs: experiments with polystyrene NPs showed no change in peroxiredoxin expression. In addition, this oxidative stress response was specific to TiO_2 NPs coated with a "corona" of adsorbed serum proteins. "Bare" TiO_2 NPs lacking this protein layer were cytotoxic at the same concentrations. Peroxiredoxin expression was also examined as a function of cell type and passage number. Overall, our experiments show that protein-TiO_2 NP complexes lead to a unique oxidative stress response in both human cancer cells (HeLa) and monkey kidney cells (BS-C-1). Because the isoforms of peroxiredoxins vary in their cellular localization, our results suggest subcellular differences in TiO_2 NP-induced oxidative stress. Moving forward, these results point to the importance of considering cellular responses to NPs at low concentrations that do not lead to cytotoxicity, but may cause more subtle cellular changes.

3.2 Results and Discussion

3.2.1 Titanium Dioxide Nanoparticle Characterization

The TiO_2 NPs used in these experiments have a primary particle size of ~21 nm determined by TEM provided by the manufacturer (Sigma) and consist of a mixture of 80% anatase and 20% rutile crystal phases. TEM carried out shows that the individual particles are fused into larger aggregates or agglomerates (mean diameter = 290 nm, n = 10). Dynamic light scattering (DLS) was used to characterize the size distribution and effective surface charge of these TiO_2 NP aggregates with and without serum proteins. Although DLS is not ideal for these nonspherical particles, it does provide a relative measure and a point of comparison to published DLS values. The addition of serum proteins reduced the diameter of the TiO_2 NPs (mean diameter = 367 ± 63 nm, PDI = 0.36) compared with TiO_2 NPs in the absence of proteins (mean diameter = 567 ± 38 nm, PDI = 0.17), suggesting a protein-mediated reduction of NP aggregation (Figure 3b). Similar size distributions in cell culture medium have been previously observed. The zeta potential of the bare TiO_2 NPs redispersed in water is −22 ± 0.5 mV, similar to the zeta potential of TiO_2 NPs incubated with FBS proteins (−24 ± 2 mV, Figure 3c). For comparison, the zeta potential of FBS (1%) in water is −18 ± 2 mV.

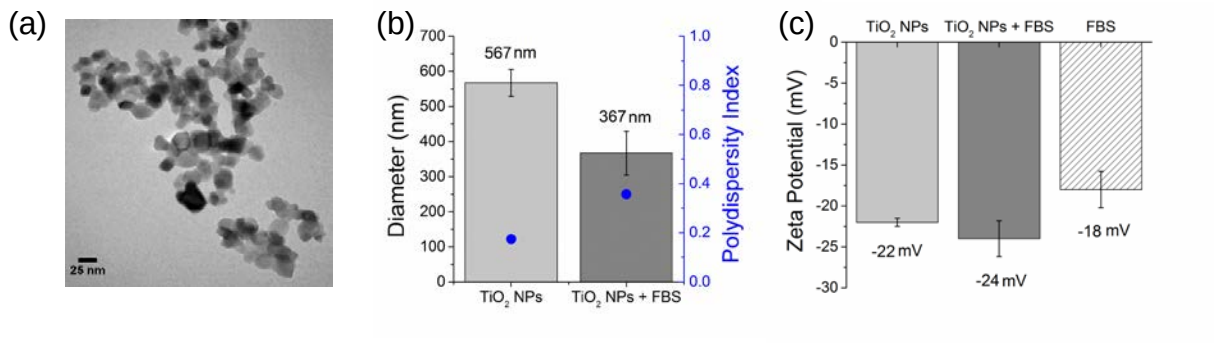

Figure 3 Characterization of the TiO_2 NPs used in these experiments. (a) TEM shows the aggregated structure and heterogeneity of the TiO_2 NPs. (b) DLS was used to measure the diameter of bare TiO_2 NPs (400 µg/mL, light grey) and TiO_2 NPs coated with FBS (dark gray). The polydispersity index (PDI) is indicated in blue. (c) Zeta potential of the bare TiO_2 NPs (400 µg/mL, light grey), TiO_2 NPs coated with FBS (dark grey), and FBS (1% in water, stripes). Measurements are the average of 3 samples and error bars represent ± standard deviation.

3.2.2 Surface analysis

BET (Brunauer, Emmett and Teller) analysis correlates the concentration of P25 TiO_2 NPs expressed in mass to specific surface area by plotting the isotherm for the adsorption of nitrogen (Figure 4).

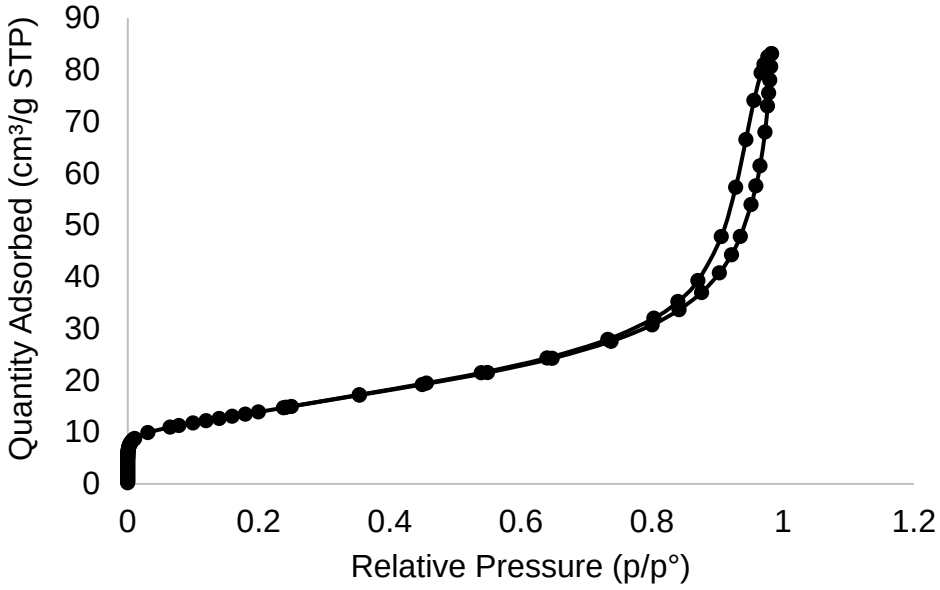

Figure 4 Adsorption isotherm of P25 TiO_2 NPs.

The BET surface area for P25 TiO_2 NPs was found to be 49.7 m^2/g. This is in agreement with previous findings.[87-88] It is important to note that this specific surface area correlates with NPs that have minimum aggregation. However, we will make the assumption that surface area scales with mass. The reproducibility of the NP experiments detailed in Chapter 2 (performed in triplicate) suggests that this is a valid assumption.

In addition to BET, through TEM, individual NPs were measured to have a mean and median of 24 nm (Figure 3a, 5a), in agreement with the manufacturer (21 nm). A representative image (Figure 3a) shows individual particles form aggregates ranging between 126-500 nm with a mean of 290 nm and median of 279 nm (Figure 5c).

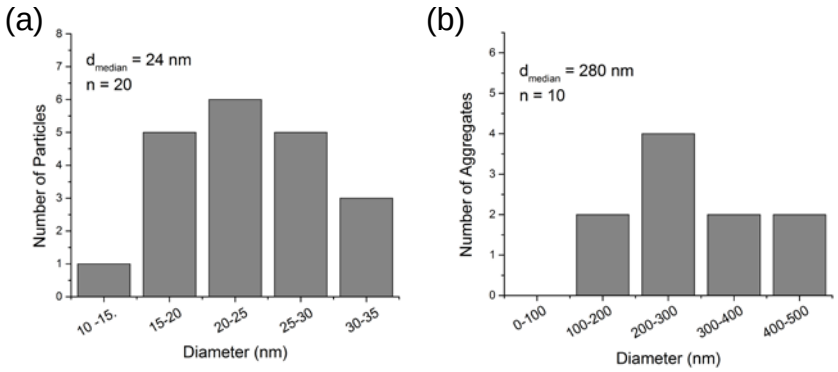

Figure 5 P25 NP size distribution. (a) Distribution function of twenty individual NPs analyzed by ImageJ software. (b) Distribution function of ten aggregates composed of individual NPs analyzed by ImageJ software.

Size analysis of individual food grade TiO_2 NPs, denoted as E171 NPs, was also performed (Figure 6). These particles were found to also generate ROS in the dark (Section 4.2.1). Through SEM analysis, the E171 NPs are shown to have a more varied diameter than P25 TiO_2 NPs (mean diameter = 110 nm, median = 99 nm, n = 50). Also, their mean aggregate size range included micron size agglomerates (mean diameter = 880 nm, median = 588, n = 50). Because our NP studies are in cellular aqueous conditions, there are

limitations in size studies using SEM and TEM of dry particles. To observe a rough particle size in an aqueous environment, DLS was used. A hydrodynamic diameter of 567 ± 38 nm with PDI = 0.17 was noted for P25 TiO_2 NPs and 210 ± 2 nm diameter with PDI = 0.37 for E171 TiO_2 NPs as noted in Sections 3.2.1 and 4.2.1.

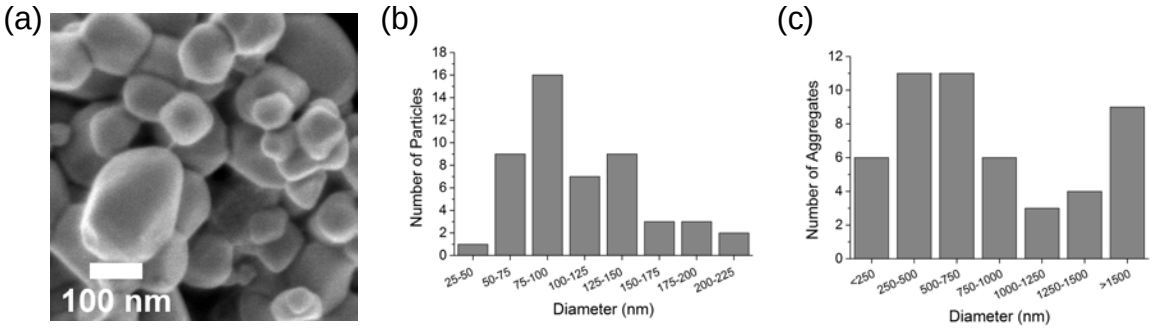

Figure 6 E171 NP size distribution. (a) Representative SEM image of TiO_2 NPs replotted from Figure 1. (b) Distribution function of 50 individual NPs analyzed by ImageJ software. (c) Distribution function of 50 aggregates composed of individual NPs analyzed by ImageJ software.

3.2.3 Nanoparticle-induced Cytotoxicity

TiO_2 NPs can damage and kill cells,[45, 47, 78-79, 82] especially at high concentrations.[78-79, 82] Our goal was to probe TiO_2 NP-cell interactions at sub-cytotoxic levels, looking for more subtle changes that can occur with apparently healthy cells. Cell health was first tested using an MTT assay to measure the activity of mitochondrial enzymes (Figure 7a). This assay confirmed that the cells (human cervical cancer, HeLa) used in the subsequent experiments were healthy, at least by this measure, following incubation with TiO_2 NPs. Based on the MTT assay, a 100x greater concentration of TiO_2 NPs was required to cause a significant decrease (68.2 ± 10.8%, compared to 100% for the control) in cell health.

The MTT assay of mitochondrial enzyme activity is generally used as a reporter of overall cell health. As additional measures of cell health, lactate dehydrogenase (LDH) and propidium iodide (PI) assays were used to test for possible membrane permeabilization. The LDH assay (Figure 7b), which measures the release of an intracellular enzyme through a damaged plasma membrane, showed minimal, non-significant, LDH release (2.6 ± 0.4%) compared to a control in the absence of TiO_2 NPs (1.9 ± 0.5%). Complete release of LDH, accomplished with a lysis buffer, was normalized to 100%. The PI assay measures the opposite effect; entry of the extracellular PI dye into the cell across a damaged plasma membrane (Figure 7c). A small (9.7 ± 1.1%), but significant, increase in PI internalization was observed for TiO_2 NP-treated cells compared to cells in the absence of TiO_2 NPs (2.5 ± 0.4%). However, this small value, in combination with the MTT and LDH assays, was not expected to cause a difference in cell function.

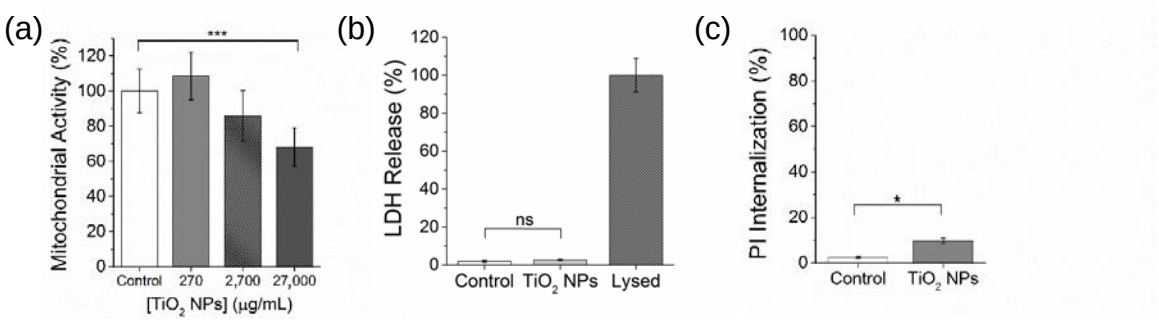

Figure 7 Cytotoxicity assays. (a) A MTT assay of mitochondrial enzyme activity was used to ensure that the concentration of TiO_2 NPs used in subsequent experiments (270 µg/mL, 12 well plate, 24 hr incubation) did not lead to decreased cell health. Measurements are the average of three wells and error bars represent ± standard deviation, ***p<0.001. There was no significant difference between the lower TiO_2 NP concentrations (270 µg/mL and 2,700 µg/mL) and the control in the absence of TiO_2 NPs. (b) A LDH assay was used to measure possible LDH release from HeLa cells in response to incubation with TiO_2 NPs (160 µg/mL, 24 well plate, 24 hrs). Complete release of LDH due to permeabilization of the membrane (lysed, dark grey) was used for normalization. Measurements are the average of three wells ± standard deviation, ns=not significant. (c) PI internalization was also used to measure membrane permeabilization of HeLa cells following incubation with TiO_2 NPs (400 µg/mL, 25 cm^2 flask, 24 hrs). Measurements are the average of three separate flasks ± standard deviation, *p<0.05.

3.2.4 Oxidative Stress-related Genes are Altered by TiO_2 NPs

To examine the cellular oxidative stress response to TiO_2 NPs, we incubated HeLa cells with TiO_2 NPs (400 µg/mL) for 24 hours. We then used a PCR array (Human Oxidative Stress Plus, Qiagen) to screen 84 different oxidative stress-related genes for changes in transcriptional response to TiO_2 NP incubation. Results from the PCR array showed that the expression of 6 genes was altered, both up- and down-regulated, in response to the TiO_2 NPs (Figure 8a). Changes in gene expression were considered significant for p-values < 0.05 for data obtained from 3 distinct experiments. Strikingly, four genes were members of the peroxiredoxin (PRDX) family of anti-oxidant enzymes. These enzymes, responsible for the degradation of peroxides, are essential to the oxidative

stress response of cells.[35, 83-86] Changes, up or down, of ~50% were observed in comparison to control cells that were not incubated with TiO_2 NPs. PCR data was validated with a western blot for peroxiredoxin 1, which showed a similar translational increase at the protein level (Figure 8b).

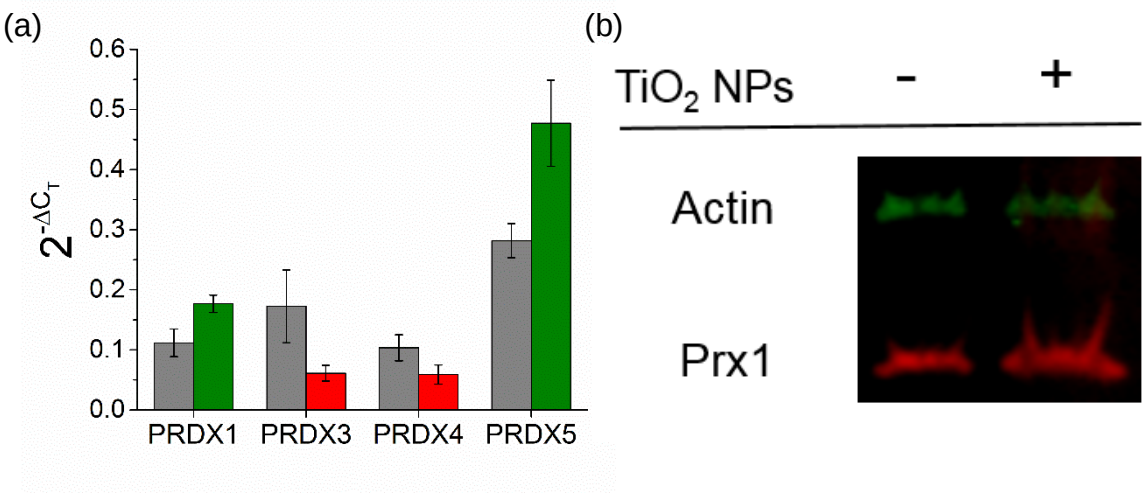

Figure 8 Changes in expression of peroxiredoxin (PRDX) genes, measured with RT-PCR, in response to incubation of HeLa cells with TiO_2 NPs (400 µg/mL) for 24 hrs. Green bars show up-regulation, down-regulation is shown in red. $p<0.05$ compared to control (gray). (b) A western blot of peroxiredoxin 1 (Prx1, red) from HeLa cell lysate was used to complement the PCR array data. Actin (green) was used as a housekeeping control. Experiments were performed in triplicate using 3 separate flasks of cells. Densitometry (ImageJ) was used to quantify the bands visible in the western blot. These experiments show an increase of 143% (p-value<0.05), in agreement with the PCR array (1.60 ± 0.42 fold).

The PCR array also included primers for PRDX2 and PRDX6, for which no change in expression was observed. In addition to the peroxiredoxins, sequestosome 1 and ferritin showed up-regulation. These proteins will be examined in future experiments.

Cellular oxidative stress, including the production of reactive oxygen species (ROS) and changes in gene expression, has been observed in previous TiO_2 NP

experiments.[23, 46, 54, 80, 89] Most relevant to this work are previous experiments using human skin cells (HaCaT) that showed small (1.1 and 1.2 fold), but significant, increases in PRDX1 and PRDX2 expression after a 6 h of incubation with TiO_2 NPs (8 μg/mL, 125 nm diameter).[81]

To determine if the changes in peroxiredoxin expression were specific to TiO_2 NPs, PCR and western blotting experiments were repeated with 200 nm carboxylate-modified polystyrene NPs. These NPs were chosen for their negative zeta potential (-31 mV ± 5 mV) and similar diameter (275 nm ± 11 nm, in water) to the TiO_2 NPs. The concentration (20 pM) was chosen to match the total polystyrene NP surface area to that of the TiO_2 NPs. After a 24 hr incubation of HeLa cells with the polystyrene NPs, PCR arrays showed no change in any of the peroxiredoxins (Figure 9b). Similarly, western blots showed no change in peroxiredoxin 1 expression (Figure 9c). These experiments show that the changes in the peroxiredoxins are specific to TiO_2 NPs, rather than a generic NP-cell interaction.

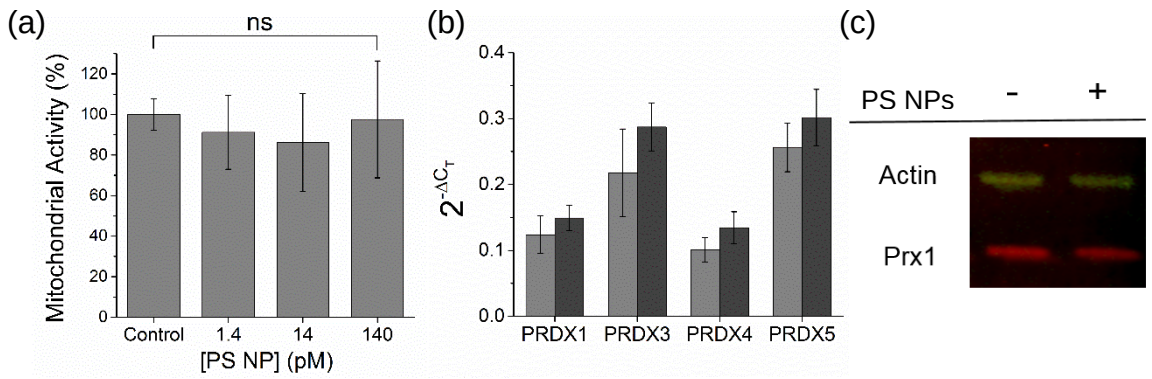

Figure 9 Polystyrene nanoparticles (PS NPs) do not lead to changes in peroxiredoxin expression in HeLa cells. (a) The concentration of polystyrene NPs (14 pM, 12 well plate) was chosen to match the surface area of the TiO_2 NPs assuming an average TiO_2 NP diameter of 370 nm. An MTT assay shows no significant change in cell health even upon addition of a 10x greater polystyrene NP concentration. Measurements are the average of three samples and error bars represent ± standard deviation. (b) A PCR array was used to measure peroxiredoxin expression following treatment (24 hrs, 20 pM, 25 cm^2 flask) with polystyrene NPs (dark grey). No significant changes in expression were detected in comparison to an untreated control (light grey). Experiments were carried out in triplicate. (c) Peroxiredoxin 1 expression (Prx1, red) was confirmed with a western blot. Actin (green) was used as a housekeeping control. Western blots were carried out in triplicate, a representative blot is shown.

3.2.5 Corona Proteins Mediate the NP-Cell Interaction

NPs generally interact with cells through a layer of proteins adsorbed on the NP surface, referred to as the protein"corona".[55, 66, 90-93] For the TiO_2 NPs, the importance of the protein corona can be evaluated by incubating HeLa cells with TiO_2 NPs (270 μg/mL, 12-well plate, 24 h) in the absence of serum proteins. An MTT assay was used to ensure that the lack of serum proteins, a nutrient source for the cells, did not decrease the viability of the cells over a 24 h period (Figure 10a). Incubation with bare TiO_2 NPs led to high levels (56.9 ± 13.2% viability) of cell death, determined by MTT assay (Figure 10b), which was also visible by eye in the cell culture flasks. In comparison, the same TiO_2 NP treatment in the presence of serum proteins led to no significant change in cell health

(Figure 7a). Because of the high level of cell death, bare TiO_2 NPs in the absence of serum proteins were not screened for an oxidative stress response.

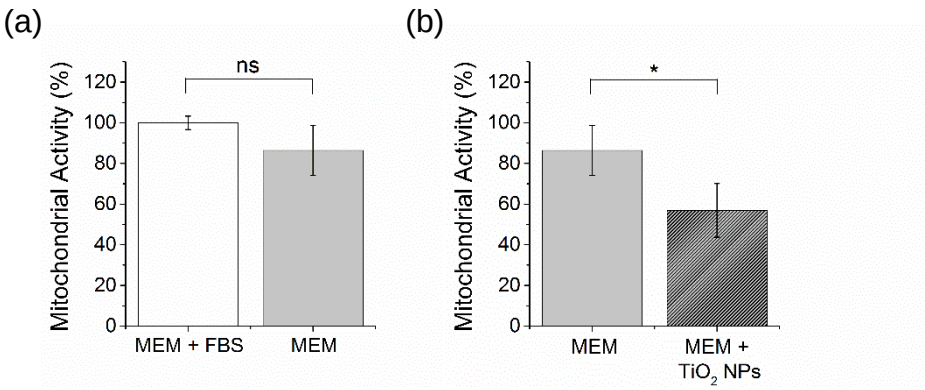

Figure 10 Bare TiO_2 NPs lead to high levels of cell death. (a) An MTT assay was used to measure the health of HeLa cells cultured in only MEM (grey) rather than MEM supplemented with 10% FBS (white) for 24 hours. Measurements are the average of three wells and error bars represent ± standard deviation, ns=not significant. (b) Incubating cells with bare TiO_2 NPs (270 µg/mL, 12 well plate, 24 hr incubation) led to a significant decrease in cell health (56.9 ± 13.2% viability). Values are normalized to cells grown in MEM supplemented with 10% FBS. Measurements are the average of three wells and error bars represent ± standard deviation, *p<0.05.

The high level of TiO_2 NP-induced cell death in the absence of serum proteins points toward the importance of the protein corona. Using mass spectrometry, we have identified the serum proteins adsorbed on the surface of TiO_2 and polystyrene NPs (Table 1). A similar corona was observed previously following incubation of TiO_2 NPs in plasma proteins,[68] although plasma also contains clotting factors (fibrinogen and kininogen), which also adsorb onto the NP surface. There is some overlap between the TiO_2 and polystyrene NP coronas. Complement C3, an immune system protein, was the most abundant protein on the surface of both TiO_2 and polystyrene NPs. The top eight most abundant proteins found on TiO_2 NPs were also found on polystyrene NPs. Of the top 10 most abundant proteins on the TiO_2 NPs, only α-2-HS glycoprotein (#9) and complement C9 (#10) were

not found on polystyrene NPs. Of the top 10 proteins adsorbed on polystyrene NPs, 6 were also present on TiO_2 NPs. To quantify the correlation between the corona proteins adsorbed on the TiO_2 and polystyrene NPs, we calculated a Spearman's rank correlation coefficient and found no significant correlation between the TiO_2 and polystyrene NP coronas.

Table 1 Ranking of protein abundance (spectral counts) on the surface of TiO_2 and polystyrene NPs. Similar results were obtained using protein identification scores.

Protein Family	Rank for TiO_2	Rank for PS
Alpha-2-HS-glycoprotein	9	-
Antithrombin-III	-	3
Beta-2-glycoprotein 1	-	8
Coagulation factor XII	8	25
Complement C3	1	1
Complement C4	-	4
Complement C5	-	6
Complement component C7	5	12
Complement component C9	10	-
Complement factor B	6	9
Complement factor H	4	17
Gelsolin	7	2
Inter-alpha (Globulin) inhibitor H4	-	10
Plasminogen	2	5
Serum Albumin	3	7

3.2.6 Biological Implications: Monkey Kidney Cells and High Passage Number HeLa Cells

It is important to determine whether the TiO_2 NP-induced changes in peroxiredoxin expression observed for the HeLa cells are specific to this cell line or more general. Western blotting experiments were repeated using monkey kidney epithelial cells (BS-C-1). Like HeLa cells, these are sturdy cells that showed no decrease in cell health in response to TiO_2 NP incubation (24 h, 304 μg/mL, concentration adjusted to account for larger cells

in a confluent monolayer, MTT assay shown in Figure 11a). The monkey kidney cells showed a decrease in peroxiredoxin 1 (53 ± 20%, Western blot) in response to TiO_2 NP treatment (Figure 11b, c).

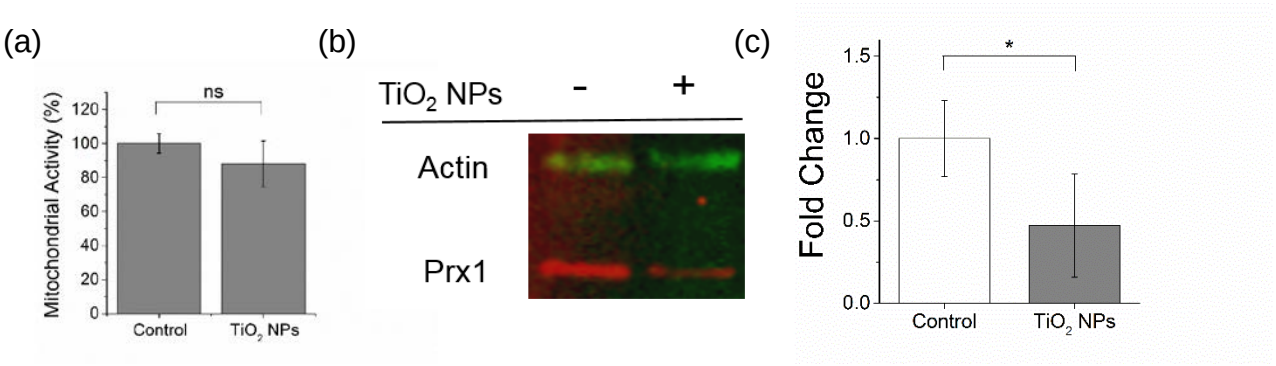

Figure 11 BS-C-1 cell health and oxidative stress. (a) Monkey kidney cells (BS-C-1) remain healthy, as measured by an MTT assay, following incubation with TiO_2 NPs (24 hr, 304 µg/mL, concentration adjusted to account for larger cells in a confluent monolayer). (b) Representative western blot of peroxiredoxin 1 (Prx1, red). Actin (green) was used as a housekeeping control. This blot is representative of 3 separate experiments. (c) Densitometric analysis of triplicate samples shows a decrease in peroxiredoxin 1 for TiO_2 NP-treated cells (grey) compared to an untreated control (white). Error bars represent ± standard deviation, ns=not significant *p<0.05.

In addition to differences between cell lines, cells from a single cell line can also show variation in protein expression, genetics, and morphology as they are repeatedly subcultured or "passaged" in the lab. Cells recently obtained from their primary source are at a low passage number. With each division in the lab, their passage number increases by one. To some extent, this represents the "age" of the cells. HeLa cells have a long history and it is not possible to assign a true passage number; instead, we can only track a relative passage number starting with the initial, relatively low passage number stock from ATCC. To determine if passage number affected the response of HeLa cells to the TiO_2 NPs, we repeated the Western blots using a high passage number cell sample (passage 28−29)

compared with the lower passage number cells (Figure 12a and Figure 8b, passage 18). While low passage number cells showed an increase in peroxiredoxin 1, these higher passage number cells showed a decrease (41 ± 10%, Figure 9a) under identical treatment conditions (400 µg/mL, 24 h). To confirm that increased passage number was responsible for this change in peroxiredoxin 1 expression, we repeated Western blotting experiments with freshly thawed, low passage number (passage 4) HeLa cells, and an increase in peroxiredoxin 1 was again observed.

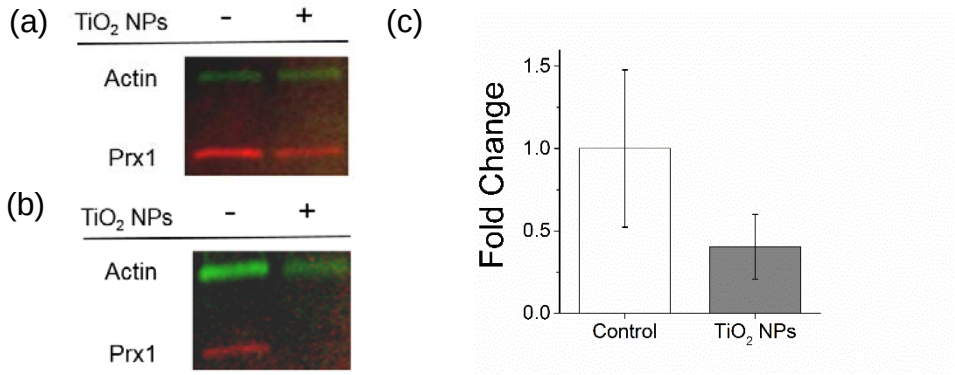

Figure 12 Western blots were used to measure expression levels of peroxiredoxin 1 in high passage number HeLa cells treated with TiO_2 NPs (24 hrs). (a) Representative western blot of peroxiredoxin 1 (Prx1, red) incubated with 400 µg/mL TiO_2 NPs. Actin (green) was used as a housekeeping control. This blot is representative of 3 separate experiments. (b) At higher TiO_2 NP concentrations (4,000 µg/mL), the peroxiredoxin 1 signal is no longer visible. This blot is representative of 3 separate experiments (c) Densitometric analysis of triplicate samples shows a decrease in peroxiredoxin 1 for TiO_2 NP-treated cells (24 hrs, 400 µg/mL, grey) compared to an untreated control (white). Error bars represent ± standard deviation.

3.2.7 Conclusions and outcomes

Our goal was to examine the cellular response to TiO_2 NPs at subcytotoxic levels with a specific focus on oxidative stress. PCR arrays and Western blotting show that expression of the peroxiredoxins, a family of antioxidant enzymes, was altered in response to TiO_2 NPs (Figure 8). These changes were specific to TiO_2 NPs because they were not observed for polystyrene NPs with a similar diameter and charge (Figure 9b, c). Both the TiO_2 NPs and polystyrene NPs are coated with a layer of adsorbed proteins (Table 1),[61, 94] known as the protein corona. For the TiO_2 NPs, the protein corona is essential to maintaining cell health. In the absence of a corona, the bare TiO_2 NPs lead to high levels of cell death (Figure 10b). Changes in peroxiredoxin expression observed for two different cell lines (HeLa and BS-C-1, Figures 8 and 11b) and the cell passage number dependence (Figure 12a, c) suggests that the cellular response to TiO_2 NPs is independent of cell type and may not lead specifically to up- or down-regulation of peroxiredoxin 1 but rather a disruption of peroxiredoxin equilibrium that results in changes in expression depending on the specifics of the system. Activity of the peroxiredoxins is highly localized and compartmentalized.[35, 83-86] It is possible that small differences in TiO_2 NP−cell interactions, such as the cell surface receptors involved, alters the peroxiredoxin response. The peroxiredoxin family of proteins has only relatively recently been discovered, and our knowledge of their characteristics and function continue to be refined. The peroxiredoxin enzymes are abundant peroxidase enzymes, and their role in clearance of H2O2 from the intracellular milieu has been quantified to be at least as large as other antioxidant mechanisms such as catalase and glutathione peroxidase.[94] The direct redox relay of oxidative equivalents to other proteins has been reported, suggesting additional functions

of the peroxiredoxins in thiolbased signaling.[95] The four isoforms identified in this study to have altered transcription by the presence of TiO_2 NPs are all 2-cysteine type peroxiredoxins; however, peroxiredoxin 5 is considered an atypical member of this enzyme class due to a lack of sequence homology.[85] Unlike peroxiredoxin 1, 3, and 4, peroxiredoxin 5 possesses the ability to detoxify peroxynitrite ($ONOO^-$); thus its up-regulation in the presence of TiO_2 NPs may reflect specificity to this reactive nitrogen species.[96] Furthermore, the subcellular distribution of these dynamic isoforms is diverse. Peroxiredoxin 1 is largely cytosolic, peroxiredoxin 3 is mitochondrial, peroxiredoxin 4 is extracellular/ secreted, while peroxiredoxin 5 is found in the cytosol, nucleus, mitochondria, and peroxisomes.[85, 97] The concomitant up-regulation of isoforms 1 and 5 may therefore point to spatial variation of TiO_2 NP-induced oxidative/nitrostative stress localized to regions of the cytosol surrounding endocytic vesicles. Overall, the heterogeneity of the TiO_2 NPs provides an interesting and challenging system for understanding this unique biological response. Future work will use changes in peroxiredoxin expression as a marker to determine which specific TiO_2 NP parameters (size, crystal structure, corona proteins) result in the oxidative stress response and address questions of localization.

This chapter was reproduced with permission from Reference 50. Copyright 2016 American Chemical Society. Figure 7a was contributed by Dipesh Khanal.

CHAPTER 4. TITANIUM DIOXIDE NANOPARTICLES OXIDIZE SERUM PROTEINS

4.1 Introduction

Titanium dioxide nanoparticles (TiO_2 NPs) are widely used as pigments and photocatalysts in consumer and industrial applications. Previous toxicology studies have shown that these NPs are non-toxic.[9-10, 20, 48] However, our lab,[50] and others,[23, 45, 47, 79-80, 82] have observed an oxidative stress response to these metal oxide NPs. While currently regarded as safe, long term exposure to even low levels of oxidative stress will ultimately affect human health. We have recently found that incubation of cells (HeLa and BS-C-1) with low, non-cytotoxic, concentrations of TiO_2 NPs, in the absence of UV light, produces an oxidative stress response, detected as changes in the expression of the peroxiredoxin family of anti-oxidant enzymes.[50] Our goal in the research described below was to determine the mechanism of metal oxide NP-induced oxidative stress in the absence of UV light.

Metal oxide NPs are very well-studied in terms of ROS generation as it is the ability to generate ROS (e.g., hydroxyl radicals, superoxide, hydrogen peroxide, singlet oxygen), that leads to their use as photocatalysts.[4, 98-99] In comparison, most human exposure to TiO_2 NPs takes place in the dark; for example, in the gut following consumption of food with white pigment TiO_2 NPs or in the lungs following inhalation of TiO_2 NPs in the factories that use them. TiO_2 NPs in sunscreen and cosmetics do not penetrate the skin and include an alumina or silica shell that adsorbs ROS generated by UV exposure.[100] Although less

studied than UV-induced ROS, we hypothesized that surface defects, such as oxygen vacancies, could generate ROS, specifically hydroxyl radicals and superoxide.[101-105] Previous work by Colvin, et al.,[82] showed that ROS produced by TiO_2 NPs in the absence of UV light was associated with oxidative stress and cytotoxicity. Additional work has found that TiO_2 NPs in the absence of light produce a classic oxidative stress response in cells including DNA damage, lipid peroxidation, and micronuclei formation.[45] Since most relevant biological exposure takes place in the dark, it is necessary to understand how ROS is generated by metal oxide NPs in the absence of UV light and determine the link between dark NP-generated ROS and cellular oxidative stress.

In considering the cellular response to NPs, it is important to note that most NPs do not interact directly with cells, but rather through a "corona" of adsorbed proteins on the NP surface.[50, 55, 60, 66, 92-93, 106-107] Both in cell culture and *in vivo*, the major source of extracellular proteins is serum. Previous work in our lab, and others, show that that serum proteins used as a nutrient source for cells in culture adsorb onto the surface of TiO_2 NPs forming a protein-TiO_2 NP complex.[50, 68, 108] The experiments described below were designed to measure ROS production by TiO_2 NPs in the dark and to determine if the ROS oxidized serum proteins. Experiments used common photocatalytic TiO_2 NPs (analogous to Degussa P25 NPs) and food grade TiO_2 (often referred to by their European Union food additive number, E171). Cellular assays measured oxidative stress in response to these NPs, showing that an oxidized protein corona serves as a cellular signal of oxidative stress. Increasing or decreasing oxygen vacancies through plasma treatment or surface passivation led to increased or decreased oxidative stress, respectively, pointing towards NP surface defects as the origin of ROS-induced oxidative stress in the dark.

4.2 Results and Discussion

4.2.1 TiO_2 NPs Generate ROS in the Absence of Light

We first probed commonly-used TiO_2 NPs, both industrial P25 NPs (DLS, hydrodynamic diameter = 567 ± 38 nm, PDI = 0.17, ZP = −22 ± 0.5 mV) and food grade E171 NPs (DLS, hydrodynamic diameter = 210 ± 2 nm, PDI = 0.37, ZP = −28 ± 0.5 mV), for possible ROS generation using H_2DCF (Figure 11a), a fluorescein derivative that becomes fluorescent upon oxidation by ROS (Excite: 488 nm, Emit: 523 nm). Polystyrene NPs, which are not expected to generate ROS, and which did not lead to oxidative stress in previous experiments,[50] were used as a negative control. Hydrogen peroxide was used as a positive control. With any light-based measurement there is the concern that light used for the measurement could excite the TiO_2 NPs or TiO_2 NPs sensitized by a dye or biomolecule. The fluorescent H_2DCF product is excited at 488 nm. Although this is lower energy than the 332 nm maximum of these TiO_2 NPs, we were careful to separate the oxidation reaction, carried out in the dark, from the light used for the measurement by removing the TiO_2 NPs (centrifugation at 8000 rcf for 15 min, Figure 13) prior to excitation in the fluorimeter. The H_2DCF assay demonstrated the production of ROS by TiO_2 NPs, both P25 and E171, in the absence of light.

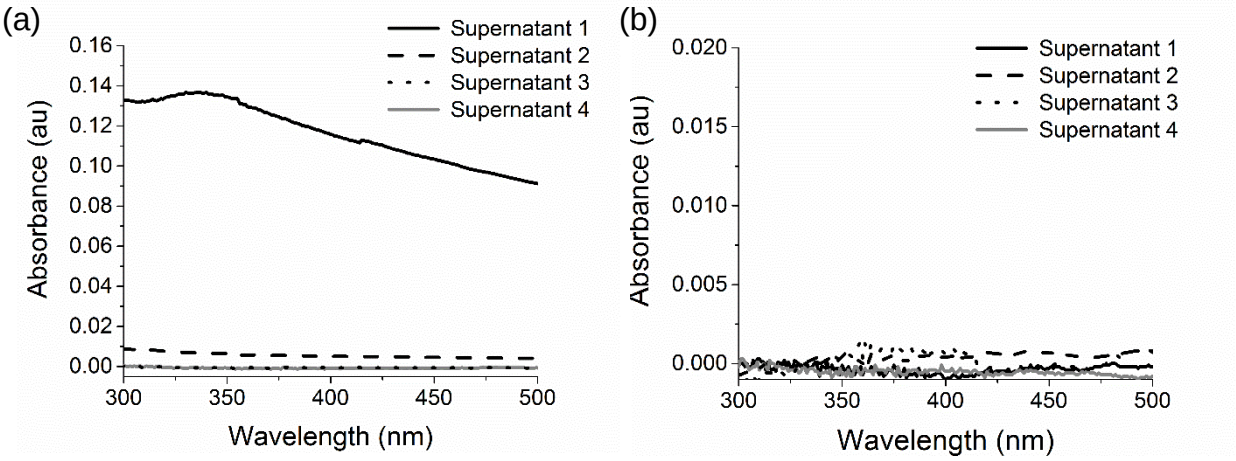

Figure 13 TiO_2 NP removal by centrifugation and concentration determination. (a) P25 and (b) E171 TiO_2 NPs were removed from solutions prior to light-based measurements using repeated (3x) centrifugation (8,000 rcf, 15 min). Supernatant 1 is the supernatant following the first centrifugation step. After 3 rounds (Supernatant 3) of centrifugation, no NPs are detected. Supernatant 4 is shown for comparison.

H_2DCF is a general probe of ROS that does not discriminate between different species.[109] To distinguish between the specific types of ROS produced, we used probes specific for hydroxyl radicals, superoxide, and hydrogen peroxide. Terephthalic acid (TA) forms a fluorescent product, 2-hydroxyl terephthalic acid (Excite: 312 nm, Emit: 434 nm), in the presence of hydroxyl radicals. Experiments show formation of a fluorescent product following incubation with TiO_2 NPs in the dark (Figure 14b), demonstrating TiO_2 NP production of hydroxyl radicals in the absence of UV light. In addition, the use of a hydroxyl radical scavenger, isopropanol, inhibited fluorescence. To confirm that TA is sensitive to only hydroxyl radicals, H_2O_2 was used as a negative control and Fenton-generated hydroxyl radicals served as a positive control (Figure 15a). To probe for superoxide we used the reaction between superoxide and Nitro blue tetrazolium (NBT, Abs: 259 nm), which leads to the formation of formazan, a water-insoluble product, and a decreased NBT signal.[110] TiO_2 NPs in the dark resulted in decreased NBT absorbance

indicating superoxide production, while polystyrene NPs did not lead to a change in signal (Figure 14c). A superoxide scavenger, superoxide dismutase (SOD), inhibited the reaction of NBT. Control experiments to ensure that NBT was specific to superoxide showed no reaction with H_2O_2 or Fenton-produced hydroxyl radicals (Figure 15b). A reaction with xanthine/xanthine oxidase was positive (Figure 15b). As with the H_2DCF assay, TiO_2 NPs were removed from the solution prior to TA and NBT measurements. An Amplex Red assay to test for possible H_2O_2 generation showed no H_2O_2 (P25 NPs, 2 mg/mL, 1 hr, room temperature, data not shown). H_2O_2 (10 μM) was used as a positive control.

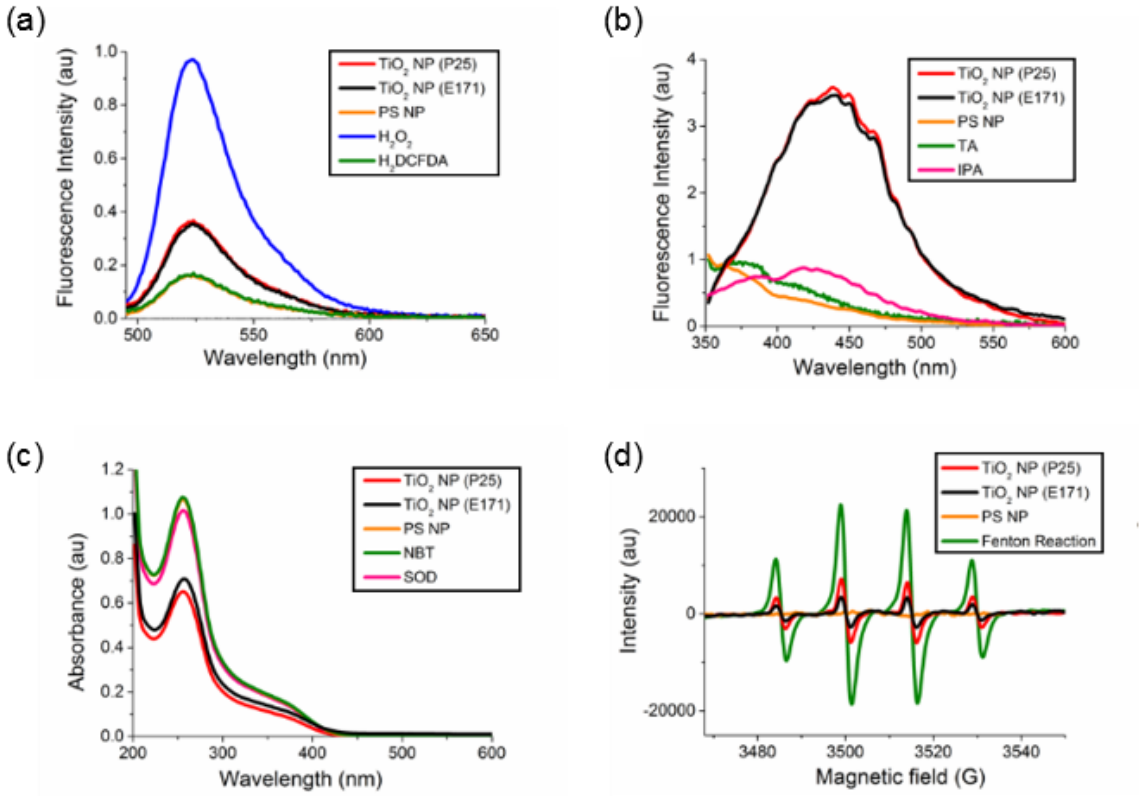

Figure 14 Generation of ROS by TiO_2 NPs in the dark. (a) Fluorescence spectra of H2DCF (5 µM) in response to ROS. TiO_2 NPs (P25 (red) and E171 (black), both 400 µg/mL) were incubated with H_2DCF in the dark (1 hr, RT). Auto-oxidation of H2DCF in blank samples (5 µM, green) results in the same signal as polystyrene (PS) NPs (20 pM, matched to the surface area of the TiO_2 NPs, orange). (b) Fluorescence spectra of terephthalic acid (TA, 2 mM) in response to hydroxyl radicals. TiO_2 NPs in the dark (P25 (red) and E171 (black), both 2 mg/mL, 1 hr, RT). No emission was observed from TA alone in blank samples (2 mM, green), similar to PS NPs (20 pM, orange). Isopropanol (4% v/v) scavenges the hydroxyl radicals produced by the TiO_2 NPs in the dark (pink). (c) Decreased absorbance of NBT indicates the production of superoxide radicals. TiO_2 NPs (2 mg/mL, 1 hr, RT) incubated with NBT in the dark (P25 (red) and E171 (black)). No change was observed from NBT alone in blank samples (2 mM, green) or polystyrene (PS) NPs (20 pM, orange). Superoxide dismutase (SOD, 5 mM) scavenges the superoxide produced by the TiO_2 NPs in the dark (pink). (d) EPR spectra of TiO_2 NPs (10 mg/mL, P25 (red) and E171 (black)) and PS NPs (100 pM, orange) with DMPO (0.02 M). Fenton-generated hydroxyl radicals (850 µM, green) were used as a positive control. For all light-based measurements, TiO_2 NPs were removed (8000 rcf for 15 min, x3) from solution prior to measurement.

In addition to light-based measurements, hydroxyl radicals and superoxide can also be detected with EPR using DMPO (Figure 14d), a spin-trapping reagent.[111] DMPO traps hydroxyl radicals to form the DMPO−OH adduct, giving a 4-peak EPR signal. DMPO traps superoxide radicals to form DMPO−OOH, which decomposes to form DMPO−OH. EPR spectra of TiO_2 NPs (P25 and E171) showed a characteristic 4-peak signal demonstrating

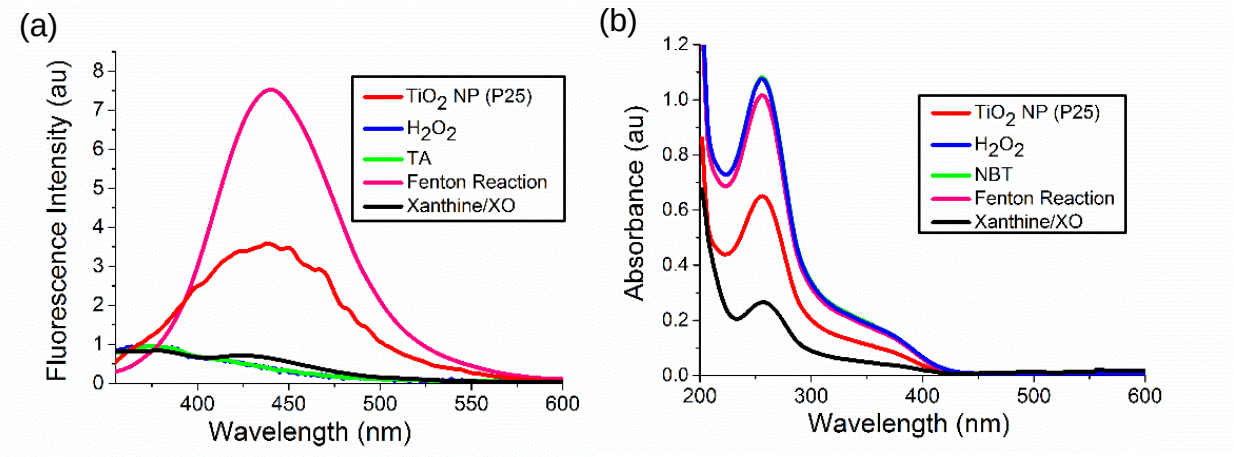

Figure 15 TA and NBT assays are specific to hydroxyl radicals and superoxides, respectively. (a) The selectivity of TA was confirmed using Fenton-generated hydroxyl radicals ($CuSO_4$ (10 μM) and H_2O_2 (1 mM), pink), H_2O_2 (blue), and xanthine (300 μM)/xanthine oxidase (XO, 0.01 U/mL)-generated superoxide (black). No emission was observed from TA alone (2 mM, green). (b) The selectivity of NBT was confirmed using xanthine (300 μM)/xanthine oxidase (XO, 0.01 U/mL)-generated superoxide (black), Fenton-generated hydroxyl radicals ($CuSO_4$ (10 μM) and H_2O_2 (1 mM), pink), and H_2O_2 (blue). No change was observed from NBT alone (2 mM, green). For both assays, measurements were made after a 1 hr incubation with TiO_2 NPs or the relevant reagent. TiO_2 NPs were removed (8000 rcf for 15 min) from the solution prior to measurement. TiO_2 NP (1 mg/mL, red), TA, and NBT data are replotted from Figure 11 for comparison.

4.2.2 TiO_2 NPs Oxidize Serum Proteins

TiO_2 NPs interact with cells through a layer or "corona" of proteins adsorbed on the NP surface.[50, 68, 108] Using proteomics, we previously identified the serum proteins adsorbed on the surface of TiO_2 NPs (P25).[50] Complement C3, an immune system protein,

was the most abundant protein on the TiO_2 NP surface followed by plasminogen and serum albumin. Based on our observation that TiO_2 NPs produce ROS in the absence of UV light (Figure 14a-d), we analyzed serum proteins to determine if this ROS oxidized serum proteins incubated with TiO_2 NPs. As a control, we used polystyrene NPs, which do not produce ROS (Figure14a-d).[50]

UV-Vis spectroscopy of a carbonyl-reactive probe (2,4-dinitrophenylhydrazine (DNPH)) was used to measure changes in the carbonyl content of serum proteins following incubation with NPs. Radical-induced peptide backbone cleavage leads to an increase in the carbonyl content of proteins.[112] DNPH reacts with carbonyls to form covalently-bound protein-dinitrophenylhydrazone (Abs: 370-385 nm). Protein oxidation is then measured based on the absorption at 375 nm following isolation of the protein from the solution (TCA precipitation and resuspension) to remove the unbound hydrazine.[36] This isolation step also means that the NPs are not present during the measurement and that any oxidation occurred prior to UV-Vis spectroscopy. FBS (10%, 3 mg/mL) incubated with TiO_2 NPs (P25 and E171, 30 min, RT) showed an increase in protein oxidation compared to FBS alone or FBS incubated with polystyrene NPs (Figure 16). In comparison, no change in carbonyl content was observed for serum proteins incubated with polystyrene NPs.

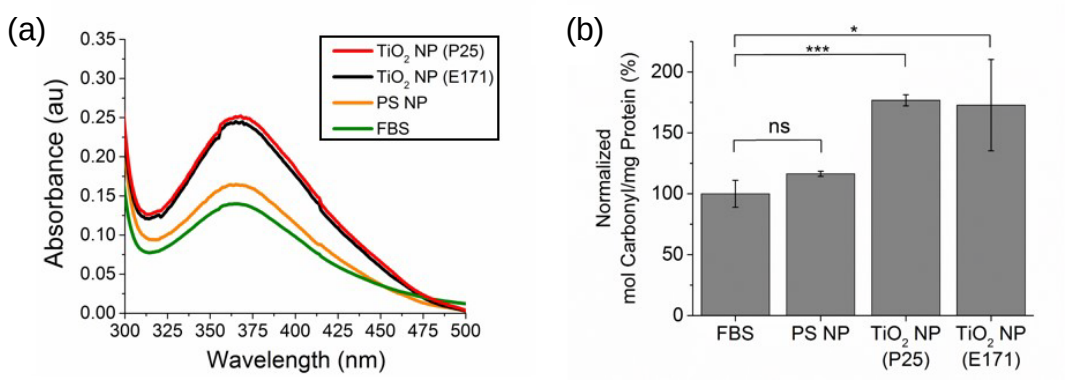

Figure 16 TiO_2 NP-induced oxidation of serum proteins. (a) Absorption spectra of FBS alone (green) or FBS incubated with TiO_2 NPs (P25 are red, E171 are black) and polystyrene (PS) NPs (orange) in the dark and then tagged with carbonyl-reactive DNPH. (b) The ratio of the 370 nm peak (DNPH) to the 280 nm peak (protein) quantifies the extent of oxidation. Error bars denote ± standard deviation for n=3. ***p<0.001, *p<0.05, ns=non-significant. A comparison of the TiO_2 NPs to the PS NPs has the same significance values as the TiO_2 NPs to FBS.

4.2.3 An Oxidized Protein Corona Leads to Oxidative Stress

To determine if the TiO_2 NP-mediated oxidation of proteins leads to oxidative stress, we used TiO_2 NPs (P25) to oxidize serum proteins, removed the TiO_2 NPs by centrifugation (8,000 rcf, 15 min, x3), and then incubated these oxidized proteins with polystyrene NPs to form an oxidized protein corona on non-oxidizing polystyrene NPs. Polystyrene NPs with a non-oxidized protein corona do not lead to oxidative stress.[50] Oxidation of the proteins was confirmed with a DNPH assay, similar to Figure 13. We then used PCR (Table 2) and western blotting (Figure 18) to determine if these oxidized protein-polystyrene NPs now alter the peroxiredoxins. The same protein bands were observed in

the oxidized and unoxidized coronas of the polystyrene NPs (gel electrophoresis, Figure 17).

Table 2 Oxidized corona-polystyrene NP-induced changes in gene expression determined by RT-PCR. Fold changes represents 2-ΔC_T ratios between untreated HeLa cells and cells incubated with oxidized protein- polystyrene NPs. $p<0.05$ for each gene, n=3 distinct samples.

Gene	Fold Change
antioxidant 1 copper chaperone	3.05 ± 1.08
24-dehydrocholesterol reductase	6.09 ± 3.06
glutathione synthetase	2.25 ± 0.48
peroxiredoxin 3	**-4.31 ± 0.16**
peroxiredoxin 4	**-2.23 ± 0.20**
peroxiredoxin 5	**2.42 ± 0.82**
prion protein	-1.94 ± 0.17
sequestosome 1	5.10 ± 1.52

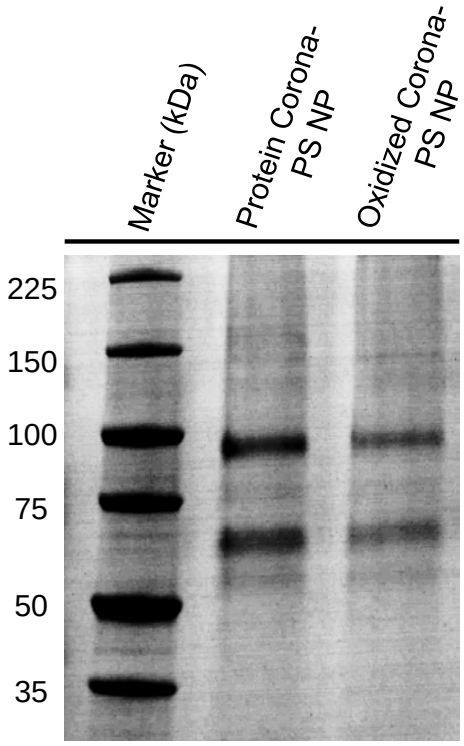

Figure 17 Gel electrophoresis was used to compare the corona formed on the surface of polystyrene (PS) NPs using FBS (unoxidized) or FBS oxidized by TiO_2 NPs, as described in Section 2.9.1. To analyze the corona, unbound and weakly bound proteins were first removed from the protein-NP mixture by centrifugation (8,000 rcf, 15 min, x3). A detergent, SDS (Laemmli loading buffer, #BP-110R, Boston BioProducts, Ashland, MA; 5 min, vortexing) was used to remove the hard corona. Protein samples were heated for 5 min at 100 ^{o}C and then loaded onto a gel (tris-glycine SDS gel, #456-1094, Bio-Rad, Hercules, CA) for SDS-PAGE (230 V, 35 min). A 5-225 kDa molecular weight marker (Lonza ProSieve Unstained Protein Marker, #50547, VWR, Rockland, ME) was included. Gels were stained for 1 hr (SimplyBlue Safe Stain, #LC6060, ThermoFisher) and then imaged. Densitometric analysis (Image J; http://rsb.info.nih.gov/ij/) was used to compare the two protein coronas. Analysis was carried out for 3 distinct samples, a representative gel is shown. No differences between the two coronas were observed.

We used a PCR array to screen 84 oxidative stress-related genes following the incubation of cells with the oxidized protein-polystyrene NPs (20 pM NPs, 24 hrs). Changes in gene expression were considered significant for p-values < 0.05 for data obtained from 3 distinct experiments. The PCR array showed 8 genes were altered in comparison to untreated control cells, including three members of the peroxiredoxin family (Table 2). This family of enzymes is responsible for the clearance of peroxides from the cell and are essential to the oxidative stress response.[35, 83, 85-86, 113] Changes in the expression of peroxiredoxin 1, 3, 4, and 5 were also detected in our previous experiments following incubation of HeLa cells with TiO_2 NPs (P25) in the presence of serum proteins.[50] Expression of the peroxiredoxins was unaffected by polystyrene NPs in unoxidized cell culture medium.[50] Oxidized proteins in solution, rather than on the surface of NPs, did not alter expression of any of the peroxiredoxins. The only gene altered by oxidized proteins in solution was heme oxygenase (0.64 ± 0.25 fold change).

Western blotting experiments compared changes in protein expression using an antibody against peroxiredoxin 4. Oxidized serum proteins, incubated with polystyrene NPs, were compared to a control in the absence of NPs with only standard cell culture media (MEM supplemented with 10% FBS) present. The western blot shows a 0.61-fold decrease (± 0.04%) in the expression of peroxiredoxin 4 following incubation with the oxidized protein-polystyrene NPs (Figure 18).

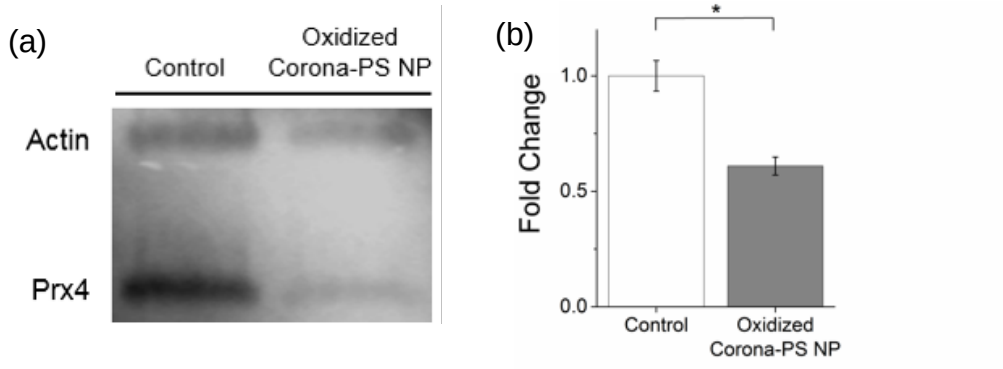

Figure 18 Western blot of peroxiredoxin 4 following treatment of HeLa cells with oxidized protein-polystyrene (PS) NPs (24 hrs, 20 pM). (a) Representative western blot of peroxiredoxin 4 (Prx4). Actin was used as a housekeeping control. Control cells, in the absence of NPs, were incubated with standard cell culture media (MEM + 10% FBS). (b) Densitometric analysis of triplicate samples shows a decrease in peroxiredoxin 4 for oxidized protein-polystyrene (PS) NP-treated cells (24 hrs, 20 pM, gray) compared to an untreated control (white). Error bars represent ± standard deviation, *p <0.05.

The results described above suggest that a protein(s) oxidized by ROS generated at the surface of TiO_2 NPs then adsorbs onto the surface of a polystyrene NP and that this oxidized protein triggers an oxidative stress response, detected as changes in peroxiredoxin expression. We do not know which specific protein is responsible, and it is likely that a combination of proteins is required since oxidative stress is not observed in response to oxidized proteins in the absence of NPs. Our previous proteomics analysis showed that of the 10 most abundant proteins found on the surface of TiO_2 NPs, 8 of these were also present on the surface of polystyrene NPs.

4.2.4 ROS Generations Correlates to Nanoparticle Surface Defects

The decrease in peroxiredoxin 4 observed with PCR (Table 2) and western blot (Figure 18) suggests that the protein corona, oxidized by the TiO_2 NPs, signals to the cells that they are under oxidative stress. Underlying this biological response is the question of

how TiO_2 NPs generate ROS in the absence of UV light. The characterization of the small amount of ROS generated by TiO_2 NPs in the absence of UV light is rarely studied, as the vast majority of research in this area focuses on the photocatalytic properties of TiO_2.[99] Studies of ROS generation in the dark have been limited to three biological studies,[45, 82, 103] and our own observations of changes in peroxiredoxins.[50] The most likely source of ROS from TiO_2 NPs in the dark are surface defects, especially oxygen vacancies.[101-105] To test the correlation between surface defects and ROS generation, we used two NP modifications to increase and decrease the surface defects of the TiO_2 NPs, confirmed with x-ray photoelectron spectroscopy (XPS) and EPR (Figure 19a and b, Table 3), and then measured ROS generation, using H_2DCF (Figure 19c), and oxidative stress, using western blotting (Figure 19d).

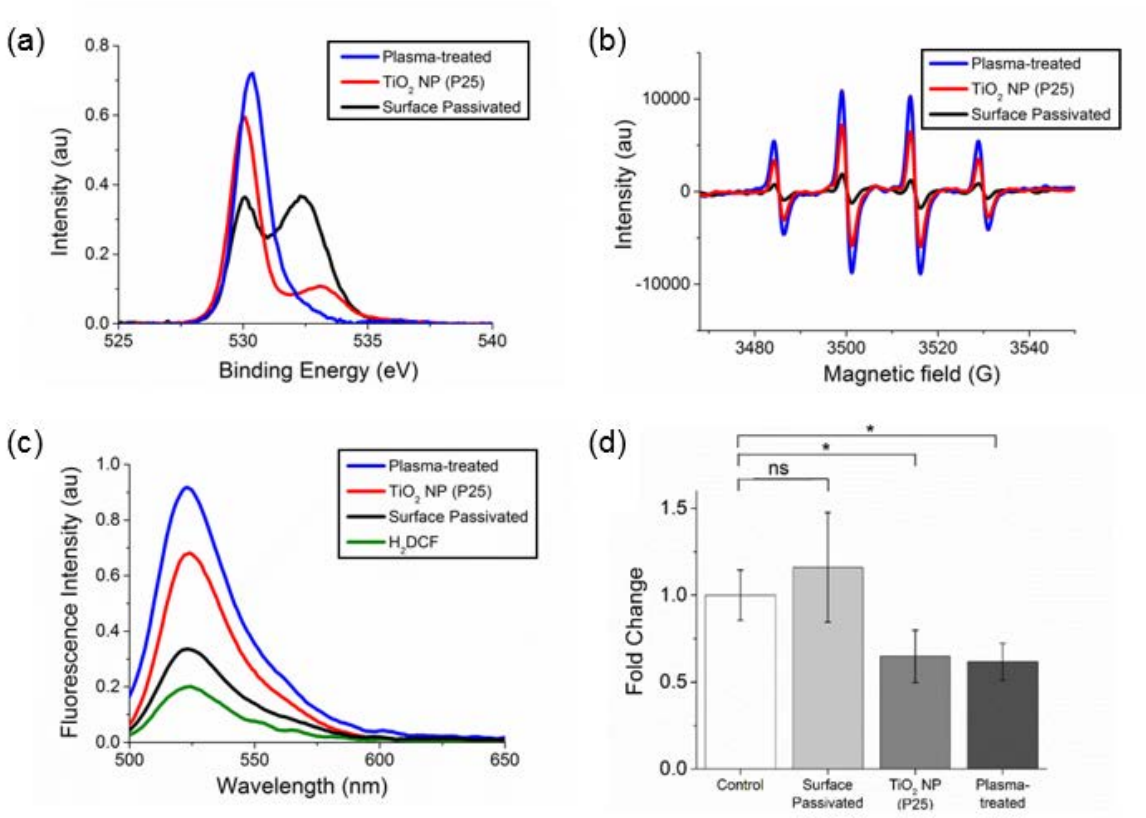

Figure 19 Increased or decreased surface defects correlate with ROS generation and oxidative stress. (a) XPS of untreated (red), plasma-treated (blue), and surface passivated (black) TiO_2 NPs was used to monitor changes in oxygen vacancies in response to surface modification. Binding energies and peak areas are listed in Table 3. (b) EPR spectra of control and surface-modified TiO_2 NPs (10 mg/mL) with DMPO (0.02 M). The TiO_2 NP spectrum is replotted from Figure 1 for comparison. (c) Fluorescence spectra of H_2DCF (5 μM) in response to ROS. All TiO_2 NPs (400 μg/mL) were incubated with H_2DCF in the dark (1 hr, RT). Auto-oxidation of H_2DCF (5 μM, green) results in a small positive signal. (d) Western blots were used to quantify changes in cellular oxidative stress as a function of surface modification of TiO_2 NPs. The control shows cells incubated with standard cell culture media (MEM + 10% FBS). Experiments were carried out in triplicate.

Table 3 XPS characterization of surface-modified TiO_2 NPs. Binding energies (B.E.) and % area under the curve are shown for unmodified, plasma-treated, and surface passivated TiO_2 NPs.

		O 1s		
		O1	O2	O3
TiO_2 NP (P25)	B.E. (eV)	530.0	531.3	533.2
	Area (%)	73.3	11.5	15.2
Plasma-treated	B.E. (eV)	530.6	531.0	536.3
	Area (%)	74.2	23.3	2.5
Passivated	B.E. (eV)	530.2	531.7	532.5
	Area (%)	35.9	0.7	63.3

Plasma treatment (10 min, 18 W, air, Harrick Plasma Cleaner) was used to increase the surface defects of the TiO_2 NPs (P25).[113-115] XPS shows an increase in the peak at 531 eV associated with oxygen vacancies (Figure 19a) as well as increased ROS generation (Figure 19b, c). To examine the effect of decreased surface defects, TiO_2 NPs (P25) were passivated with a silica-aluminum shell on the NP surface,[116] confirmed with XPS (Figure 16a) and EPR (Figure 19b). In addition to the XPS scan for oxygen, peaks were also measured for Al 2p and Si 2p (Figure 20). This surface passivation decreased the amount of ROS generated by the NPs (Figure 19c).

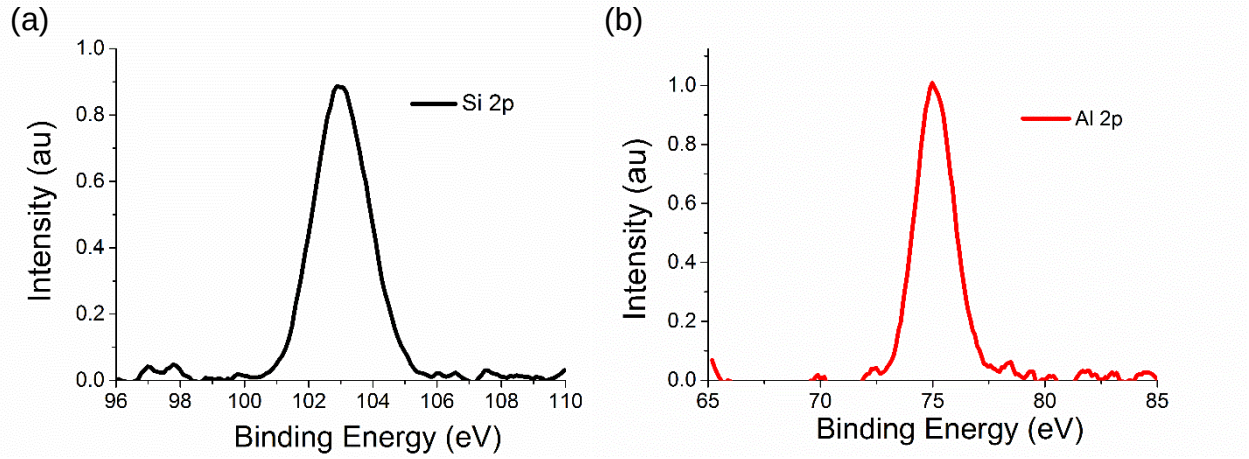

Figure 20 XPS of surface passivated TiO_2 NPs. XPS measured for (a) Si 2p and (b) Al 2p confirms that TiO_2 NPs (P25) were passivated with a silica-aluminum shell on the NP surface. Measurements were carried on 4 distinct samples (2 mg/mL, dried), representative spectra are shown.

Western blots from three cell samples show that surface passivated TiO_2 NPs (400 μg/mL, 24 hrs) do not alter peroxiredoxin 4 (Figure 19d and Figure 21a). In comparison, plasma-treated and unmodified TiO_2 show a similar decrease in peroxiredoxin 4 (Figure 19d and Figure 21a), suggesting a threshold response to oxidative stress. An MTT assay of cell health confirmed that the plasma-treated and surface passivated TiO_2 NPs did not decrease cell viability (Figure 21b).

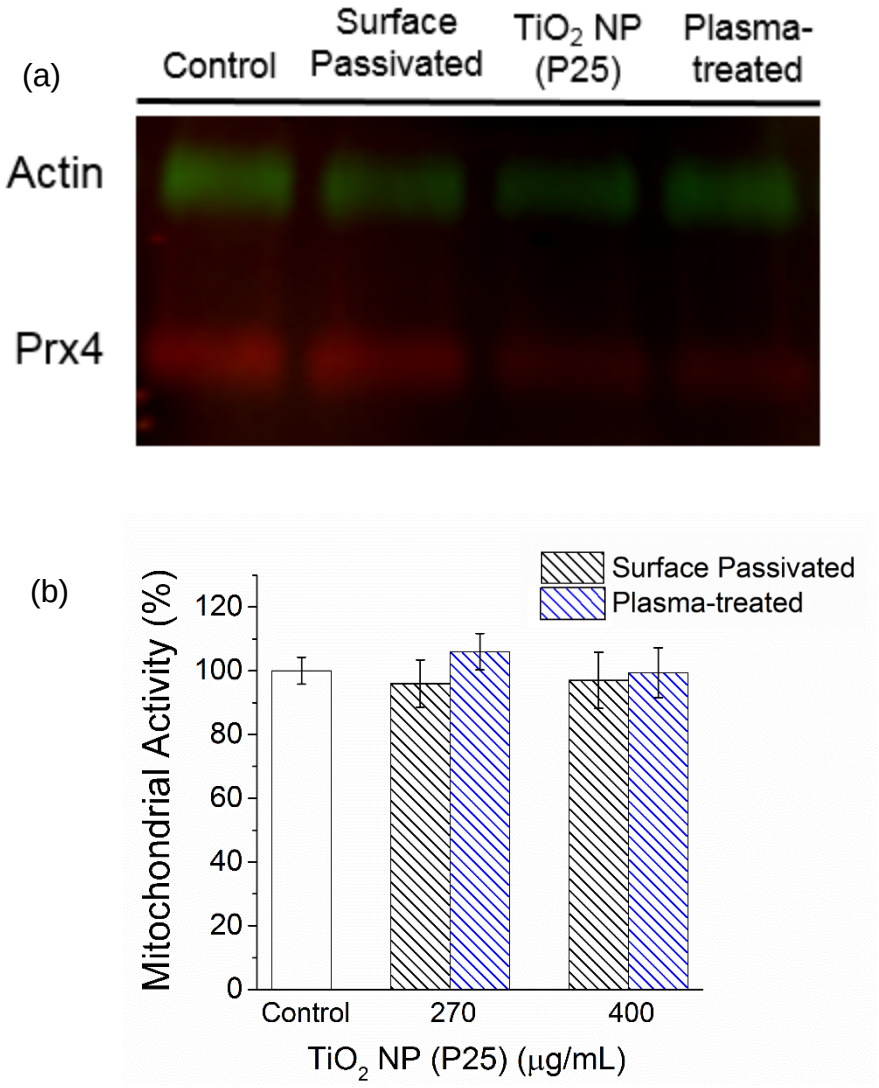

Figure 21 Cellular response to plasma-treated and surface passivated TiO_2 NPs. (a) Representative western blot of peroxiredoxin 4 (Prx4, red) following incubation with TiO_2 NPs (400 μg/mL 24 hrs, red). Actin (green) was used as a housekeeping control. Cells lacking NPs (Control) were incubated with standard cell culture media (MEM + 10% FBS). This blot is representative of three trials with densitometric analysis shown in Figure 16d. (b) Cytotoxicity. An MTT assay of mitochondrial enzyme activity was used to ensure that the concentration of plasma-treated and surface passivated TiO_2 NPs (270 μg/mL, 12-well plate, 24 h incubation) did not lead to decreased cell health. Measurements are the average of three wells and error bars represent ± standard deviation. MTT activity (%) is normalized against a control in the absence of NPs. There was no significant difference between the control and the concentration of TiO_2 NPs used for experiments (400 μg/mL), which was used to confirm that we were working in a non-cytotoxic regime.

4.2.5 Conclusions

Overall, our experiments show that TiO_2 NPs, both industrial P25 and food grade E171 NPs, produce ROS even in the absence of UV light (Figure 14). This ROS generation, which is correlated with TiO_2 NP surface defects (Figure 19), oxidizes the serum proteins that adsorb on the surface of the TiO_2 NPs (Figure 16). These oxidized proteins lead to an oxidative stress response in cells, observed as changes in the peroxiredoxin family of anti-oxidant enzymes (Table 3, Figure 18, 22 (E171)). While previous work showed that TiO_2 NPs produce low levels of ROS in the dark and that TiO_2 NPs in the dark can cause oxidative stress,[45, 82] the experiments described above are the first to link TiO_2 NP-induced oxidation of corona proteins to oxidative stress.

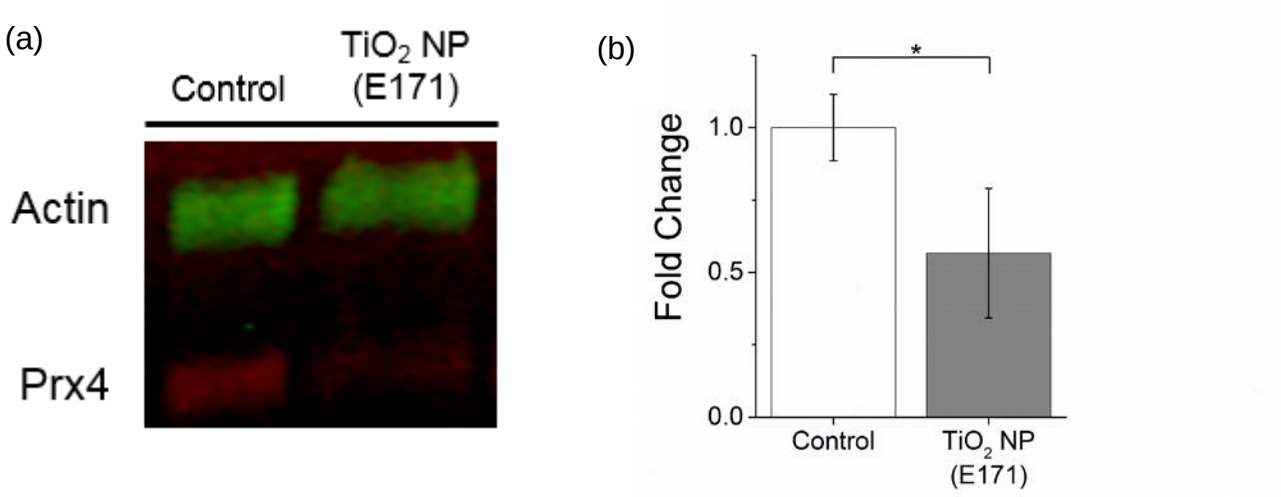

Figure 22 Food grade E171 TiO_2 NPs induce oxidative stress. (a) Representative western blot of peroxiredoxin 4 (Prx4, red) following incubation with E171 TiO_2 NPs (400 µg/mL 24 hrs, red). Actin (green) was used as a housekeeping control. Cells lacking NPs (Control) were incubated with standard cell culture media (MEM + 10% FBS). This blot is representative of three trials. (b) Densitometric analysis of (a) *$p<0.05$.

The P25 TiO_2 NPs used in these experiments are the same NPs used in many photocatalytic applications, making them relevant to human health, especially for workers who may inhale them during production.[26, 76, 100] In addition, all people routinely encounter TiO_2 NPs as a white pigment in paint or in food, such as frostings and powders, taking advantage of their high index of refraction for a bright white color. Although both types of NPs are non-toxic based on conventional toxicology assays,[9-10, 20, 48, 50] it is important to note that long-term exposure to even low levels of oxidative stress can be detrimental to human health. The contemporary theory on human exposome is based upon small cumulative contributors to disease through lifestyle and environment.[45, 117-118] Our results provide evidence of one such low-level oxidative burden, through TiO_2 NP exposure, that may add to a summative effect on cellular function.

This chapter was reproduced with permission from reference 124. Copyright 2017 Royal Society of Chemistry. Figures 12-13, 15, 17-21, and Table 3 were contributed by Dr. Dhanya Jayaram.

CHAPTER 5. TITANIUM DIOXIDE NANOPARTICLE-INDUCED OXIDATION OF THE PLASMA MEMBRANE

5.1 Introduction

Titanium dioxide nanoparticles (TiO_2 NPs) are estimated to be produced at levels of >200,000 metric tons each year for use as pigments and photocatalysts.[119-121] This high level of production has raised concerns about human exposure, both the workers responsible for processing of TiO_2 NP-containing materials and consumers who are routinely exposed to the white TiO_2 NP-based pigments in food, cosmetics, and paint.[18, 26, 48, 51, 122-123] Previous work from our lab, and others, have shown that TiO_2 NPs lead to oxidative stress in cells, even in the absence of UV light.[45, 50, 82] Experiments in the absence of UV light are important as the major exposure pathways, inhalation and ingestion, preclude exposure to UV light. TiO_2 NPs used in sunscreens are coated with alumina, silica, or silicone dioxide, or doped with metals to reduce the generation of reactive oxygen species and increase photostability.[12, 100]

Recent work from our lab has shown that TiO_2 NP-induced oxidative stress is due to oxidation of the protein "corona,"[124] the layer of non-specifically adsorbed serum proteins that form an interface between the cell and the NP.[50, 55, 66, 92-93, 107] Oxidation of the protein corona leads to an oxidative stress response,[50, 124] characterized by changes in expression of the peroxiredoxin family of antioxidant enzymes.[35, 68, 83-85] In the course of this previous research, we observed that "bare" TiO_2 NPs, lacking a protein corona, were more cytotoxic than TiO_2 NPs in the presence of serum proteins. Having confirmed that TiO_2 NPs oxidize

proteins,[124] we hypothesized that a direct oxidation of the plasma membrane lipids could be responsible for the greater cytotoxicity of bare TiO_2 NPs.

Our current research examines the TiO_2 NP-induced oxidation of the plasma membrane. We find that bare TiO_2 NPs lead to lipid peroxidation, quantified with a malondialdehyde (MDA) assay, and that peroxidation can be inhibited by passivation of the NP surface with an alumina-silica shell or the presence of Trolox, an antioxidant. Importantly, a protein corona has a similar inhibitory effect, slowing lipid peroxidation. We used super-resolution fluorescence microscopy to image the protein corona formed on the surface of TiO_2 NPs and observed small clusters of proteins, rather than a diffuse layer. The protein corona is displaced by free proteins over a 24 hr period. The clustering and dynamic nature of the protein corona suggests that inhibition of lipid peroxidation will be incomplete. This is in agreement with our observation that lipid peroxidation is similar to that of bare TiO_2 NPs at 24 hours. Interestingly, lipid peroxidation does not correlate with cytotoxicity, pointing towards a more complex pathway for cell death.

5.2 Results and Discussion

5.2.1 Bare TiO_2 NPs Oxidize the Plasma Membrane

HeLa cells incubated with TiO_2 NPs (124 μg/mL, 12 hrs), in the absence of serum proteins, show the majority of NPs bound to the cell surface with some possibly internalized into the cells (Figure 23a). Based on our previous work examining TiO_2 NP-induced protein oxidation,[124] we hypothesized that TiO_2 NP-induced lipid peroxidation of the plasma membrane could result from these TiO_2 NPs lacking a protein corona. A MDA assay was used to measure lipid peroxidation following incubation of HeLa cells with TiO_2

NPs (400 μg/mL, scaled for consistent NP:cell ratio) at 2 hours, 4 hours, 6 hours, and 12 hours. MDA is a cellular product of lipid peroxidation.[125-127] The reaction of MDA with thiobarbituric acid leads to a colored product (Abs: 540 nm) that allows quantification of lipid peroxidation normalized against protein concentration (Abs: 280 nm). The lipid peroxidation of cells incubated with bare TiO_2 NPs was compared to cells cultured in only minimum essential medium (MEM). Previous work from our lab showed that the lack of serum proteins in the cell culture media for this period of time did not affect cell health (86% viability compared to 100% with FBS present, no significant difference).[50] Following incubation of HeLa cells with TiO_2 NPs for up to 4 hours, no significant difference was observed in MDA concentration (Figure 23b). After a 6 hour incubation, the MDA concentration increased to 0.27 ± 0.01 nmol MDA/mg protein, compared to 0.15 ± 0.03 nmol MDA/mg protein, demonstrating TiO_2 NP-induced lipid peroxidation of the plasma membrane. At 12 hours, lipid peroxidation was similar, 0.28 ± 0.05 nmol MDA/mg protein, compared to 0.18 ± 0.03 nmol MDA/mg protein.

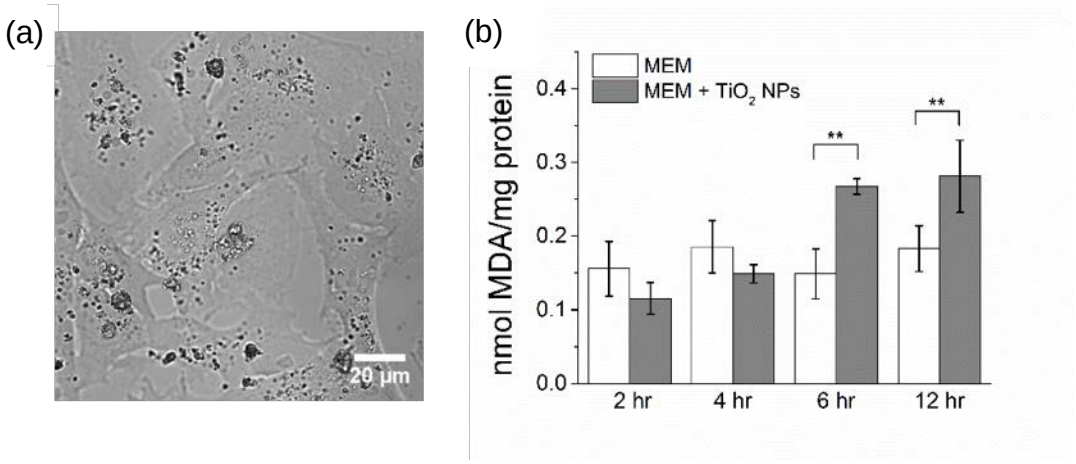

Figure 23 Cellular response to TiO_2 NPs. (a) Brightfield microscopy image of HeLa cells incubated with TiO_2 NPs (124 μg/mL, 12 hrs, MEM). (b) Lipid peroxidation following the incubation of HeLa cells with TiO_2 NPs (400 μg/mL, concentration scaled for consistent NP:cell ratio) was quantified by a MDA assay. Error bars show standard deviation for n=3 distinct experiments. **p<0.01

5.2.2 Lipid Peroxidation is Inhibited by Serum Proteins, Surface Passivation, and a ROS Scavenger

Previous MTT assays of mitochondrial activity from our lab had shown that bare TiO_2 NPs (270 μg/mL) were cytotoxic with a decrease to 57% viability over 24 hrs.[50] In comparison, the same concentration of TiO_2 NPs did not decrease cell health when serum proteins were present. To determine if serum proteins inhibited lipid peroxidation, MDA assays were repeated in the presence of 10% FBS, a standard concentration for culturing cells. In the presence of 10% FBS, no TiO_2 NP-induced lipid peroxidation was observed (Figure 24). This experiment showed that serum proteins inhibit lipid peroxidation in comparison to bare TiO_2 NPs. The underlying cause of NP-induced lipid peroxidation is expected to be ROS generation by the NPs. It is important to note that these TiO_2 NPs produce low levels of ROS,[124, 128] even in the absence of UV light. To confirm the link

between ROS generation and lipid peroxidation, we tested two methods of ROS inhibition; TiO_2 NP surface passivation and the addition of Trolox, a biocompatible antioxidant. The TiO_2 NPs were passivated with an alumina-silica shell, confirmed with XPS, that prevents ROS formation.[124] A MDA assay, in the absence of serum proteins, shows that this surface passivation inhibits lipid peroxidation (Figure 24). Similarly, supplementing the cell culture medium (MEM) with Trolox (0.5 mM, 12 hr) also inhibits lipid peroxidation (Figure 24).

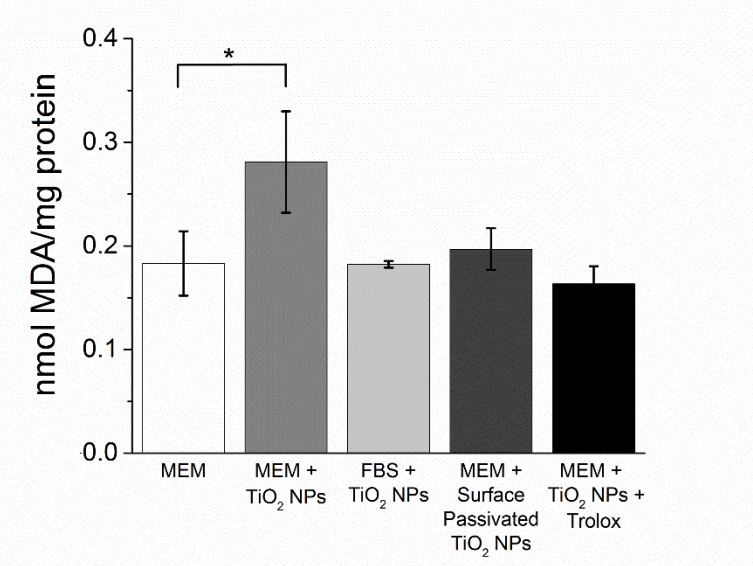

Figure 24 TiO_2 NP-induced lipid peroxidation is inhibited by supplementing MEM with 10% serum proteins (FBS + TiO_2 NPs, light gray), surface passivation of the TiO_2 NPs (dark gray), and a ROS scavenger (Trolox, black). All treatments used 400 μg/mL TiO_2 NPs and 12 hr incubations. MEM (white) and MEM + TiO_2 NPs (gray) are replotted from Figure 1 for comparison. Except for the bare TiO_2 NPs (gray), no significant changes were observed compared to MEM in the absence of NPs. Error bars show standard deviation for n=3 assays. *p<0.05

5.2.3 Serum Proteins Slow Lipid Peroxidation

Serum itself is an antioxidant.[129-130] It is important to determine if the adsorbed proteins on the surface of the NP, in addition to the free proteins, can serve as a surface-specific antioxidant. Serum proteins interact directly with NPs in two ways; as a highly dynamic, weakly bound, soft corona or as a tightly bound hard corona.[50, 92-93, 131-133] We first used super-resolution fluorescence microscopy to characterize the distribution of a hard corona of protein on the surface of TiO_2 NPs (Figure 25a and b). Bovine serum albumin (BSA) was labeled with AlexaFluor647 for STORM imaging.[134-137] In comparison to conventional fluorescence microscopy (Figure 25a), STORM provides sub-diffraction images (Figure 25b), allowing us to resolve proteins on the NP surface. These images showed that BSA is distributed in clusters of BSA molecules (47.5% of clusters consisting of 10-20 localizations/cluster; localizations are proportional to the number of proteins; Figure 26) on the surface of the TiO_2 NPs, rather than an evenly distributed layer. Similar clustering, of both albumin and complement C3, was observed on the surface of mesoporous silica NPs also using STORM super-resolution fluorescence microscopy.[70]

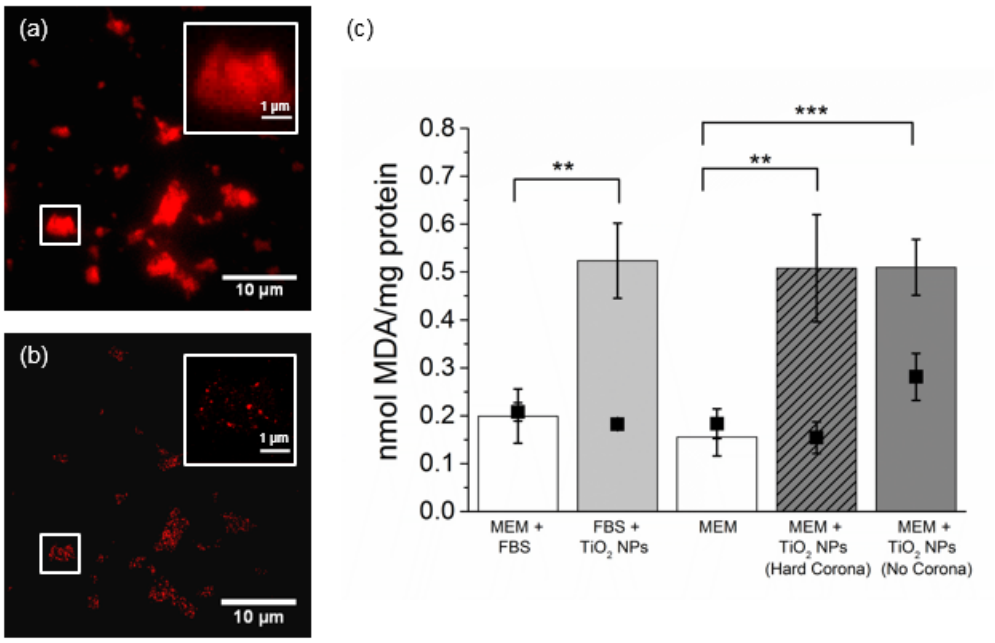

Figure 25 A protein corona slows lipid peroxidation. (a) Conventional epi-fluorescence microscopy image of BSA (red) adsorbed on the surface of TiO_2 NPs. (b) A super-resolution fluorescence microscopy image (STORM) shows that BSA (red) is clustered on the TiO_2 NP surface. The inset is representative of 56 particles. (c) A MDA assay was used to quantify lipid peroxidation following incubation of HeLa cells with TiO_2 NPs (400 μg/mL TiO_2 NPs) following 12 hr (black squares) and 24 hr (bars) incubations in the absence of NPs (MEM+FBS and MEM, white), in MEM supplemented with 10% FBS resulting in the formation of a hard and soft corona (gray), a hard corona (striped), or bare TiO_2 NPs (dark gray). 12 hr data, with the exception of MEM+FBS and TiO_2 NPs with a hard corona, is replotted from Figure 2 for comparison. Error bars show standard deviation for n=3 assays. p-values are shown for 24 hr data. **p<0.01, ***p<0.001

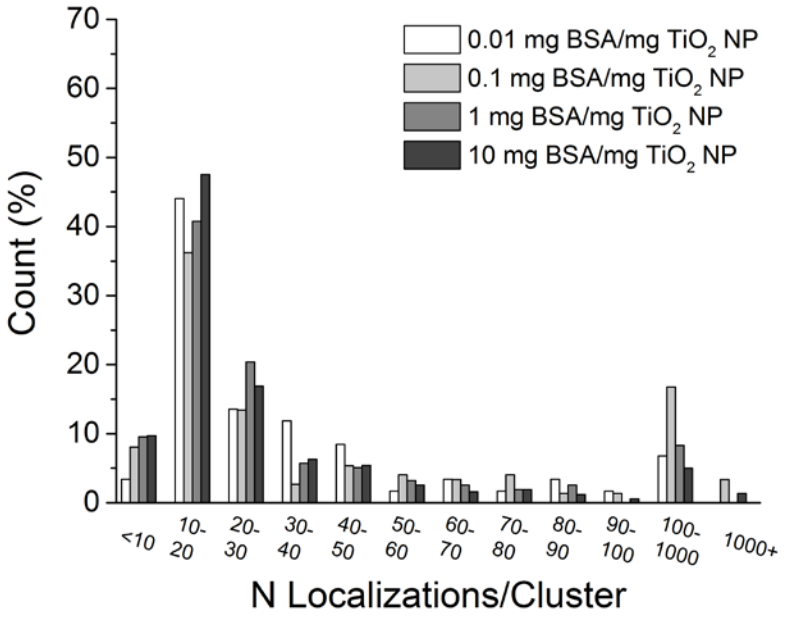

Figure 26 Protein clustering analysis of 0.01-10 mg BSA/mg TiO_2 NPs. Protein distributions were similar at all concentrations, with 47% of clusters having 10-20 localizations per cluster.

To determine if this hard corona was sufficient to prevent lipid peroxidation, TiO_2 NPs were incubated with 10% FBS for 30 min. Unbound and weakly bound proteins were removed by centrifugation (8,000 rcf, 15 min, x3, Figure 27) and the TiO_2 NPs (400 μg/mL), with the associated hard corona, were added to cells in MEM for a 12 hr incubation.

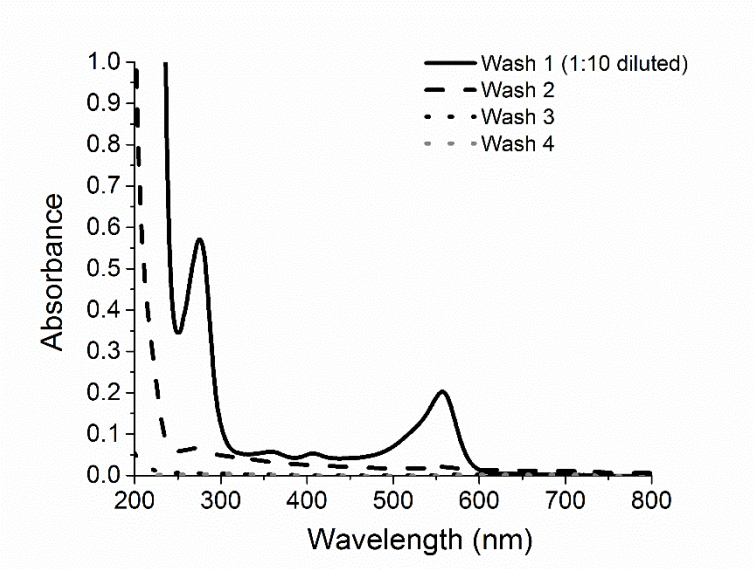

Figure 27 Unbound and weakly bound proteins were removed from TiO_2 NPs by repeated centrifugation (8,000 rcf, 15 min) and resuspension of the TiO_2 NPs, with a tightly bound hard corona, in water. The UV-vis absorption spectrum of the supernatant is shown at each wash step. Three wash steps were used prior to experiments using a hard corona. A 4th wash (gray, dotted) is plotted for comparison. The peak at 557 nm is the phenol red used in cell culture medium.

A MDA assay shows that a hard corona is sufficient to inhibit lipid peroxidation at 12 hrs with no significant difference between a hard corona and cell culture medium supplemented with 10% FBS (Figure 25c). However; MDA assays following 24 hr incubation with TiO_2 NPs, both with 10% FBS present and only a hard corona, shows that lipid peroxidation at this longer time is independent of protein corona or free serum proteins in solution (Figure 23c). Similar results were obtained with a second cell line (Figure 28), human epithelial lung cells (A549).

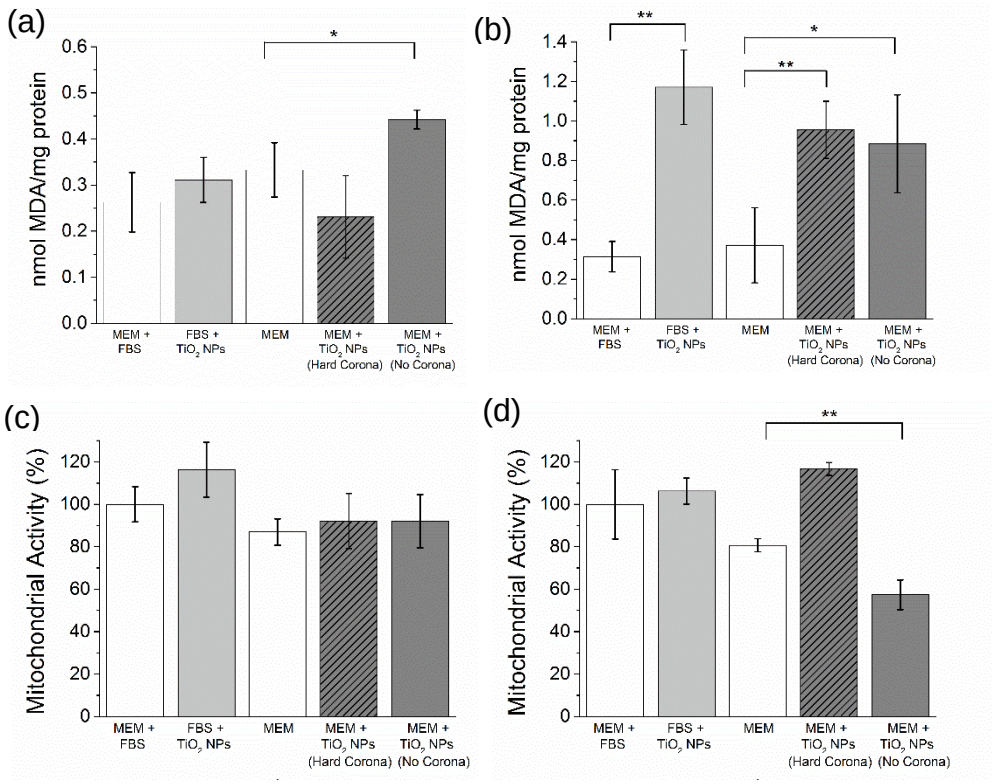

Figure 28 Lipid peroxidation and cytotoxicity in A549 cells. (a) A MDA assay was used to quantify lipid peroxidation following incubation of A549 cells with TiO_2 NPs (1.1 mg/mL TiO_2 NPs) following 12 hr incubations in the absence of NPs (MEM+FBS and MEM, white), in MEM supplemented with 10% FBS resulting in the formation of a hard and soft corona (gray), a hard corona (striped), or bare TiO_2 NPs (dark gray). (b) Identical experiments following a 24 hr incubation. Error bars show standard deviation for n=3 assays. *p<0.05, **p<0.01, ***p<0.001 (c) Cell health was quantified by a MTT assay following a 12 hr of A549 cells with TiO_2 NPs (744 μg/mL) in the presence of 10% FBS (MEM+FBS, light gray) and only a hard corona (striped gray) in comparison to MEM in the absence of serum proteins (MEM, white). MEM+FBS was normalized to 100%. (d) Identical cell health experiments following a 24 hr incubation. Error bars show standard deviation for n=3 assays. **p<0.01, all other comparisons were not significant.

At 12 hrs, the hard corona inhibits lipid peroxidation, but at 24 hrs lipid peroxidation by TiO_2 NPs with a hard corona (0.51 ± 0.11 nmol MDA/mg protein) is identical to that observed for bare TiO_2 NPs (0.51 ± 0.06 nmol MDA/mg protein) (Figure 25c). While the hard corona is conventionally defined as the adsorbed proteins that are tightly bound to the

NP surface, efforts to quantify the difference in hard and soft coronas has been limited.[125, 138-143] To determine if the hard corona on these TiO_2 NPs could be displaced over a 24 hr period, we fluorescently labeled the mixture of proteins in FBS with AlexaFluor647 and used these fluorescent proteins to form a hard corona, identical to the formation of the hard corona described above (Figure 25a, b). We then imaged the hard corona with the NPs at 10 min, 6 hr, 12 hr, 18 hr, and 24 hr in the presence and absence of unlabeled 10% FBS (Figure 29), similar to an approach used previously with polystyrene NPs.[60]

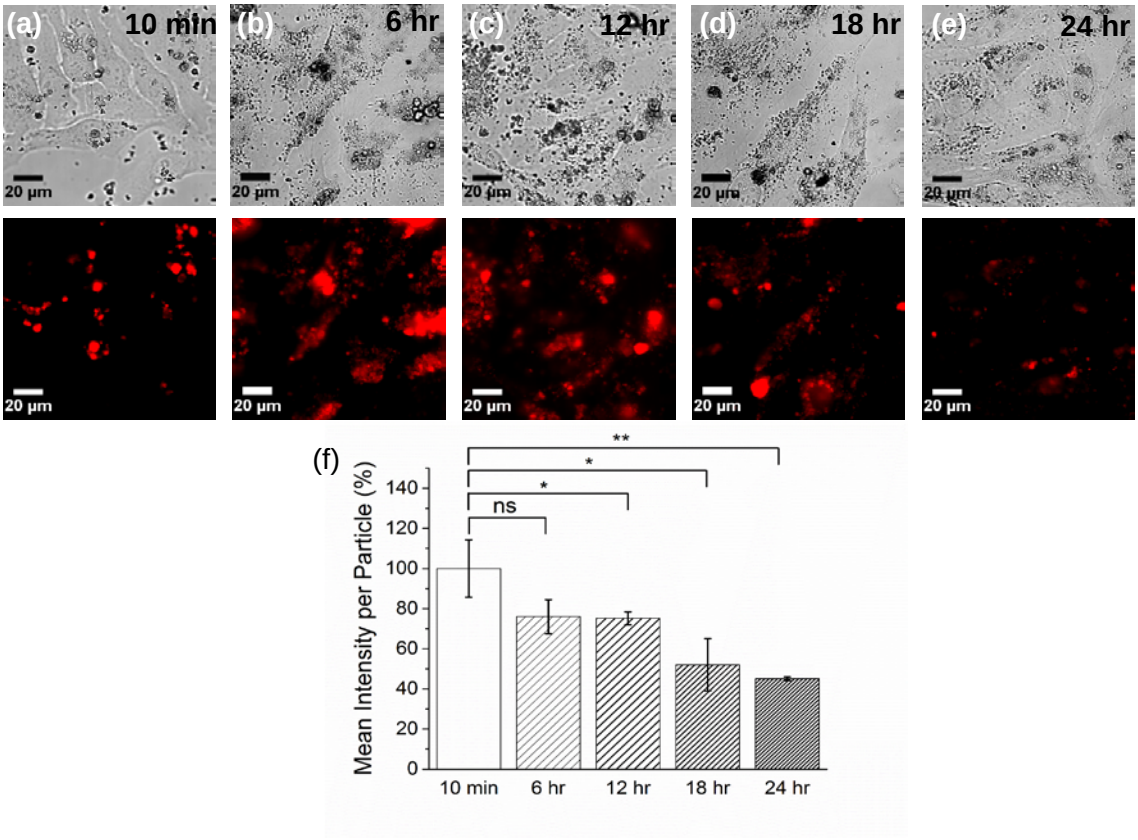

Figure 29 Displacement of hard corona proteins from the surface of TiO_2 NPs as a function of time, in the presence of unlabeled 10% FBS. (a) Representative brightfield microscopy image (top) and fluorescence microscopy image (bottom) and showing AlexaFluor647-labeled FBS (red) adsorbed on TiO_2 NPs and incubated with HeLa cells at 4 °C for 10 min. (b) 6 hour incubation at 37 °C. (c) 12 hour incubation at 37 °C. (d) 18 hour incubation at 37 °C. (e) 24 hour incubation at 37 °C. (f) Average mean intensity/particle at each time point. Ten NPs or NP aggregates, from three images at each time point, were used for analysis (n=30). *p<0.05, **p<0.01

If the fluorescent hard corona is displaced by unlabeled FBS, we expect to observe a decrease in the fluorescent intensity of the NPs. Following a 10 min cold binding at 4° C, the fluorescently-labeled proteins are adsorbed on the surface of the TiO_2 NPs, with the fluorescence intensity normalized to 100% (100 ± 14.3%, n=30 NPs or NP aggregates from 3 images) with the TiO_2 NPs visible in the corresponding brightfield images. At 12 hrs, the average fluorescence intensity decreases to 75.2 ± 3.2% (n=30). At 18 hrs and 24 hrs, fluorescence intensity decreases further (52.0 ± 13% and 45.0 ± 1.0%, respectively, n=30), suggesting that the free, unlabeled, FBS displaces the hard corona. In comparison, the same experiment carried out in MEM, in the absence of unlabeled protein, showed no decrease in fluorescence intensity at 24 hrs (93.8 ± 12.4%, n=30, Figure 30).

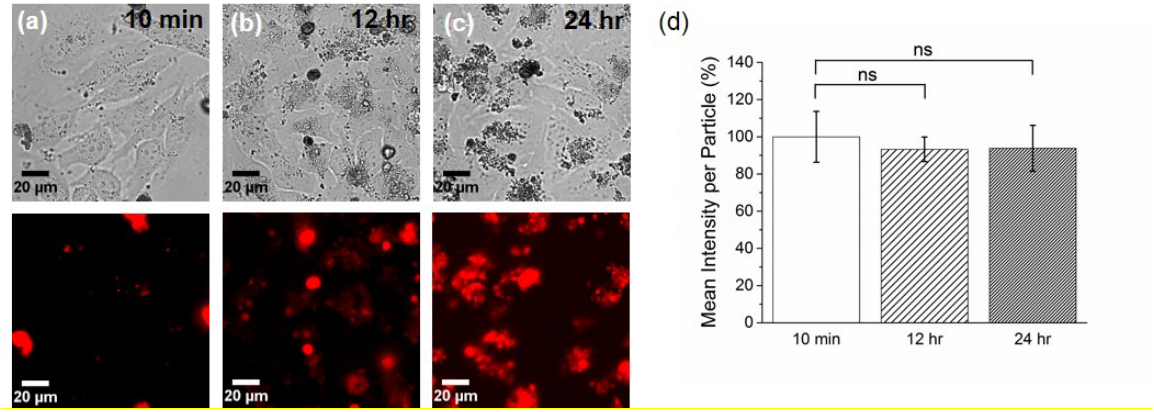

Figure 30 Hard corona on the surface of TiO_2 NPs as a function of time in the absence of free serum proteins. (a) Representative brightfield microscopy image (top) and fluorescence microscopy image (bottom) showing AlexaFluor647-labeled FBS (red) adsorbed on TiO_2 NPs and incubated with cells at 4 °C for 10 min. (b) 12 hour incubation at 37 °C. (c) 24 hour incubation at 37 °C. (d) Average mean intensity/particle at each time point. Ten NPs, or NP aggregates, from three images at each time point, were used for analysis.

5.2.4 Bare TiO_2 NPs are Cytotoxic

Our initial interest in understanding TiO_2 NP-induced lipid peroxidation stemmed from the observation that at 24 hrs TiO_2 NPs (270 μg/mL) did not damage cells when serum proteins were present, but were cytotoxic in the absence of serum proteins.[50] A control experiment showed that the lack of serum proteins in the cell culture media did not affect cell health (86% viability compared to 100% with 10% FBS present, no significant difference).[50] The results described above demonstrate that bare TiO_2 NPs oxidize the lipids of the plasma membrane (Figure 24 and 25c). Serum proteins, even a hard corona, slows lipid peroxidation, but at 24 hrs lipid peroxidation is observed in response to any form of TiO_2 NP incubation (Figure 25c), suggesting a more complex relationship between lipid peroxidation and cell health. A MTT assay of mitochondrial activity was used as a measure of cell health following incubation of cells with TiO_2 NPs (270 μg/mL) for 12 hrs and 24 hrs (Figure 31). Cells cultured in MEM supplemented with 10% FBS was used as a positive control for cell health and normalized to 100%. At both 12 hrs and 24 hrs, with a hard corona present on the TiO_2 NPs, no decrease in cell health was observed compared to a control in the absence of NPs (MEM alone, Figure 31). In comparison, at 12 hrs, bare TiO_2 NPs were slightly cytotoxic (71.4 ± 9.1% viability) compared to cells cultured in only MEM (88.8 ± 3.3% viability). At 24 hours, bare NPs show a further decrease in viability (57%),[50] while cells incubated with TiO_2 NPs with a hard corona remain healthy (96.5 ± 9.8% viability) (Figure 31). Taken together, these results show that at 24 hrs TiO_2 NPs with a hard corona, which is dynamic and displaced by free proteins (Figure 29), does oxidize the lipids of the plasma membrane, but that this lipid peroxidation is not cytotoxic (Figure

31). This result points towards the possibility of a cellular response capable of mitigating the effects of lipid peroxidation.

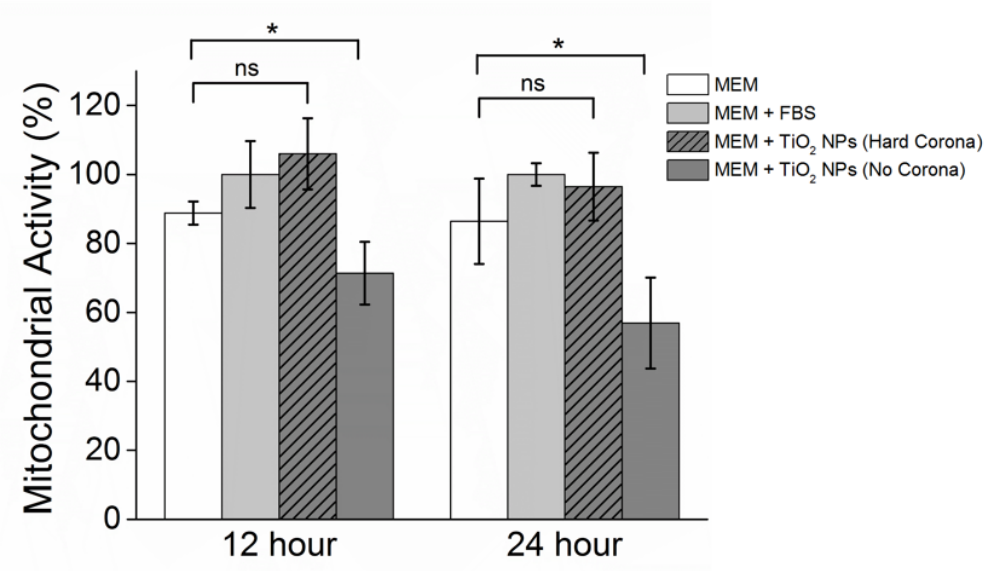

Figure 31 TiO_2 NP-induced cytotoxicity. (a) Cell health was quantified by a MTT assay following a 12 hr or 24 hr incubation of HeLa cells with TiO_2 NPs (270 µg/mL) in the presence of 10% FBS (MEM+FBS, light gray) and only a hard corona (striped gray) in comparison to MEM in the absence of serum proteins (MEM, white). MEM+FBS was normalized to 100%. The data for bare TiO_2 NPs (MEM/TiO_2 NPs, dark gray) at 24 hrs is replotted from Ref. 10. Error bars show standard deviation for n=3 assays. ns=not significant, *p<0.05

5.3 Conclusions

TiO_2 NPs, in the absence of serum proteins, bind to the surface of cells and oxidize the lipids of the plasma membrane, determined by MDA assay for both HeLa and A549 cells (Figure 25c and Figure 28). Similar lipid peroxidation in response to TiO_2 NPs has been observed previously for a range of cell types including human bronchial epithelial cells,[45] red blood cells,[144] brains of mice,[145-147] and the liver, brain, and gills of carp.[148] Lipid peroxidation is not unique to TiO_2 NPs, and has also been detected in response to nano-C_{60},[82] gold NPs (20 nm),[149] cerium oxide NPs (20 nm),[150] and single-walled carbon nanotubes.[151] Unique to these experiments is the focus on the role of the protein corona in

this oxidative response. Lipid peroxidation is inhibited by passivation of the TiO_2 NPs with an alumina-silica shell and the addition of Trolox, a radical scavenger, to the cell culture media (Figure 24). These are both treatments that reduce ROS production. Supplementing the cell culture medium with 10% FBS leads to a similar reduction in lipid peroxidation with the serum proteins in solution serving as antioxidants (Figure 24).[129-130] Super-resolution fluorescence microscopy (Figure 25a and b) shows that the hard corona that forms on the surface of the TiO_2 NPs is better described as protein clusters, rather than a diffuse layer of proteins. These protein clusters slow the oxidation of the plasma membrane with peroxidation levels (0.15 ± 0.03 nmol MDA/mg protein) similar to that of TiO_2 NPs in MEM supplemented with 10% FBS (0.18 ± 0.003 nmol MDA/mg protein, Figure 25c) at 12 hrs. At 24 hrs, increased levels of lipid peroxidation are observed for TiO_2 NPs, independent of serum proteins (Figure 25c). It is possible that the protein corona, even in the form of clusters, slows lipid peroxidation by reducing the surface area of the bare TiO_2 NPs in contact with the plasma membrane. In addition, the displacement of the hard corona proteins over 24 hours shows that even a hard corona is dynamic (Figure 29). It is important to note that free proteins are required to displace adsorbed proteins (Figure 30). The similar levels of lipid peroxidation at 24 hrs for a soft corona (10% FBS), a hard corona with no free protein for displacement, and bare TiO_2 NPs (Figure 25c) points towards the relative magnitude and kinetics of this process. For both the hard and soft corona, ROS will oxidize adsorbed proteins, but this process, even with the exchange of proteins, likely does not deplete all ROS. Over longer times (24 hrs), it is possible that ROS concentration exceeds the protective effect of the protein corona and that low levels of ROS present throughout the 24 hr period have a cumulative effect on lipid peroxidation. Interestingly, cytotoxicity

does not correlate with lipid peroxidation. At 24 hrs, similar levels of lipid peroxidation are observed for bare TiO_2 NPs, TiO_2 NPs with a hard corona, and TiO_2 NPs in 10% FBS, leading to both a hard and soft corona.[124] Only the bare TiO_2 NPs lead to decreases in cell viability, suggesting the length of exposure, rather than just exposure level, may be an important parameter in understanding NP-induced oxidative stress and points towards the complexity of NP-induced cytotoxicity.[152-153]

CHAPTER 6. CONCLUSIONS AND FUTURE WORK

6.1 Conclusions and Outlook

Given the prevalence of titanium dioxide nanoparticles (TiO_2 NPs) in applications that range from aesthetics to photocatalysis, exposure to these nanoparticles through inhalation and ingestion must be addressed. We investigated the oxidative stress response in human cervical cancer cells, and other cell lines, after incubation with a non-cytotoxic concentration of TiO_2 NPs. Cellular oxidative stress is characterized by an imbalance in reactive oxygen species (ROS).[35] ROS capture and quantification within cells remains difficult due to their turnover rate, location, and limited methods of detection and resolution. To bypass these limitations, a measure of oxidative stress can be characterized by changes in gene expression for oxidative stress-related enzymes. These enzymes are implicated in numerous pathways to reduce or oxidize ROS. Four members of the peroxiredoxin family of anti-oxidant enzyme were found to be either up- or down-regulated in response to TiO_2 NPs. This response is specific to TiO_2 NPs, and polystyrene nanoparticles do not induce any changes in peroxiredoxin concentrations. We further examined this intracellular response by means of the protein corona. The TiO_2 NP protein corona was characterized by proteomics, spatial mapping, and confirmation of its oxidative modifications. We observed that an oxidized corona led to oxidative stress (Table 2, Figure 18 and 32).

NP-protein interactions contribute to a complex and dynamic system (Figure 32). Corona proteins were observed to dissociate off the NP surface over time. This, coupled with incomplete surface coverage, resulting “bare patches” add to the complexity of investigating nanomaterial-cell interactions. Lipid peroxidation of the plasma membrane was observed in both the presence and absence of serum proteins, suggesting that serum proteins slow down lipid peroxidation but not inhibit it.

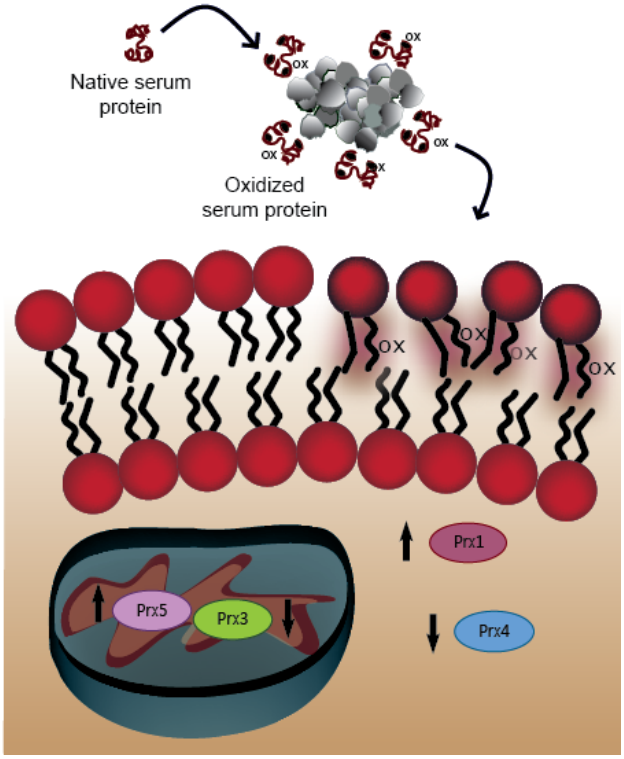

Figure 32 Oxidative stress and damage by titanium dioxide nanoparticles. TiO_2 NPs oxidize serum proteins, creating an oxidized corona, which induces oxidative stress as seen by changes in expression of peroxiredoxins. TiO_2 NPs induce lipid peroxidation, leading to an oxidized plasma membrane.

The oxidation of serum proteins and the plasma membrane can be attributed to ROS production by the TiO_2 NP in the absence of light. This phenomena was correlated back to

surface defects, mainly oxygen vacancies, that naturally occur on both industrial and food grade TiO_2 NPs.

This dissertation has addressed the oxidative stress response with regards to the protein corona. These findings confirm the protein corona mediates the cell-NP interaction and plays a fundamental role in cellular outcomes.

6.2 Future Work

6.2.1 Serum Protein Specificity

With the addition of TiO_2 NPs, the model *in vitro* setting which we explored can be characterized as a multi-component system, where bio-macromolecule oxidation and oxidative stress occur. While we explored the oxidation of the protein corona, there are many distinct connections between an oxidized corona and biological pathways left to be explored. The series of events that lead to the gene expression of peroxiredoxins were found to be triggered by an oxidized corona. The subsequent steps are yet to be addressed or known. To narrow down an affected biological pathway leading to oxidative stress, it is crucial to know if a specific protein on the corona or multiple corona proteins trigger a response through binding to a specific cellular receptor.

Initial studies used bovine serum albumin (BSA) as a possible corona protein of interest. BSA, the most abundant protein in serum,[130] was present in the hard corona of TiO_2 NPs (Section 3.2.5). Should a BSA corona trigger oxidative stress, we would expect changes in the peroxiredoxins when Hela cells are incubated with TiO_2 NPs in MEM supplemented with 10% BSA. A preliminary western blot observed no changes in

peroxiredoxin 1 (prx1) upon 24 hour incubation with 400 μg/mL TiO_2 NPs in MEM + 10% BSA. A 10% BSA volume has a concentration of 3 mg/mL BSA. No significant changes were detected between cells grown in 10% BSA and 10% BSA with nanoparticles, indicating that BSA is not the protein of interest that mediates the oxidative stress response (Figure 33).

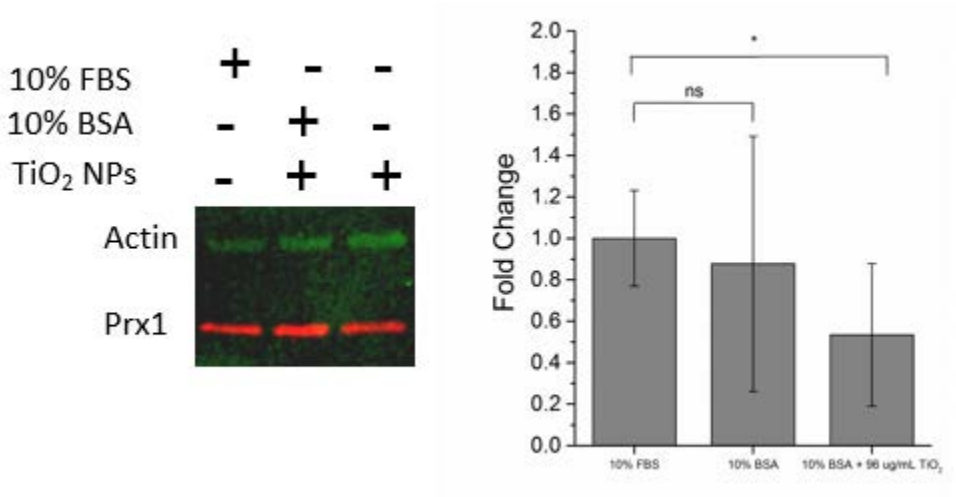

Figure 33 Changes in peroxiredoxin 1 (prx1) in response to bovine serum albumin and TiO_2 NP incubation. Western blot of prx1 under 10% FBS, 10% BSA, and 10% BSA + 400 μg/mL TiO_2 NPs (left). Quantification of western blots in triplicate (right).

6.2.2 A Kinetic Study of TiO_2 NPs in the Absence of Ultraviolet Light.

6.2.2.1 Introduction

TiO_2 NPs are well-studied for their photocatalytic properties. Interestingly, our experiments suggest that TiO_2 NPs can generate low levels of reactive oxygen species (ROS) in the absence of ultraviolet light (Chapter 4). A proposal of future experiments include laying the groundwork to determine whether the NPs react in a catalytic or stoichiometric fashion to produce ROS.

As a first step, we measured ROS production using the 2',7'-dichlorodihydrofluorescein (H_2DCF) fluorescent probe in both the presence and absence of ultraviolet light. As a second experiment, methylene blue (MB) was selected as a well-established reagent for the measurement of NP photocatalytic activity. This was carried out through the measurement of change in concentration (MB/MB_0) of MB (UV-Vis; 664 nm absorbance) as a function of TiO_2 NP concentration and time.[154-158] MB is stable under exposure to UV light, but does adsorb onto the surface of TiO_2 NPs.[155-158] A decrease in concentration due to adsorption on the NPs must be accounted for during experiments. Experiments were carried out in aqueous solutions at pH 6.6 where MB absorbance can be measured at 664 nm.

6.2.2.2 H_2DCF

Our previous results detected ROS production by TiO_2 NPs using the general ROS probe H_2DCF after one hr (Figure 11a). We used the fluorescent probe H_2DCF to observe general ROS production over time by the NPs after UV exposure. It should be noted that the UV lamp is not ideal for this experiments as its spectrum (Figure 34) is not matched to the absorption maxima of the TiO_2 NPs (330 nm).

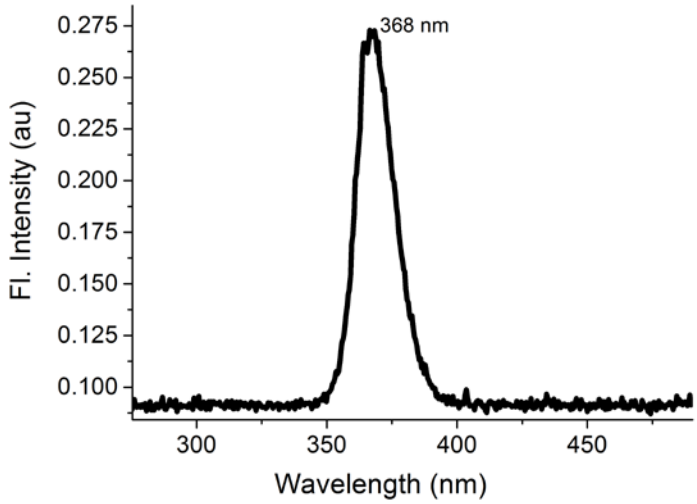

Figure 34 Fluorescence emission of UV lamp used for H_2DCF and MB experiments. Peak fluorescence is 368 nm.

Measurements were taken after every 15 minutes of UV exposure for 135 minutes (Figure 35a). The use of H_2DCF is limited by the auto-oxidation of H_2DCF by UV light, previously observed in literature.[159] To address this issue, H_2DCF was added immediately to TiO_2 NPs after UV exposure. This method limits the reaction to occur with ROS present at the end of each time point as opposed to ROS produced throughout. The use of a second ROS probe, methylene blue (MB) is suggested. MB is insensitive to UV light unlike H_2DCF and is proposed to be used for determining the kinetic profile of ROS production by TiO_2 NPs.[155]

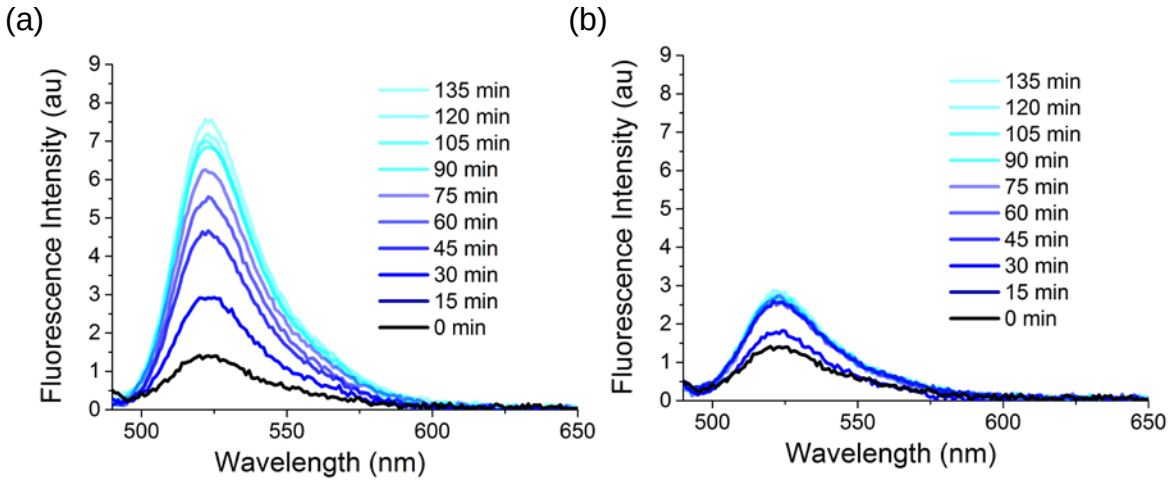

Figure 35 Time dependent fluorescence spectra of H_2DCF by TiO_2 NPs in the presence and absence of UV light. (a) H_2DCF spectra was measured after 15 minute increments of TiO_2 incubation under UV-irradiation for 135 minutes. (b) TiO_2 NPs generate low levels of ROS without UV-irradiation.

6.2.2.3 Methylene Blue (MB)

Unlike H_2DCF, MB is unresponsive to UV light and therefore was used to measure the rate of ROS production by the TiO_2 NPs. Concentration of MB was determined by the absorbance peak at 664 nm.[155] MB also has characteristic peaks in the ultraviolet range at 245 and 292 nm, although these peaks are typically not used quantitatively.

As a first step, we optimized conditions and concentrations by varying concentrations of TiO_2 NPs incubated with 6 μM MB for one hour without external light. A decrease in absorbance is seen after incubation with all NP concentrations (0.01-1 mg/mL). From this, an optimal concentration of 1 mg/mL TiO_2 NPs was used to next examine MB degradation with respect to time.

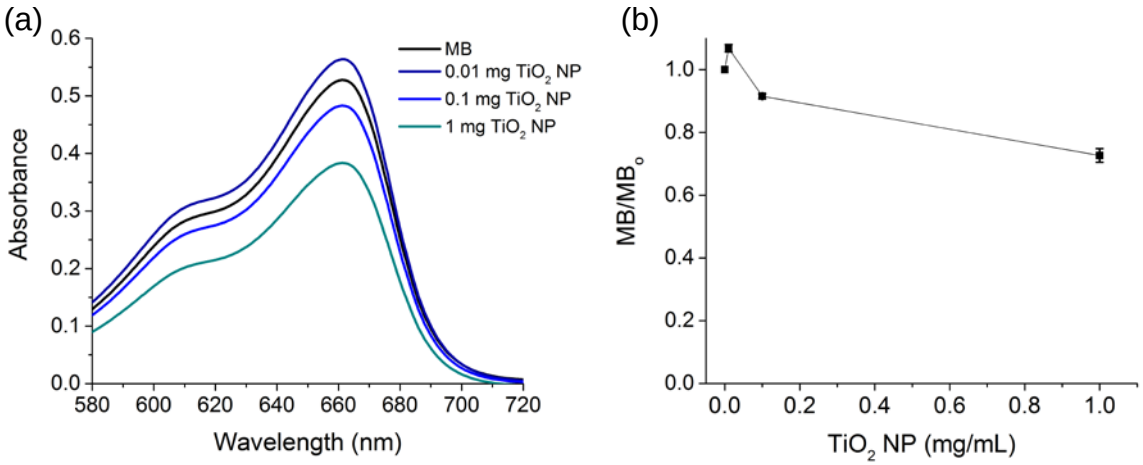

Figure 36 Methylene Blue (MB) degradation after 1 hour incubation with TiO_2 NPs in the absence of UV light. (a) MB was incubated with varying concentrations of TiO_2 NPs. A decrease in absorbance at 664 nm correlates with degradation of MB or adsorption of MB onto the NP surface. (b) Changes in MB concentration plotted as a function of TiO_2 NP concentration in (a).

The observed MB/MB_o with respect to NP concentration (Figure 36b) was not linear, suggesting any adsorption onto or reactivity of the nanoparticle surface with the dye is not stoichiometric. After one hour incubation with 1 mg/mL TiO_2 NPs, MB absorbance measurements decreased to 72 ± 2%. From these results, a 1 mg/mL TiO_2 NP concentration and 6 μM MB concentration is suggested for future experiments.

To further examine MB degradation over time, a kinetic study over two hours examined the degradation of MB by the NPs. As a positive control, we observed the kinetics of this reaction where TiO_2 NPs and MB solutions were exposed to UV light for

varying times. MB degradation was observed after 30 seconds, and the dye was no longer visible after 8 minutes of irradiation (Figure 37a).

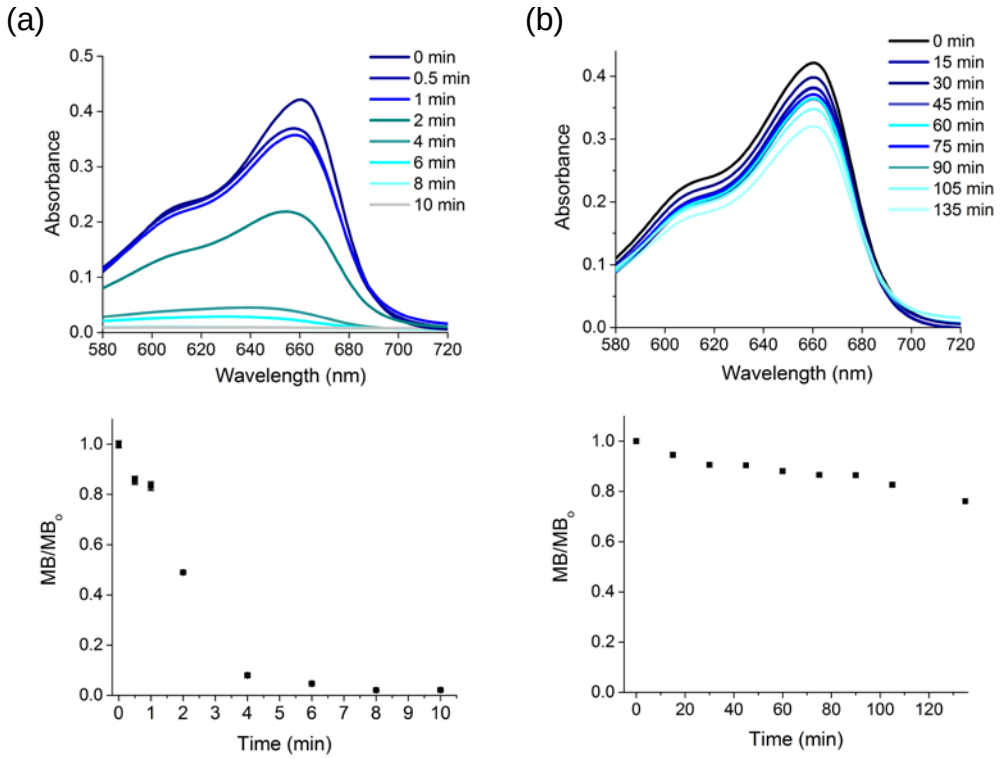

Figure 37 Time dependent methylene blue (MB) degradation by TiO_2 NPs in the presence and absence of UV light. (a) MB concentration decreases by TiO_2 NPs (1 mg/mL) and UV exposure with respect to time (top), characterized by a decrease in absorbance at 664 nm (bottom). (b) MB concentration decreases by TiO_2 NPs (1 mg/mL) in the dark over two hours (top), characterized by a decrease in absorbance at 664 nm (bottom).

The degradation kinetics seen using an MB/MB_0 plot is in agreement with first order kinetics with a rate constant of 0.53 s^{-1}. Similar degradation kinetics are seen by TiO_2 without UV light (Figure 37b) with a rate constant of 0.002 s^{-1}. It is important to note that MB adsorbs onto the NPs. Therefore, the initial drop in MB can be attributed to any ROS-induced degradation and adsorption. To further this experiment, the concentration of MB adsorbed must be determined. The H_2DCF results in the absence of light (Figure 35)

ensures that the MB changes are not attributed to only adsorption, but rather ROS production indeed occurs.

A calculation can be made to relate MB concentration to the specific surface area of TiO_2 NPs. Assuming the surface area of one MB molecule is roughly 62×10^{-20} m^2, this leads to 0.022 m^2 MB adsorbed or degraded by 0.1 mg NPs for 1 hr.[160] Performing the same calculation for 1 mg TiO_2 NPs gives about 0.072 m^2 MB absorbed or degraded.

The proposed experiment includes measuring MB degradation as a function of time with varying TiO_2 NP concentration. Should the NPs react catalytically with MB, we would expect zero-order kinetics. Should the TiO_2 NP react stochiometrically with MB, a non-zero-order rate plot is expected where the rate is dependent on NP concentration. It is also proposed that kinetic experiments be conducted with E171 TiO_2 NPs in the presence and absence of UV light. The MB degradation kinetics in the presence of E171 TiO_2 NPs and UV-irradiation can be cross compared to that of P25 TiO_2 NPs. These studies would be beneficial in tracing the relationship between NP surface area and catalytic activity.

APPENDIX A. EXPERIMENTAL DESIGN AND METHOD SUGGESTIONS

The following appendix lists experimental parameters and details that were incorporated into the work of this dissertation. Future work and experiments conducted can use these optimized conditions and suggestions.

A.1 TiO_2 NP Experiments

A.1.1 Cell Experiments

For NP-cell experiments, TiO_2 NP solutions were made fresh daily in minimal essential medium (MEM) with or without 10% FBS. Storing this solution overnight increases the basicity. Therefore, the solution must be made fresh prior to cell incubation. The NP solution should be wrapped in foil so as to avoid any photoactivation of the NPs by ambient light. The cells should be at ~70-80% confluency at the time of NP addition.

A.1.2 NP Experiments in the Absence of Light

TiO_2 NP experiments performed in the dark were carried out by addition of the NPs in the desired media (water, PBS, or MEM ± 10% FBS) inside plastic tubes (Eppendorf or Falcon) wrapped in foil and under constant vortexing. For protein oxidation, insufficient vortexing can lead to insufficient contact between the NP and proteins and increased variability in reproducibility.

A.2 Stochastic Optical Reconstruction Microscopy (STORM)

STORM experiments were conducted at the Institute for Photonic Sciences in Castelldefels, Barcelona, Spain. Imaging was performed on a commercial Nikon setup using a 100x oil-immersion objective, 1.49 NA. For sample preparation, BSA was labelled with AlexaFluor647 at a 1:1 ratio. An over-labeled (more than 1 fluorophore per protein) sample is advised against since this will require a longer photobleaching time. After NP-protein incubation and wash steps, the NP-protein pellet samples need to be re-dispersed in 100 μL of Millipore water and transferred to an 8-well borosilicate glass chamber with 0.13-0.17 mm thickness and allowed two minutes to adhere. The sample must be washed at least six times with Millipore water to remove unbound NPs and the excess dissociated proteins that adhere onto the substrate. 100 μL of imaging buffer (5% glucose, 1% glucose oxidase/catalase, and 10% ethanolamine) is an adequate volume to add to the substrate prior to imaging. Ethanolamine buffer should be made fresh in 6 M HCl.

NP samples should be imaged the day of preparation, and imaging buffer should be made fresh daily.

Photobleaching prior to imaging takes between one and five minutes depending on the fluorophore concentration. Activation of the AlexaFluor647 was performed through a series of one 20 ms exposure activation frame of 488 nm, followed three collection frames at 652 nm. About 30,000 collection frames were taken for each dSTORM image. Collection files are saved as either .dax or .nd2 files. Both are compatible with Insight3 v4.29.1, the software used to compile and reconstruct dSTORM images.

A drift correction must be administered prior to analysis under the STORM tab of Insight3. This automatically corrects for any drift in sample by dividing each .dax or .nd2 file into bins of 100 frames and performing a localization-based drift correction.

For analysis, the CCD baseline, CCD pixel size, and photons per count value must be input. These values were predetermined by the commercial company to be 157, 600, and 0.41, respectively. A simple Gaussian fit model was used with a minimum width of 200 nm and maximum width of 400 nm. The resulting STORM image should be saved as a .bin file. Each individual cluster size and fluorescence can be evaluated using the Fiji software. To find clusters and clustering patterns, a script written by Joe Bordley was used. Variables to input include the height and width of the image as well as cluster definition parameters. These parameters are variable, but it is necessary to define what a protein cluster is. To find the clusters and clustering patterns, a region of interest and threshold must be defined. The STORM images in this dissertation have a region of interest of 5x5 pixel area. To further consider a cluster, a threshold value for three was given. This means that the sum of the pixels of each ROI must be greater than 3 for it to be considered a cluster.

A.3 Proteomics

HPLC-MS/MS proteomics was carried out by Bioproximity using a Q-Exactive Orbitrap mass spectrometry. For analysis, 20 milligrams of protein is sufficient. To isolate the corona from the NP for analysis, the NP-protein pellet should be run on a gel (230 V, 5 minutes) to separate the NPs from the proteins. The resolved band can then be excised

with a razor blade, placed in an Eppendorf tube with 0.5% acetic acid solution, and mailed out for analysis.

Proteomics was repeated with similar results at the Georgia Tech Systems Mass Spectrometry Core. The following protocol was written by Dr. David Smalley and used for analysis of the excised band: 200 µL of an 8 M urea/100 mM ammonium bicarbonate solution was added to the protein sample to dissolve the sample followed by 16 µL of 1 M DTT to further denature the proteins. The mixture was incubated at room temperature for 30 min, followed by the addition of 64 µL of 0.5 M indole-3-acetic acid. The sample was incubated in the dark for 30 min. Another 16 µL of 1 M DTT was added, and after 30 minutes, 840 µL of 100 mM ammonium bicarbonate was added. The sample was trypsinized (3 µg in 100 mM ammonium bicarbonate) and incubated overnight at 37 ^{o}C. The pH was adjusted to be less than 4 using acetic acid. The protein supernatant was removed from the beads and dried using a vacuum concentrator. 100 µL water was added to 33 µL of the sample and desalted using a Pierce C18 Spin Column. The sample was dried and 20 µL of 2% acetonitrile/0.1% formic acid was added prior to mass spectrometry.

Protein abundance is determined by computing the total spectral counts for each protein. The protein identities, molecular weights, and functions can be found on the UniProt database. Actin and keratin are artifacts of contamination and their spectral counts are discarded in the analysis. It is important to note that many proteins have multiple isoforms. For the analysis in this dissertation, the spectral count for all isoforms of a given protein were combined to determine abundance of that protein.

A.4 Reverse Transcriptase Polymerase Chain Reaction (RT-PCR)

Gene expression is highly dependent on cell type, health, culture condition, passage number, and confluency among others. RT-PCR should be performed for low passage cells (below passage ~20) although this may be hard to concretely determine. Each experiment should be performed in triplicate over cells at the same passage number. Cells should not be overconfluent, and, if treated with NPs, should be washed at least six times to remove all excess unbound NPs, as they may interfere with the RNA isolation steps.

RNAse Away should always be used on gloves, lab benches, pipette tips, and tube holders near samples. All dilution steps should be performed with nuclease free water. Autoclaved Millipore, distilled, or tap water all contain RNAse which will degrade nucleic acids. RNA elution should be carried out in 30 μL nuclease-free water. RNA concentration should be determined using a NanoDrop. An absorbance peak at 230 nm is indicative of salts or contaminants. An ideal sample should have an Abs_{260}/Abs_{230} greater than 2. For $1x10^6$ cells, about ~1000 ng/μL RNA yield correlates to a well performed RNA isolation. Conversion to cDNA must be performed directly after RNA isolation. RNA is single-stranded and not as stable as DNA. DNA samples should be stable in -20 ^oC for one week. Samples should always be kept on ice, covered from light and protected from biological contaminants.

Data analysis can be performed via Excel, or through the Qiagen data analysis center. Output values are given in C_T, or threshold cycle values. A value above 35 indicated poor cDNA concentration and is discarded. Ideal C_T values range roughly between 9 and 22. These C_T values for housekeeping genes are averaged and used to normalize gene of

interest C_T values, and should therefore should be roughly identical or in close proximity to each other. Variances in C_T values for housekeeping genes indicate varying cell passage numbers, contamination, or insufficient starting cDNA concentrations.

REFERENCES

1. Bell, N. J.; Yun, H. N.; Du, A. J.; Coster, H.; Smith, S. C.; Amal, R., Understanding the Enhancement in Photoelectrochemical Properties of Photocatalytically Prepared TiO_2-Reduced Graphene Oxide Composite. *J Phys Chem C* **2011,** *115* (13), 6004-6009.

2. Chen, X.; Mao, S. S., Titanium dioxide nanomaterials: Synthesis, properties, modifications, and applications. *Chem Rev* **2007,** *107* (7), 2891-2959.

3. Gazquez, M. J.; Bolivar, J. P.; Garcia-Tenorio, R.; Vaca, F., Physicochemical Characterization of Raw Materials and Co-products From the Titanium Dioxide Industry. *J Hazard Mater* **2009,** *166* (2-3), 1429-1440.

4. Linsebigler, A. L.; Lu, G. Q.; Yates, J. T., Photocatalysis on TiO_2 Surfaces - Principles, Mechanisms, and Selected Results. *Chem Rev* **1995,** *95* (3), 735-758.

5. Tan, T. H.; Scott, J.; Ng, Y. H.; Taylor, R. A.; Aguey-Zinsou, K. F.; Amal, R., Understanding Plasmon and Band Gap Photoexcitation Effects on the Thermal-Catalytic Oxidation of Ethanol by TiO_2-Supported Gold. *ACS Catal* **2016,** *6* (3), 1870-1879.

6. Vance, M. E.; Kuiken, T.; Vejerano, E. P.; McGinnis, S. P.; Hochella, M. F.; Rejeski, D.; Hull, M. S., Nanotechnology in the Real World: Redeveloping the Nanomaterial Consumer Products Inventory. *Beilstein J Nanotechnol* **2015,** *6*, 1769-1780.

7. Hanaor, D. A. H.; Sorrell, C. C., Review of the Anatase to Rutile Phase Transformation. *J Mater Sci* **2011,** *46* (4), 855-874.

8. Chen, J.; Ollis, D. F.; Rulkens, W. H.; Bruning, H., Photocatalyzed Oxidation of Alcohols and Organochlorides in the Presence of Native TiO_2 and Metallized TiO_2 Suspensions. Part (II): Photocatalytic Mechanisms. *Water Res* **1999,** *33* (3), 669-676.

9. Xia, T.; Kovochich, M.; Brant, J.; Hotze, M.; Sempf, J.; Oberley, T.; Sioutas, C.; Yeh, J. I.; Wiesner, M. R.; Nel, A. E., Comparison of the Abilities of Ambient and Manufactured Nanoparticles to Induce Cellular Toxicity According to an Oxidative Stress Paradigm. *Nano Lett* **2006,** *6* (8), 1794-1807.

10. Xia, T.; Kovochich, M.; Liong, M.; Madler, L.; Gilbert, B.; Shi, H. B.; Yeh, J. I.; Zink, J. I.; Nel, A. E., Comparison of the Mechanism of Toxicity of Zinc Oxide and Cerium Oxide Nanoparticles Based on Dissolution and Oxidative Stress Properties. *ACS Nano* **2008,** *2* (10), 2121-2134.

11. Lu, P. J.; Cheng, W. L.; Huang, S. C.; Chen, Y. P.; Chou, H. K.; Cheng, H. F., Characterizing Titanium Dioxide and Zinc Oxide Nanoparticles in Sunscreen Spray. *Int J Cosmetic Sci* **2015,** *37* (6), 620-626.

12. Smijs, T. G.; Pavel, S., Titanium Dioxide and Zinc Oxide Nanoparticles in Sunscreens: Focus on their Safety and Effectiveness. *Nanotechnol Sci Appl* **2011,** *4*, 95-112.

13. Jovanovic, B., Critical Review of Public Health Regulations of Titanium Dioxide, a Human Food Additive. *Integr Environ Assess Manag* **2015,** *11* (1), 10-20.

14. Weir, A.; Westerhoff, P.; Fabricius, L.; Hristovski, K.; von Goetz, N., Titanium Dioxide Nanoparticles in Food and Personal Care Products. *Environ Sci Technol* **2012,** *46* (4), 2242-2250.

15. Sato, S.; White, J. M., Photocatalytic Water Decomposition and Water-Gas Shift Reactions over Naoh-Coated, Platinized TiO_2. *J Catal* **1981,** *69* (1), 128-139.

16. Heinrich, U.; Fuhst, R.; Rittinghausen, S.; Creutzenberg, O.; Bellmann, B.; Koch, W.; Levsen, K., Chronic Inhalation Exposure of Wistar Rats and 2 Different Strains of

Mice to Diesel-Engine Exhaust, Carbon-Black, and Titanium-Dioxide. *Inhal Toxicol* **1995,** *7* (4), 533-556.

17. Lee, K. P.; Trochimowicz, H. J.; Reinhardt, C. F., Pulmonary Response of Rats Exposed to Titanium Dioxide (TiO_2) by Inhalation for Two Years. *Toxicol Appl Pharmacol* **1985,** *79* (2), 179-192.

18. Pelclova, D.; Zdimal, V.; Fenclova, Z.; Vlckova, S.; Schwarz, J.; Pusman, J.; Zikova, N.; Syslova, K.; Kuzma, M.; Navratil, T.; Zakharov, S.; Kacer, P., Markers of Oxidative Stress Are Elevated in Workers Exposed to Nanoparticles. *Nanocon 2012, 4th International Conference* **2012**, 654-658.

19. Fryzek, J. P.; Chadda, B.; Marano, D.; White, K.; Schweitzer, S.; McLaughlin, J. K.; Blot, W. J., A Cohort Mortality Study among Titanium Dioxide Manufacturing Workers in the United States. *J Occup Environ Med* **2003,** *45* (4), 400-409.

20. Boffetta, P.; Soutar, A.; Cherrie, J. W.; Granath, F.; Andersen, A.; Anttila, A.; Blettner, M.; Gaborieau, V.; Klug, S. J.; Langard, S.; Luce, D.; Merletti, F.; Miller, B.; Mirabelli, D.; Pukkala, E.; Adami, H. O.; Weiderpass, E., Mortality Among Workers Employed in the Titanium Dioxide Production Industry in Europe. *Cancer Causes Control* **2004,** *15* (7), 697-706.

21. Bernard, B. K.; Osheroff, M. R.; Hofmann, A.; Mennear, J. H., Toxicology and Carcinogenesis Studies of Dietary Titanium Dioxide-Coated Mica in Male and Female Fischer 344 Rats. *J Toxicol Env Health* **1990,** *29* (4), 417-429.

22. Bettini, S.; Boutet-Robinet, E.; Cartier, C.; Comera, C.; Gaultier, E.; Dupuy, J.; Naud, N.; Tache, S.; Grysan, P.; Reguer, S.; Thieriet, N.; Refregiers, M.; Thiaudiere, D.; Cravedi, J. P.; Carriere, M.; Audinot, J. N.; Pierre, F. H.; Guzylack-Piriou, L.; Houdeau,

E., Food-grade TiO_2 Impairs Intestinal and Systemic Immune Homeostasis, Initiates Preneoplastic Lesions and Promotes Aberrant Crypt Development in the Rat Colon. *Sci Rep* **2017,** *7*.

23. De Angelis, I.; Barone, F.; Zijno, A.; Bizzarri, L.; Russo, M. T.; Pozzi, R.; Franchini, F.; Giudetti, G.; Uboldi, C.; Ponti, J.; Rossi, F.; De Berardis, B., Comparative Study of ZnO and TiO_2 Nanoparticles: Physicochemical Characterisation and Toxicological Effects on Human Colon Carcinoma Cells. *Nanotoxicology* **2013,** *7* (8), 1361-1372.

24. Wang, S. Q.; Lim, H. W., Current Status of the Sunscreen Regulation in the United States: 2011 Food and Drug Administration's Final Rule on Labeling and Effectiveness Testing. *J Am Acad Dermatol* **2011,** *65* (4), 863-869.

25. Food and Drug Administration, Code of Federal Regulations Title 21. 2016; Vol. 1.

26. Occupational Exposure to Titanium Dioxide. *Centers for Disease Control and Prevention and National Institute for Occupational Safety and Health* **2011**.

27. Hancock, J. T.; Desikan, R.; Neill, S. J., Role of Reactive Oxygen Species in Cell Signalling Pathways. *Biochem Soc Trans* **2001,** *29*, 345-350.

28. Zhang, J. X.; Wang, X. L.; Vikash, V.; Ye, Q.; Wu, D. D.; Liu, Y. L.; Dong, W. G., ROS and ROS-Mediated Cellular Signaling. *Oxid Med Cell Longev* **2016**.

29. Sies, H., Biochemistry of Oxidative Stress. *Angew Chem Int Ed* **1986,** *25* (12), 1058-1071.

30. Orient, A.; Donko, A.; Szabo, A.; Leto, T. L.; Geiszt, M., Novel Sources of Reactive Oxygen Species in the Human Body. *Nephrol Dial Transpl* **2007,** *22* (5), 1281-1288.

31. Nathan, C., Specificity of a Third Kind: Reactive Oxygen and Nitrogen Intermediates in Cell Signaling. *J Clin Invest* **2003,** *111* (6), 769-778.

32. Fridovich, I., Superoxide Anion Radical ($O\cdot^-_2$ Radical Anion), Superoxide Dismutases, and Related Matters. *J. Biol. Chem.* **1997,** *272* (30), 18515-18517.

33. Schieber, M.; Chandel, N. S., ROS Function in Redox Signaling and Oxidative Stress. *Curr Biol* **2014,** *24* (10), R453-R462.

34. Poljsak, B.; Suput, D.; Milisav, I., Achieving the Balance between ROS and Antioxidants: When to Use the Synthetic Antioxidants. *Oxid Med Cell Longev* **2013**.

35. Finkel, T., Signal Transduction by Reactive Oxygen Species. *J Cell Biol* **2011,** *194* (1), 7-15.

36. Cross, C. E.; Halliwell, B.; Borish, E. T.; Pryor, W. A.; Ames, B. N.; Saul, R. L.; Mccord, J. M.; Harman, D., Oxygen Radicals and Human-Disease. *Ann Intern Med* **1987,** *107* (4), 526-545.

37. Somasundaram, V.; Nadhan, R.; Hemalatha, S. K.; Sengodan, S. K.; Srinivas, P., Nitric Oxide and Reactive Oxygen Species: Clues to Target Oxidative Damage Repair Defective Breast Cancers. *Crit Rev Oncol Hemat* **2016,** *101*, 184-192.

38. Zhang, B.; Bailey, W.; McVicar, A.; Gensel, J., Age Increases Reactive Oxygen Species Production in Macrophages and Potentiates Oxidative Damage after Spinal Cord Injury. *J Neurotraum* **2016,** *33* (13), A14-A14.

39. Wood, Z. A.; Poole, L. B.; Karplus, P. A., Peroxiredoxin Evolution and the Regulation of Hydrogen Peroxide Signaling. *Science* **2003,** *300* (5619), 650-653.

40. Wells, P. G.; Miller-Pinsler, L.; Bhatia, S.; Drake, D.; Shapiro, A. M., Reactive Oxygen Species (ROS) Formation, Oxidative DNA Damage and Repair in Teratogenesis. *Birth Defects Res A* **2015,** *103* (5), 359-359.

41. Bongarzone, E. R.; Pasquini, J. M.; Soto, E. F., Oxidative Damage to Proteins and Lipids of Cns Myelin Produced by in-Vitro Generated Reactive Oxygen Species. *J Neurosci Res* **1995,** *41* (2), 213-221.

42. Jeon, K. I.; Park, E.; Park, H. R.; Jeon, Y. J.; Cha, S. H.; Lee, S. C., Antioxidant Activity of Far-Infrared Radiated Rice Hull Extracts on Reactive Oxygen Species Scavenging and Oxidative DNA Damage in Human Lymphocytes. *J Med Food* **2006,** *9* (1), 42-48.

43. Shimizu, I.; Shimamoto, N.; Saiki, K.; Furujo, M.; Osawa, K., Lipid Peroxidation in Hepatic Fibrosis. *Lipid Peroxidation* **2012**, 483-492.

44. Frijhoff, J.; Winyard, P. G.; Zarkovic, N.; Davies, S. S.; Stocker, R.; Cheng, D.; Knight, A. R.; Taylor, E. L.; Oettrich, J.; Ruskovska, T.; Gasparovic, A. C.; Cuadrado, A.; Weber, D.; Poulsen, H. E.; Grune, T.; Schmidt, H. H. H. W.; Ghezzi, P., Clinical Relevance of Biomarkers of Oxidative Stress. *Antioxid Redox Sign* **2015,** *23* (14), 1144-1170.

45. Gurr, J. R.; Wang, A. S. S.; Chen, C. H.; Jan, K. Y., Ultrafine Titanium Dioxide Particles in the Absence of Photoactivation can Induce Oxidative Damage to Human Bronchial Epithelial Cells. *Toxicology* **2005,** *213* (1-2), 66-73.

46. Iavicoli, I.; Leso, V.; Fontana, L.; Bergamaschi, A., Toxicological Effects of Titanium Dioxide Nanoparticles: a Review of In Vitro Mammalian Studies. *Eur Rev Med Pharmacol* **2011,** *15* (5), 481-508.

47. Jin, C. Y.; Zhu, B. S.; Wang, X. F.; Lu, Q. H., Cytotoxicity of Titanium Dioxide Nanoparticles in Mouse Fibroblast Cells. *Chem Res Toxicol* **2008,** *21* (9), 1871-1877.

48. Llop, J.; Estrela-Lopis, I.; Ziolo, R. F.; Gonzalez, A.; Fleddermann, J.; Dorn, M.; Vallejo, V. G.; Simon-Vazquez, R.; Donath, E.; Mao, Z. G.; Gao, C. Y.; Moya, S. E., Uptake, Biological Fate, and Toxicity of Metal Oxide Nanoparticles. *Part Part Syst Char* **2014,** *31* (1), 24-35.

49. Magdolenova, Z.; Collins, A.; Kumar, A.; Dhawan, A.; Stone, V.; Dusinska, M., Mechanisms of Genotoxicity. A Review of In Vitro and In Vivo Studies with Engineered Nanoparticles. *Nanotoxicology* **2014,** *8* (3), 233-278.

50. Runa, S.; Khanal, D.; Kemp, M. L.; Payne, C. K., TiO_2 Nanoparticles Alter the Expression of Peroxiredoxin Antioxidant Genes. *J Phys Chem C* **2016,** *120* (37), 20736-20742.

51. Shi, H. B.; Magaye, R.; Castranova, V.; Zhao, J. S., Titanium Dioxide Nanoparticles: a Review of Current Toxicological Data. *Part Fibre Toxicol* **2013,** *10.*

52. Winter, M.; Beer, H. D.; Hornung, V.; Kramer, U.; Schins, R. P. F.; Forster, I., Activation of the Inflammasome by Amorphous Silica and TiO_2 Nanoparticles in Murine Dendritic Cells. *Nanotoxicology* **2011,** *5* (3), 326-340.

53. Cedervall, T.; Lynch, I.; Lindman, S.; Berggard, T.; Thulin, E.; Nilsson, H.; Dawson, K. A.; Linse, S., Understanding the Nanoparticle-Protein Corona Using Methods

to Quantify Exchange Rates and Affinities of Proteins for Nanoparticles. *Proc Natl Acad Sci U.S.A.* **2007,** *104* (7), 2050-2055.

54. Unfried, K.; Albrecht, C.; Klotz, L. O.; Von Mikecz, A.; Grether-Beck, S.; Schins, R. P. F., Cellular Responses to Nanoparticles: Target Structures and Mechanisms. *Nanotoxicology* **2007,** *1* (1), 52-71.

55. Walczyk, D.; Bombelli, F. B.; Monopoli, M. P.; Lynch, I.; Dawson, K. A., What the Cell "Sees" in Bionanoscience. *J Am Chem Soc* **2010,** *132* (16), 5761-5768.

56. Yang, S. T.; Liu, Y.; Wang, Y. W.; Cao, A. N., Biosafety and Bioapplication of Nanomaterials by Designing Protein Nanoparticle Interactions. *Small* **2013,** *9* (9-10), 1635-1653.

57. Yoon, J. Y.; Kim, J. H.; Kim, W. S., Interpretation of Protein Adsorption Phenomena onto Functional Microspheres. *Colloid Surf B* **1998,** *12* (1), 15-22.

58. Ruge, C. A.; Schaefer, U. F.; Herrmann, J.; Kirch, J.; Canadas, O.; Echaide, M.; Perez-Gil, J.; Casals, C.; Muller, R.; Lehr, C. M., The Interplay of Lung Surfactant Proteins and Lipids Assimilates the Macrophage Clearance of Nanoparticles. *PLoS One* **2012,** *7* (7).

59. Cedervall, T.; Lynch, I.; Foy, M.; Berggad, T.; Donnelly, S. C.; Cagney, G.; Linse, S.; Dawson, K. A., Detailed Identification of Plasma Proteins Adsorbed on Copolymer Nanoparticles. *Angew Chem Int Ed* **2007,** *46* (30), 5754-5756.

60. Doorley, G. W.; Payne, C. K., Cellular Binding of Nanoparticles in the Presence of Serum Proteins. *Chem Commun* **2011,** *47* (1), 466-468.

61. Fleischer, C. C.; Payne, C. K., Nanoparticle Surface Charge Directs the Cellular Binding of Nanoparticle-Protein Complexes. *Biophys J* **2013,** *104* (2), 524a-524a.

62. Fleischer, C. C.; Payne, C. K., Secondary Structure of Corona Proteins Determines the Cell Surface Receptors Used by Nanoparticles. *J Phys Chem B* **2014,** *118* (49), 14017-14026.

63. Nel, A. E.; Madler, L.; Velegol, D.; Xia, T.; Hoek, E. M. V.; Somasundaran, P.; Klaessig, F.; Castranova, V.; Thompson, M., Understanding Biophysicochemical Interactions at the Nano-Bio Interface. *Nat Mater* **2009,** *8* (7), 543-557.

64. Zhang, Y. Y.; Leu, Y. R.; Aitken, R. J.; Riediker, M., Inventory of Engineered Nanoparticle-Containing Consumer Products Available in the Singapore Retail Market and Likelihood of Release into the Aquatic Environment. *Int J Env Res Pub He* **2015,** *12* (8), 8717-8743.

65. Vroman, L.; Adams, A. L.; Fischer, G. C.; Munoz, P. C., Interaction of High Molecular-Weight Kininogen, Factor XII, and Fibrinogen in Plasma at Interfaces. *Blood* **1980,** *55* (1), 156-159.

66. Fleischer, C. C.; Payne, C. K., Nanoparticle-Cell Interactions: Molecular Structure of the Protein Corona and Cellular Outcomes. *Accounts Chem Res* **2014,** *47* (8), 2651-2659.

67. Del Pino, P.; Pelaz, B.; Zhang, Q.; Maffre, P.; Nienhaus, G. U.; Parak, W. J., Protein Corona Formation Around Nanoparticles - From the Past to the Future. *Mater Horizons* **2014,** *1* (3), 301-313.

68. Deng, Z. J.; Mortimer, G.; Schiller, T.; Musumeci, A.; Martin, D.; Minchin, R. F., Differential Plasma Protein Binding to Metal Oxide Nanoparticles. *Nanotechnology* **2009,** *20* (45).

69. Lesniak, A.; Fenaroli, F.; Monopoli, M. R.; Aberg, C.; Dawson, K. A.; Salvati, A., Effects of the Presence or Absence of a Protein Corona on Silica Nanoparticle Uptake and Impact on Cells. *ACS Nano* **2012,** *6* (7), 5845-5857.

70. Clemments, A. M.; Botella, P.; Landry, C. C., Spatial Mapping of Protein Adsorption on Mesoporous Silica Nanoparticles by Stochastic Optical Reconstruction Microscopy. *J Am Chem Soc* **2017,** *139* (11), 3978-3981.

71. Hlady, V.; Buijs, J., Protein Adsorption on Solid Surfaces. *Curr Opin Biotech* **1996,** *7* (1), 72-77.

72. Morgan, P. E.; Sturgess, A. D.; Davies, M. J., Increased Levels of Serum Protein Oxidation and Correlation with Disease Activity in Systemic Lupus Erythematosus. *Arthritis Rheum* **2005,** *52* (7), 2069-2079.

73. Pan, H.; Qin, M.; Meng, W.; Cao, Y.; Wang, W., How Do Proteins Unfold upon Adsorption on Nanoparticle Surfaces? *Langmuir* **2012,** *28* (35), 12779-12787.

74. Roach, P.; Farrar, D.; Perry, C. C., Interpretation of Protein Adsorption: Surface-Induced Conformational Changes. *J Am Chem Soc* **2005,** *127* (22), 8168-8173.

75. Treuel, L.; Brandholt, S.; Maffre, P.; Wiegele, S.; Shang, L.; Nienhaus, G. U., Impact of Protein Modification on the Protein Corona on Nanoparticles and Nanoparticle-Cell Interactions. *ACS Nano* **2014,** *8* (1), 503-513.

76. Nel, A.; Xia, T.; Madler, L.; Li, N., Toxic Potential of Materials at the Nanolevel. *Science* **2006,** *311* (5761), 622-627.

77. Sharifi, S.; Behzadi, S.; Laurent, S.; Forrest, M. L.; Stroeve, P.; Mahmoudi, M., Toxicity of Nanomaterials. *Chem Soc Rev* **2012,** *41* (6), 2323-2343.

78. Gerloff, K.; Fenoglio, I.; Carella, E.; Kolling, J.; Albrecht, C.; Boots, A. W.; Forster, I.; Schins, R. P. F., Distinctive Toxicity of TiO_2 Rutile/Anatase Mixed Phase Nanoparticles on Caco-2 Cells. *Chem Res Toxicol* **2012,** *25* (3), 646-655.

79. Hussain, S. M.; Hess, K. L.; Gearhart, J. M.; Geiss, K. T.; Schlager, J. J., In Vitro Toxicity of Nanoparticles in BRL 3A Rat Liver Cells. *Toxicol in Vitro* **2005,** *19* (7), 975-983.

80. Jugan, M. L.; Barillet, S.; Simon-Deckers, A.; Herlin-Boime, N.; Sauvaigo, S.; Douki, T.; Carriere, M., Titanium Dioxide Nanoparticles Exhibit Genotoxicity and Impair DNA Repair Activity in A549 Cells. *Nanotoxicology* **2012,** *6* (5), 501-513.

81. Kumar, A.; Khan, S.; Dhawan, A., Comprehensive Molecular Analysis of the Responses Induced by Titanium Dioxide Nanoparticles in Human Keratinocyte Cells. *J Transl Toxicol* **2014,** *1* (1), 28-39.

82. Sayes, C. M.; Gobin, A. M.; Ausman, K. D.; Mendez, J.; West, J. L.; Colvin, V. L., Nano-C-60 Cytotoxicity is Due to Lipid Peroxidation. *Biomaterials* **2005,** *26* (36), 7587-7595.

83. Fujii, J.; Ikeda, Y., Advances in our Understanding of Peroxiredoxin, a Multifunctional, Mammalian Redox Protein. *Redox Rep* **2002,** *7* (3), 123-130.

84. Rabilloud, T.; Heller, M.; Gasnier, F.; Luche, S.; Rey, C.; Aebersold, R.; Benahmed, M.; Louisot, P.; Lunardi, J., Proteomics Analysis of Cellular Response to Oxidative Stress - Evidence for In Vivo Overoxidation of Peroxiredoxins at their Active Site. *J Biol Chem* **2002,** *277* (22), 19396-19401.

85. Rhee, S. G.; Chae, H. Z.; Kim, K., Peroxiredoxins: A Historical Overview and Speculative Preview of Novel Mechanisms and Emerging Concepts in Cell Signaling. *Free Radic Biol Med* **2005,** *38* (12), 1543-1552.

86. Wood, Z. A.; Schroder, E.; Harris, J. R.; Poole, L. B., Structure, Mechanism and Regulation of Peroxiredoxins. *Trends Biochem Sci* **2003,** *28* (1), 32-40.

87. Kipling, J. J.; Wilson, R. B., Adsorptive Properties of Polymer Carbons 2. Determination of Pore Sizes. *J Chem Soc Faraday Trans* **1960,** *56* (4), 562-569.

88. Nagaveni, K.; Hegde, M. S.; Ravishankar, N.; Subbanna, G. N.; Madras, G., Synthesis and Structure of Nanocrystalline TiO_2 with Lower Band Gap Showing High Photocatalytic Activity. *Langmuir* **2004,** *20* (7), 2900-2907.

89. Long, T. C.; Saleh, N.; Tilton, R. D.; Lowry, G. V.; Veronesi, B., Titanium dioxide (P25) Produces Reactive Oxygen Species in Immortalized Brain Microglia (BV2): Implications for Nanoparticle Neurotoxicity. *Environ Sci Technol* **2006,** *40* (14), 4346-4352.

90. Brun, E.; Sicard – Roselli, C., Could Nanoparticle Corona Characterization Help for Biological Consequence Prediction? *Cancer Nanotechnol* **2014,** *5* (1), 7.

91. Ge, C.; Tian, J.; Zhao, Y.; Chen, C.; Zhou, R.; Chai, Z., Towards Understanding of Nanoparticle–Protein Corona. *Arch Toxicol* **2015,** *89* (4), 519-539.

92. Park, S.; Hamad-Schifferli, K., Nanoscale Interfaces to Biology. *Curr Opin Chem Biol* **2010,** *14* (5), 616-622.

93. Treuel, L.; Nienhaus, G. U., Toward a Molecular Understanding of Nanoparticle–Protein Interactions. *Biophys Rev* **2012,** *4* (2), 137-147.

94. Adimora, N. J.; Jones, D. P.; Kemp, M. L., A Model of Redox Kinetics Implicates the Thiol Proteome in Cellular Hydrogen Peroxide Responses. *Antioxid Redox Sign* **2010,** *13* (6), 731-743.

95. Sobotta, M. C.; Liou, W.; Stocker, S.; Talwar, D.; Oehler, M.; Ruppert, T.; Scharf, A. N. D.; Dick, T. P., Peroxiredoxin-2 and STAT3 Form a Redox Relay for H_2O_2 Signaling. *Nat Chem Biol* **2015,** *11* (1), 64-70.

96. Xu, A.; Chai, Y. F.; Nohmi, T.; Hei, T. K., Genotoxic Responses to Titanium Dioxide Nanoparticles and Fullerene in Gpt Delta Transgenic MEF Cells. *Part Fibre Toxicol* **2009,** *6*.

97. Knoops, B.; Goemaere, J.; Van der Eecken, V.; Declercq, J. P., Peroxiredoxin 5: Structure, Mechanism, and Function of the Mammalian Atypical 2-Cys Peroxiredoxin. *Antioxid Redox Sign* **2011,** *15* (3), 817-829.

98. Diebold, U., The Surface Science of Titanium Dioxide. *Surf Sci Rep* **2003,** *48* (5-8), 53-229.

99. Fujishima, A.; Zhang, X. T.; Tryk, D. A., TiO_2 Photocatalysis and Related Surface Phenomena. *Surf Sci Rep* **2008,** *63* (12), 515-582.

100. EPA. Nanomaterial Case Studies: Nanoscale Titanium Dioxide in Water Treatment and Topical Sunscreen 2010.

101. Diebold, U.; Lehman, J.; Mahmoud, T.; Kuhn, M.; Leonardelli, G.; Hebenstreit, W.; Schmid, M.; Varga, P., Intrinsic Defects on a TiO_2 (110) (1x1) Surface and Their Reaction with Oxygen: a Scanning Tunneling Microscopy Study. *Surf Sci* **1998,** *411* (1-2), 137-153.

102. Hugenschmidt, M. B.; Gamble, L.; Campbell, C. T., The Interaction of H_2O with a TiO_2 (110) Surface. *Surf Sci* **1994,** *302* (3), 329-340.

103. Prasanna, V. L.; Vijayaraghavan, R., Insight into the Mechanism of Antibacterial Activity of ZnO: Surface Defects Mediated Reactive Oxygen Species Even in the Dark. *Langmuir* **2015,** *31* (33), 9155-9162.

104. Schaub, R.; Thostrup, P.; Lopez, N.; Laegsgaard, E.; Stensgaard, I.; Norskov, J. K.; Besenbacher, F., Oxygen Vacancies as Active Sites for Water Dissociation on Rutile TiO_2 (110). *Phys Rev Lett* **2001,** *87* (26).

105. Wendt, S.; Schaub, R.; Matthiesen, J.; Vestergaard, E. K.; Wahlstrom, E.; Rasmussen, M. D.; Thostrup, P.; Molina, L. M.; Laegsgaard, E.; Stensgaard, I.; Hammer, B.; Besenbacher, F., Oxygen Vacancies on TiO_2 (110) and Their Interaction with H_2O and O_2: A Combined High-Resolution STM and DFT Study. *Surf Sci* **2005,** *598* (1-3), 226-245.

106. Doorley, G. W.; Payne, C. K., Nanoparticles Act as Protein Carriers During Cellular Internalization. *Chem Commun* **2012,** *48* (24), 2961-2963.

107. Lynch, I.; Cedervall, T.; Lundqvist, M.; Cabaleiro-Lago, C.; Linse, S.; Dawson, K. A., The Nanoparticle - Protein Complex as a Biological Entity; a Complex Fluids and Surface Science Challenge for the 21st Century. *Adv Colloid Interface Sci* **2007,** *134-35*, 167-174.

108. Prasad, R. Y.; Wallace, K.; Daniel, K. M.; Tennant, A. H.; Zucker, R. M.; Strickland, J.; Dreher, K.; Kligerman, A. D.; Blackman, C. F.; DeMarini, D. M., Effect of Treatment Media on the Agglomeration of Titanium Dioxide Nanoparticles: Impact on Genotoxicity, Cellular Interaction, and Cell Cycle. *ACS Nano* **2013,** *7* (3), 1929-1942.

109. Goto, H.; Hanada, Y.; Ohno, T.; Matsumura, M., Quantitative Analysis of Superoxide Ion and Hydrogen Peroxide Produced from Molecular Oxygen on Photoirradiated TiO_2 Particles. *J Catal* **2004,** *225* (1), 223-229.

110. Lipovsky, A.; Levitski, L.; Tzitrinovich, Z.; Gedanken, A.; Lubart, R., The Different Behavior of Rutile and Anatase Nanoparticles in Forming Oxy Radicals Upon Illumination with Visible Light: An EPR Study. *Photochem Photobiol* **2012,** *88* (1), 14-20.

111. Berlett, B. S.; Stadtman, E. R., Protein Oxidation in Aging, Disease, and Oxidative Stress. *J Biol Chem* **1997,** *272* (33), 20313-20316.

112. Hawkins, C. L.; Morgan, P. E.; Davies, M. J., Quantification of Protein Modification by Oxidants. *Free Radic Biol Med* **2009,** *46* (8), 965-988.

113. Nakamura, I.; Negishi, N.; Kutsuna, S.; Ihara, T.; Sugihara, S.; Takeuchi, E., Role of Oxygen Vacancy in the Plasma-Treated TiO_2 Photocatalyst with Visible Light Activity for NO Removal. *J Mol Catal A: Chem* **2000,** *161* (1-2), 205-212.

114. Ihara, T.; Miyoshi, M.; Ando, M.; Sugihara, S.; Iriyama, Y., Preparation of a Visible-Light-Active TiO_2 Photocatalyst by RF Plasma Treatment. *J Mater Sci* **2001,** *36* (17), 4201-4207.

115. Jun, J.; Shin, J. H.; Dhayal, M., Surface State of TiO_2 Treated with Low Ion Energy Plasma. *Appl Surf Sci* **2006,** *252* (10), 3871-3877.

116. Frerichs, S. R. M., W. H. Passivated Nano-Titanium Dioxide Particles and Method of Making the Same. US11011670 2005.

117. Miller, G. W.; Jones, D. P., The Nature of Nurture: Refining the Definition of the Exposome. *Toxicol Sci* **2014,** *137* (1), 1-2.

118. Wild, C.; Delgado, L., Foreword. *Cancer Epidemiol* **2016,** *44*, S1-S2.

119. U. G. Mineral and Commodity Summaries 2015: Titanium and Titanium Dioxide. Reston, VA, 2015.

120. Robichaud, C. O.; Uyar, A. E.; Darby, M. R.; Zucker, L. G.; Wiesner, M. R., Estimates of Upper Bounds and Trends in Nano- TiO_2 Production As a Basis for Exposure Assessment. *Environ Sci Technol* **2009,** *43* (12), 4227-4233.

121. Sun, T. Y.; Gottschalk, F.; Hungerbuhler, K.; Nowack, B., Comprehensive Probabilistic Modelling of Environmental Emissions of Engineered Nanomaterials. *Environ Pollut* **2014,** *185*, 69-76.

122. Otani, N.; Ishimatsu, S.; Mochizuki, T., Acute Group Poisoning by Titanium Dioxide: Inhalation Exposure May Cause Metal Fume Fever. *Am J Emerg Med* **2008,** *26* (5), 608-611.

123. Sha, B. Y.; Gao, W.; Cui, X. Y.; Wang, L.; Xu, F., The Potential Health Challenges of TiO_2 Nanomaterials. *J Appl Toxicol* **2015,** *35* (10), 1086-1101.

124. Jayaram, D. T.; Runa, S.; Kemp, M. L.; Payne, C. K., Nanoparticle-induced Oxidation of Corona Proteins Initiates an Oxidative Stress Response in Cells. *Nanoscale* **2017,** *9* (22), 7595-7601.

125. Bekdemir, A.; Stellacci, F., A Centrifugation-based Physicochemical Characterization Method for the Interaction Between Proteins and Nanoparticles. *Nat Commun* **2016,** *7*.

126. Lewinski, N.; Colvin, V.; Drezek, R., Cytotoxicity of Nanoparticles. *Small* **2008,** *4* (1), 26-49.

127. Niehaus, W. G.; Samuelsson, B., Formation of Malonaldehyde from Phospholipid Arachidonate during Microsomal Lipid Peroxidation. *Eur J Biochem* **1968,** *6* (1), 126-130.

128. Sayes, C. M.; Wahi, R.; Kurian, P. A.; Liu, Y. P.; West, J. L.; Ausman, K. D.; Warheit, D. B.; Colvin, V. L., Correlating Nanoscale Titania Structure with Toxicity: A Cytotoxicity and Inflammatory Response Study with Human Dermal Fibroblasts and Human Lung Epithelial Cells. *Toxicol Sci* **2006,** *92* (1), 174-185.

129. Stocks, J.; Gutteridge, J. M.; Sharp, R. J.; Dormandy, T. L., Inhibition of Lipid Autoxidation by Human-Serum and its Relation to Serum-Proteins and Alpha-Tocopherol. *Clin Sci Mol Med* **1974,** *47* (3), 223-233.

130. Roche, M.; Rondeau, P.; Singh, N. R.; Tarnus, E.; Bourdon, E., The Antioxidant Properties of Serum Albumin. *FEBS Lett* **2008,** *582* (13), 1783-1787.

131. Fleischer, C. C.; Payne, C. K., Nanoparticle-cell interactions: Molecular Structure of the Protein Corona and Cellular Outcomes. *Acc Chem Res* **2014,** *47*, 2651-2659.

132. Walczyk, D.; Bombelli, F. B.; Monopoli, M. P.; Lynch, I.; Dawson, K. A., What the Cell "Sees" in Bionanoscience. *J Am Chem Soc* **2010,** *132*, 5761-5768.

133. Lynch, I.; Cedervall, T.; Lundqvist, M.; Cabaleiro-Lago, C.; Linse, S.; Dawson, K. A., The Nanoparticle - Protein Complex as a Biological Entity; a Complex Fluids and Surface Science Challenge for the 21st Century. *Adv Colloid Interfac* **2007,** *7* (134-135), 167-174.

134. Oddone, A.; Vilanova, I. V.; Tam, J.; Lakadamyali, M., Super-resolution Imaging with Stochastic Single-molecule Localization: Concepts, Technical Developments, and Biological Applications. *Microsc Res Tech* **2014,** *77* (7), 502-509.

135. Durisic, N.; Cuervo, L. L.; Lakadamyali, M., Quantitative Super-resolution Microscopy: Pitfalls and Strategies for Image Analysis. *Curr Opin Chem Biol* **2014,** *20*, 22-28.

136. Rust, M. J.; Bates, M.; Zhuang, X., Sub-diffraction-limit Imaging by Stochastic Optical Reconstruction Microscopy (STORM). *Nat Methods* **2006,** *3* (10), 793-796.

137. Heilemann, M.; Van De Linde, S.; Schüttpelz, M.; Kasper, R.; Seefeldt, B.; Mukherjee, A.; Tinnefeld, P.; Sauer, M., Subdiffraction-resolution Fluorescence Imaging with Conventional Fluorescent Probes. *Angew Chem Int Edit* **2008,** *47* (33), 6172-6176.

138. Ashby, J.; Pan, S. Q.; Zhong, W. W., Size and Surface Functionalization of Iron Oxide Nanoparticles Influence the Composition and Dynamic Nature of Their Protein Corona. *ACS Appl Mater Inter* **2014,** *6* (17), 15412-15419.

139. Milani, S.; Bombelli, F. B.; Pitek, A. S.; Dawson, K. A.; Radler, J., Reversible versus Irreversible Binding of Transferrin to Polystyrene Nanoparticles: Soft and Hard Corona. *ACS Nano* **2012,** *6* (3), 2532-2541.

140. Sasidharan, A.; Riviere, J. E.; Monteiro-Riviere, N. A., Gold and Silver Nanoparticle Interactions with Human Proteins: Impact and Implications in Biocorona Formation. *J Mater Chem B* **2015,** *3* (10), 2075-2082.

141. Wang, A. L.; Perera, Y. R.; Davidson, M. B.; Fitzkee, N. C., Electrostatic Interactions and Protein Competition Reveal a Dynamic Surface in Gold Nanoparticle-Protein Adsorption. *J Phys Chem C* **2016,** *120* (42), 24231-24239.

142. Wang, A. L.; Vangala, K.; Vo, T.; Zhang, D. M.; Fitzkee, N. C., A Three-Step Model for Protein-Gold Nanoparticle Adsorption. *J Phys Chem C* **2014,** *118* (15), 8134-8142.

143. Monopoli, M. P.; Walczyk, D.; Campbell, A.; Elia, G.; Lynch, I.; Bombelli, F. B.; Dawson, K. A., Physical-Chemical Aspects of Protein Corona: Relevance to in Vitro and in Vivo Biological Impacts of Nanoparticles. *J Am Chem Soc* **2011,** *133* (8), 2525-2534.

144. Li, S.-Q.; Zhu, R.-R.; Zhu, H.; Xue, M.; Sun, X.-Y.; Yao, S.-D.; Wang, S.-L., Nanotoxicity of TiO_2 Nanoparticles to Erythrocyte in Vitro. *Food Chem. Toxicol.* **2008,** *46* (12), 3626-3631.

145. Wang, J.; Liu, Y.; Jiao, F.; Lao, F.; Li, W.; Gu, Y.; Li, Y.; Ge, C.; Zhou, G.; Li, B., Time-dependent Translocation and Potential Impairment on Central Nervous System by Intranasally Instilled TiO_2 Nanoparticles. *Toxicology* **2008,** *254* (1), 82-90.

146. Wang, J.; Chen, C.; Liu, Y.; Jiao, F.; Li, W.; Lao, F.; Li, Y.; Li, B.; Ge, C.; Zhou, G., Potential Neurological Lesion after Nasal Instillation of TiO_2 Nanoparticles in the Anatase and Rutile Crystal Phases. *Toxicol Lett* **2008,** *183* (1), 72-80.

147. Ma, L.; Liu, J.; Li, N.; Wang, J.; Duan, Y.; Yan, J.; Liu, H.; Wang, H.; Hong, F., Oxidative Stress in the Brain of Mice Caused by Translocated Nanoparticulate TiO_2 Delivered to the Abdominal Cavity. *Biomaterials* **2010,** *31* (1), 99-105.

148. Linhua, H.; Zhenyu, W.; Baoshan, X., Effect of Sub-acute Exposure to TiO_2 Nanoparticles on Oxidative Stress and Histopathological Changes in Juvenile Carp (Cyprinus carpio). *J Environ Sci* **2009,** *21* (10), 1459-1466.

149. Li, J. J.; Hartono, D.; Ong, C.-N.; Bay, B.-H.; Yung, L.-Y. L., Autophagy and Oxidative Stress Associated with Gold Nanoparticles. *Biomaterials* **2010,** *31* (23), 5996-6003.

150. Lin, W.; Huang, Y.-w.; Zhou, X.-D.; Ma, Y., Toxicity of Cerium Oxide Nanoparticles in Human Lung Cancer Cells. *Int J Toxicol* **2006,** *25* (6), 451-457.

151. Shvedova, A.; Castranova, V.; Kisin, E.; Schwegler-Berry, D.; Murray, A.; Gandelsman, V.; Maynard, A.; Baron, P., Exposure to Carbon Nanotube Material:

Assessment of Nanotube Cytotoxicity using Human Keratinocyte Cells. *J Toxicol Environ Health A* **2003,** *66* (20), 1909-1926.

152. Feliu, N.; Docter, D.; Heine, M.; del Pino, P.; Ashraf, S.; Kolosnjaj-Tabi, J.; Macchiarini, P.; Nielsen, P.; Alloyeau, D.; Gazeau, F., In Vivo Degeneration and the Fate of Inorganic Nanoparticles. *Chem Soc Rev* **2016,** *45* (9), 2440-2457.

153. Ma, Z.; Bai, J.; Jiang, X., Monitoring of the Enzymatic Degradation of Protein Corona and Evaluating the Accompanying Cytotoxicity of Nanoparticles. *ACS Appl. Mater. Interfaces* **2015,** *7* (32), 17614-17622.

154. Heger, D.; Jirkovsky, J.; Klan, P., Aggregation of Methylene Blue in Frozen Aqueous Solutions Studied by Absorption Spectroscopy. *J Phys Chem A* **2005,** *109* (30), 6702-6709.

155. Jia, Z.; Duan, X. G.; Zhang, W. C.; Wang, W. M.; Sun, H. Q.; Wang, S. B.; Zhang, L. C., Ultra-sustainable $Fe^{78}Si^{9}B^{13}$ Metallic Glass as a Catalyst for Activation of Persulfate on Methylene Blue Degradation under UV-Vis Light. *Sci Rep* **2016,** *6*.

156. Maurya, R.; Ghosh, T.; Paliwal, C.; Shrivastav, A.; Chokshi, K.; Pancha, I.; Ghosh, A.; Mishra, S., Biosorption of Methylene Blue by De-Oiled Algal Biomass: Equilibrium, Kinetics and Artificial Neural Network Modelling. *Plos One* **2014,** *9* (10).

157. Wu, C. H.; Chern, J. M., Kinetics of Photocatalytic Decomposition of Methylene blue. *Ind Eng Chem Res* **2006,** *45* (19), 6450-6457.

158. Yang, S. J.; He, H. P.; Wu, D. Q.; Chen, D.; Ma, Y. H.; Li, X. L.; Zhu, J. X.; Yuan, P., Degradation of Methylene Blue by Heterogeneous Fenton Reaction Using Titanomagnetite at Neutral pH Values: Process and Affecting Factors. *Ind Eng Chem Res* **2009,** *48* (22), 9915-9921.

159. Palomero, J.; Pye, D.; Kabayo, T.; Spiller, D. G.; Jackson, M. J., In Situ Detection and Measurement of Intracellular Reactive Oxygen Species in Single Isolated Mature Skeletal Muscle Fibers by Real Time Fluorescence Microscopy. *Antioxid Redox Sign* **2008,** *10* (8), 1463-1474.

160. Santamarina, J. C.; Klein, K. A.; Wang, Y. H.; Prencke, E., Specific Surface: Determination and Relevance. *Can Geotech J* **2002,** *39* (1), 233-241.

VITA

Sabiha Runa was born in Barberton, Ohio in 1990 and raised in Huntsville, Alabama. She graduated from The University of Alabama in Huntsville in 2012 with a B.S. in chemistry and a B.S.E. in chemical engineering with magna cum laude distinction. A strong believer in “science for all”, she has dedicated much of her time outside of the research lab volunteering for programs that provide STEM (science, technology, engineering and mathematics) education and opportunities for a K-12 audience. She is the creator of the Science Haiku Contest for the Atlanta Science Festival, and has worked as part of the communications team at The Center for Education Integrating Science, Mathematics, and Computing at Georgia Tech.